Oxidative Cracking of n-Hexane

a catalytic pathway to olefins

Graduation committee

Prof. Dr. P.J. Kelly, chairman	University of Twente
Prof. Dr. Ir. L. Lefferts, promoter	University of Twente
Dr. K. Seshan, assistant promoter	University of Twente
Prof. Dr. Ir. H. van den Berg	University of Twente
Prof. Dr. J.G.E. Gardeniers	University of Twente
Prof. Dr. Ir. G. Mul	University of Twente
Prof. Dr. Ir. M.C.M van de Sanden	Technical University of Eindhoven
Dr. B.L. Mojet	University of Twente
Dr. G. Meima	Dow Benelux, B.V.

The research described in this thesis was carried out at the Catalytic Processes and Materials group of the University of Twente. Financial support by ASPECT project n^{o} 053.62.011 is gratefully acknowledged.

Cover design: Bedo Demirdjian, Cassia Boyadjian and Bert Geerdink.

Publisher
Gildeprint, Enschede, the Netherlands

ISBN: 978-90-365-3081-1

Author email: cassia.boyadjian@gmail.com

Oxidative Cracking of n-Hexane
a catalytic pathway to olefins

DISSERTATION

to obtain
the degree of doctor at the University of Twente,
on the authority of the rector magnificus,
Prof. Dr. H. Brinksma
on account of the decision of the graduation committee,
to be publicly defended on
Friday September 24th 2010 at 16:45 hrs

by

Cassia Boyadjian

born on 17 January 1978
in Bourj Hammoud, Lebanon

This dissertation has been approved by the promoter
Prof. Dr. Ir. L. Lefferts
and the assistant promoter
Dr. K. Seshan

To my parents, brother and Bedo

“Life is not easy for any of us. But what of that? We must have perseverance and above all confidence in ourselves. We must believe that we are gifted for something, and that this thing, at whatever cost, must be attained.”

Marie Curie

Acknowledgements

I would like to express my deepest gratitude to all those who believed in me and contributed in this work, and in bringing my PhD journey successfully to an end.

I am grateful to my promoter Prof. Leon Lefferts for offering me the opportunity of a life altering experience, which taught me every second to believe more and more in myself. His constant critical view of my work developed my already not simple mind into an even more detailed scientific analytical thinking.

I deeply thank my supervisor Dr. K. Seshan, for his unique approach and guidance, which are the seeds of this fruitful work. With him I learnt to think beyond answering the simple questions, as science is not to explain the trivial. By time, I observed myself developing with him, from an amateur to a professional researcher.

It is an honor for me to acknowledge each one of Prof. Henk van den Berg, Prof. Han Gardeniers, Dr. Barbara Mojet, Dr. Igor Babich and Dr. Louis van der Ham for their scientific contribution in this work.

My deepest gratitude goes to Ing. Bert Geerdink for his significant contribution in this thesis.

I heartily thank all my friends and colleagues, this mosaic of individuals at the Catalytic Processes and Materials group of the University of Twente, who colored my PhD experience and contributed in this achievement.

Dejan Radivojevic, Sergio Pacheco Benito, Marijana Kovacevic, Berta Matas Güell, Kumar Chintaginjala, Digvijay Thakur, Anil Agiral, Davide Crapanzano, Cristiano Trionfetti, Khalid Azzam, Zeljko Kotanjac, Inga Tuzovskaya, Elizaveta Vereshchagina, Hrudya Nair, Louise Vrielink, Karin Altena-Schildkamp, Lianne Bode, Dennis de Vlieger, Astrid Hoeppener; my students Bart van der Veer and Arnau Carné Sánchez; the process design team R.M. van Dorp, J.T.G. te Braake, Y. ter Mors, F.N.H. Schrama, R. Veneman; and so many others whom I am not mentioning here, I thank you all!

Last but not least, I am indebted to my parents Antranig and Alice Boyadjians and brother Raffi, for their patience and sacrifice of having me abroad specially in moments when they needed me most; my grandmother for her constant encouraging words; my uncle Garo Nercessian and his family for believing in me; Dr. Carla Garapedian for her inspiration and motivation; my dearest friends Silva Hairabedian and Mirna Sunna for their non stop moral support and advices; and finally Bedo, whose presence provided the ultimate meaning and balance to my life.

Cassia Boyadjian
Groningen, Sept. 2010

Summary

Steam cracking, the major, current existing route for light olefin production, is the most energy consuming process in the chemical industry. The need for an energy efficient processes, urged substantial research work for the development of new catalytic technologies for light olefin production.

Steam cracking maximizes ethylene formation and propylene is produced only as a secondary product. The faster increase in demand of propylene than that of ethylene makes steam cracking a less attractive route for the production of propylene. Thus, catalytic pathways that provide for more propylene formation are essential.

The present thesis investigates catalytic pathways for n-hexane cracking, as a model compound of naphtha, in the presence of oxygen. Compared to steam cracking, this work aims towards achieving; (i) lower cracking temperatures making the overall process less energy consuming and (ii) higher selectivities to both propylene and butylenes.

For the oxidative conversion of low alkanes (methane, ethane and propane) to light olefins, the design of efficient catalysts that minimize combustion and maximize olefin yields has been the bottleneck. The ideal catalyst should possess non-red-ox properties in order to minimize, in presence of oxygen, combustion reactions, and to maintain high selectivity to olefins. The catalyst studied here is the sol-gel synthesized Li/MgO. Chapter one explores the performance of this catalyst for the oxidative cracking of n-hexane. Li/MgO has no formal red-ox character and together with its inherent strong Bronsted basicity, minimizes re-adsorption and sequential combustion of formed olefins. Therefore, the catalyst has shown to be promising for the oxidative conversion of low alkanes (ethane, propane and butane) with ~60 mol% selectivity to light olefins ($C_2^=$ -$C_3^=$).

In the oxidative cracking of n-hexane, Li/MgO shows a similar behavior as in oxidative dehydrogenation of ethane, propane and butane; *i.e.,* heterogeneously initiated homogeneous reaction. However, as hexane is more active than C_2-C_4 alkanes, consequently it is possible to operate at lower reaction temperatures (575 ^oC). Due to the low oxidation activity of Li/MgO limited hexane conversions (28 mol%), however excellent selectivities to C_2-C_4 olefins (60 mol%) are observed. Selectivities obtained are similar to those achieved during oxidative conversion of C_2-C_4 alkanes. Moreover, in agreement with the non-red-ox characteristics of Li/MgO, olefin selectivities which are invariant with hexane conversions are observed.

Studies of the influence of oxygen concentrations in chapter one, demonstrate that oxygen in the feed plays a significant role in (i) regenerating the active sites, (ii) accelerating the radical chemistry, and (iii) inhibiting coke formation.

Despite of its promising performance for the oxidative cracking of n-hexane, the sol-gel synthesized Li/MgO catalyst suffers from the following two drawbacks. Firstly, the catalyst undergoes sintering when exposed to high temperature treatments (> 500 ^oC). Unlike the conventional impregnation route, the sol-gel synthesis route allows the incorporation of Li into MgO lattice at milder temperatures (500 ^oC). This results in high surface area catalyst

and enhanced [Li^+O^-] active sites. However, even with this preparation route, not complete incorporation of Li is achieved. Un-incorporated Li stays as Li_2O which through interaction with ambient CO_2 forms Li_2CO_3. Li_2CO_3 makes the catalyst susceptible for sintering when exposed to high temperature treatment.

A second drawback of the Li/MgO catalyst is that during oxidative cracking reaction, it undergoes partial deactivation due to the poisoning of the [Li^+O^-] active sites by product CO_2.

Chapter two, thus, further investigates catalyst improvement. Promotion of Li/MgO with Mo results in significant improvements in both surface area and stability of the catalyst. It is established, that minimum loadings of Mo (~0.3wt%) is sufficient to (i) reduce the amount of Li_2CO_3 originally present in Li/MgO, thus promoting the catalyst to maintain higher surface area upon high temperature treatment, and (ii) prevent the poisoning of the [Li^+O^-] by product CO_2 during reaction, hence improving stability of the catalyst. Increase in Mo loadings above 0.3 wt%, however, affects both catalyst activity and selectivity negatively.

Further in chapter three, the chemical structure of the different molybdena species is identified and their presence is correlated to the high surface area and stability, as well as the activity and selectivity of the Mo promoted catalysts. Characterization with Raman spectroscopy shows that (i) amorphous lithium molybdate species enhance catalyst stability by hindering Li_2CO_3 formation from catalytically active [Li^+O^-] sites during oxidative cracking reaction, and (ii) formation of lithium molybdates (Li_2MoO_4, $Li_2Mo_4O_{13}$) from reaction of MoO_3 with Li_2CO_3, reduce the amount of Li_2CO_3 originally present in the catalyst, thus prevent sintering when exposed to high temperatures. At the high Mo loadings, however, the formation of the dispersed phases is enhanced, leading to poor activity and selectivity.

It is agreed generally for the oxidative conversion reactions, that C-H bond splitting in the alkane is the rate limiting step. Even in the presence of strong H• abstractor, high temperatures ≥550 ^oC are still required to induce this step. The use of plasma, however, is an alternative way to achieve C-H and C-C bond activation at lower temperatures. Thus, in an attempt to enhance C-H and C-C bond cleavage in n-hexane, catalytic oxidative cracking in the presence of plasma is studied in chapter four. Plasma introduces additional pathways for hexane and oxygen activation *via* electron impact excitations. Combination of plasma and Li/MgO results in a synergistic effect, hence significantly higher C_2-C_5 olefin yields (35 mol%) than those achieved with plasma in the absence of catalyst (15 mol%) or with catalyst in the absence of plasma (19 mol%). Temperature has clear influence on the performance of the integrated plasma-Li/MgO system. At 500 ^oC, plasma chemistry is dominant leading to significant formation of acetylene (17 mol%) and ethylene (32 mol%) and low formation of the high olefins ($C_3^=$-$C_5^=$ =11 mol%). At the higher temperature (600 ^oC), however, contribution of the catalyst both in hexane activation and olefin formation becomes significant leading to more formation of C_3-C_5 olefins (38 mol%) than ethylene (26 mol%).

Finally, a technical and economical feasibility study of the catalytic oxidative cracking, as an alternative process to steam cracking, is presented in chapter five. The key differences between both processes are established. Catalytic oxidative cracking operates at lower temperatures (575 ^oC) than steam cracking (800 ^oC). Oxygen in the feed allows for an autothermal operation where part of the heat of reaction is provided *in situ* from combustion of part of the feed, thus reducing the external fuel combustion. The presence of the Li/MgO catalyst controls the olefin distribution increasing the ratio of ($C_4^=$ +$C_3^=$)/$C_2^=$. In comparison to steam cracking, catalytic oxidative cracking process is more energy efficient and consumes 53% less of total duty.

However, a preliminary economical evaluation illustrates that oxidative cracking still can not compete with the steam cracking process. This is due to carbon loss in the former, as result of combustion of part of the valuable naphtha feed. It is established that the profitability of the catalytic oxidative cracking process is highly dependent on the design of more selective catalysts as well as optimal reactors.

Samenvatting

Kraken met behulp van stoom, de huidige route voor de productie van lichte olefinen, is het meest energie consumerende proces binnen de chemische industrie. De behoefte aan energie efficiënte processen lag ten grondslag aan de ontwikkeling van nieuwe katalytische technologieën voor lichte olefinen productie.

Kraken met behulp van stoom maximaliseert de ethyleen productie en propyleen wordt alleen als secundair product geproduceerd. De snelle toename in vraag naar propyleen ten opzichte van ethyleen maakt kraken met behulp van stoom een minder aantrekkelijke route voor propyleen productie. Om deze reden zijn katalytische routes die meer propyleen productie opleveren essentieel.

Voor deze thesis werden katalytische reactie routes onderzocht voor het kraken van n-hexaan, die dienen als model samenstelling voor nafta, in de aanwezigheid van zuurstof. Vergeleken met kraken met behulp van stoom, spitst dit werk zich toe op het bereiken van; (i) lagere kraak temperaturen die het gehele proces minder energie consumerend maken en (ii) hogere selectiviteit voor propyleen en butyleen.

Het ontwikkelen van efficiënte katalysatoren die verbranding minimaliseren en olefine opbrengst maximaliseren, is altijd problematisch geweest. Deze katalysatoren zijn nodig voor de oxidatieve conversie van lichte alkanen (methaan, ethaan en propaan) naar lichte olefinen.

De ideale katalysator zou non-red-ox eigenschappen moeten bezitten om, in aanwezigheid van zuurstof, verbrandings reacties te minimaliseren en hoge selectiviteit voor olefinen te behouden. De bestudeerde katalysator voor deze thesis is de sol-gel gesynthetiseerde Li/MgO. Li/MgO heeft geen red-ox karakter en samen met zijn inherente Bronsted basiciteit, minimaliseert de katalysator re-absorptie en verbranding van de gevormde olefinen. Om deze reden heeft de katalysator veelbelovende eigenschappen laten zien voor de oxidatieve omzetting van lichte alkanen (ethaan, methaan en butaan) met ~60mol% selectiviteit voor lichte olefinen ($C_2^=$-$C_3^=$). Hoofdstuk een onderzoekt de werking van deze katalysator voor het oxidatieve kraken van n-hexaan.

Li/MgO vertoont vergelijkbaar gedrag tijdens het oxidatieve kraken van n-hexaan als in de oxidatieve dehydrogenering van ethaan, propaan en butaan; bv., heterogeen geïnitieerde homogene reacties. Echter, hexaan is actiever dan C_2-C_4 alkanen wat resulteert in de mogelijkheid om lagere reactie temperaturen (575 ^oC) te gebruiken. De lage oxidatieve activiteit van Li/MgO leidt tot beperkte hexaan conversies (28 mol%), maar goede selectiviteit voor C_2-C_4 olefinen (60 mol%). De verkregen selectiviteit(en) zijn vergelijkbaar met die van oxidatieve omzetting van C_2-C_4 alkanen. Bovendien is er hogere olefine selectiviteit waargenomen die onafhankelijk zijn met hexaan conversies. Dit is in overeenkomst met de non-red-ox karakteristieken van Li/MgO.

Onderzoek naar de invloed van zuurstof concentraties in hoofdstuk een, demonstreert dat zuurstof in de toevoer, een significante rol speelt in (i) regeneratie van de actieve sites, (ii) acceleratie van radicaal chemie, en (iii) remming van coke formatie.

Ondanks de veelbelovende prestatie voor het oxidatief kraken van n-hexaan, heeft de sol-gel gesynthetiseerde Li/MgO katalysator twee nadelen. Ten eerste ondergaat de katalysator sintering als deze wordt blootgesteld aan behandeling bij hoge temperaturen (>500 ^{o}C). In tegenstelling tot de conventionele impregnatie route, maakt de sol-gel synthese route incorporatie van Li in het MgO netwerk mogelijk bij milde temperaturen (500 ^{o}C). Dit resulteert in een groter reactie oppervlak van de katalysator en versterkte [$Li^{+}O$] reactie sites. Echter, zelfs met deze productie route is er geen complete incorporatie van Li bereikt. Niet ingebouwd Li blijft als Li_2O aanwezig en zal Li_2CO_3 vormen door interacties met omringend CO_2. Li_2CO_3 maakt de katalysator ontvankelijk voor sintering zodra deze wordt blootgesteld aan behandeling met hoge temperaturen.

Een tweede nadeel van de Li/MgO katalysator is partiële deactivatie tijdens de oxidatieve kraak reacties. Dit is te wijten aan het vergiftigen van de [$Li^{+}O^{-}$] actieve sites door het ontstane product CO_2.

Om deze reden zal hoofdstuk twee het onderzoek naar verbeteringen voor de katalysator beschrijven. Het bevorderen van Li/MgO met Mo resulteert in significante verbeteringen op het gebied van reactie oppervlak en stabiliteit van de katalysator. Het is vastgesteld dat minimale Mo lading (0.3 wt%) genoeg is voor (i) het terugbrengen van de Li_2CO_3 hoeveelheid die oorspronkelijk aanwezig is in Li/MgO en hierdoor de katalysator aanzet tot het behouden van een groter reactie oppervlak bij hoge temperatuur behandeling en (ii) Mo voorkomt CO_2 vergiftiging van de [$Li^{+}O^{-}$] tijdens de reactie en verbetert daardoor de stabiliteit van de katalysator. Toename in Mo belading boven 0.3 wt% heeft een negatieve invloed op zowel de activiteit als de selectiviteit van de katalysator.

Verder wordt in hoofdstuk drie de chemische structuur van de verschillende geïdentificeerde molybdeen soorten beschreven. Deze aanwezigheid is gecorreleerd aan het grote reactie oppervlak en stabiliteit en eveneens aan de activiteit en selectiviteit van de Mo bevattende katalysator. Karakterisatie met behulp van Raman spectroscopie toont aan dat (i) amorfe lithium molybdaat soorten de stabiliteit van de katalysator versterken door de formatie van Li_2CO_3 op katalytisch actieve [$Li^{+}O^{-}$] sites, tijdens de oxidatieve kraak reactie, te verhinderen en (ii) de formatie van lithium molybdates (Li_2MoO_4, $Li_2Mo_4O_{13}$) uit de reactie van MoO_3 met Li_2CO_3 verlaagt de hoeveelheid Li_2CO_3 dat oorspronkelijk in de katalysator aanwezig is resulterend in voorkoming van sintering zodra de katalysator wordt blootgesteld aan hoge temperaturen. Bij te hoge Mo lading/toevoeging wordt de formatie van verscheidene fasen versterkt resulterend in zwakke activiteit en selectiviteit.

Het is algemeen bekend dat het splitsen van de C-H binding in het alkaan, de beperkende stap is voor de oxidatieve omzettings reactie. Zelfs in aanwezigheid van een sterkte H abstractor, zijn er nog steeds hoge temperaturen (≥ 550 ^{o}C) vereist om deze stap te induceren. Echter, het gebruik van plasma is een alternatieve manier om C-H en C-C bindingen te activeren bij lagere temperaturen. Zodoende is de ondernomen poging om het verbreken van C-H en C-C bindingen te versterken in n-hexaan, door middel van katalytisch oxidatieve kraking in aanwezigheid van plasma, beschreven in hoofdstuk vier. Plasma introduceert supplementaire reactiewegen voor de activering van hexaan en zuurstof via electron impact excitaties. De combinatie van plasma en Li/MgO resulteert in een synergetisch effect, leidende tot significant hogere C_2-C_5 olefine opbrengst (35 mol%) dan die bereikt met plasma in afwezigheid van de katalysator (15 mol%) of met de katalysator in afwezigheid van plasma (19 mol%). Temperatuur heeft duidelijk invloed op het functioneren van het geïntegreerde plasma-Li/MgO systeem. Bij 500 ^{o}C zal de plasma chemie zorgen voor significante formatie van acetyleen (17 mol%) en ethyleen (32 mol%) en weinig formatie van de lichte olefinen ($C_3^{=}$-$C_5^{=}$ = 11 mol%). Bij de hogere temperatuur (600 ^{o}C) zal de contributie

van de katalysator in zowel hexaan activatie en olefine productie significant worden, wat resulteert in hogere C_3-C_5 olefinen formatie (38 mol%) ten opzichte van ethyleen (26 mol%).

Ter afsluiting wordt een technisch en economisch haalbaarheids studie naar de katalytische oxidatieve kraking als alternatief voor kraken met behulp van stoom, besproken in hoofdstuk vijf. De belangrijkste verschillen tussen beide processen zijn vastgesteld. Katalytisch oxidatieve kraking vindt plaats bij lagere temperaturen (575 ^{o}C) dan kraken met behulp van stoom (800 ^{o}C). De toevoer van zuurstof zorgt voor een autothermische operatie waardoor een deel van de reactiewarmte *in situ* verkregen wordt door verbranding van een deel van de voeding. Dit leidt tot een lagere verbranding van de externe brandstof. De aanwezigheid van de Li/MgO katalysator controleert de olefine distributie waardoor de ratio van ($C_4^{=}$ +$C_3^{=}$)/$C_2^{=}$ toeneemt. Vergeleken met kraken met behulp van stoom, is het katalytisch oxidatieve kraak proces energetisch efficiënter en consumeert het 53% minder energie.

Niettemin illustreert een voortijdige economische evaluatie dat oxidatieve kraking nog steeds niet kan concurreren met het kraken met stoom. Dit is te wijten aan koolstof verlies in de laatst genoemde als resultaat van de verbranding van een deel van de waardevolle nafta voeding. Het is vastgesteld dat de winstgevendheid van het katalytische oxidatieve kraking proces sterk afhankelijk is van het ontwerp van meer selectieve katalysatoren en het ontwerp van optimale reactoren.

Contents

Introduction

Light olefins are the building blocks for the petrochemical industry. In a rapidly growing world with continuous development in the production of new synthetic materials, the demand of these petrochemicals is increasing tremendously. Propylene and butylene yields from current production technologies (steam cracking, fluidized catalytic cracking (FCC), oxidative dehydrogenation (ODH)) are insufficient to satisfy these growing demands, urging interest in alternative processes for light olefin production.

1 Current technologies for olefin production

Petrochemistry is the core of the modern material technology. Light olefins (ethylene, propylene, butylenes) are the building blocks for the petrochemical industry, thus the basis for a broad range of consumables. The worldwide demand and production of olefins are higher than any other chemical. The current production for ethylene and propylene in Western Europe are around 19 and 14 mln tonnes, respectively [1]. About 60% of the demand is devoted to the manufacture of polymers; *e.g.*, poly-ethylene and poly-propylene, and the remaining 40% is converted to chemical intermediates such as ethylene and propylene oxides, vinylchloride as well as acrylonitrile and acrylic acid [2]. Butylenes in addition to synthesis of poly-butylenes, are commonly used for the synthesis of fuels, such as gasoline by butylene/butane alkylation.

In a rapidly growing world with continuous development in the production of new synthetic materials, the demand of these petrochemicals is increasing tremendously. Figure 1 shows a vast increase in production of both ethylene and propylene in Western Europe (the strong decline in production observed for 2008 is the result of the economic crisis) [1].

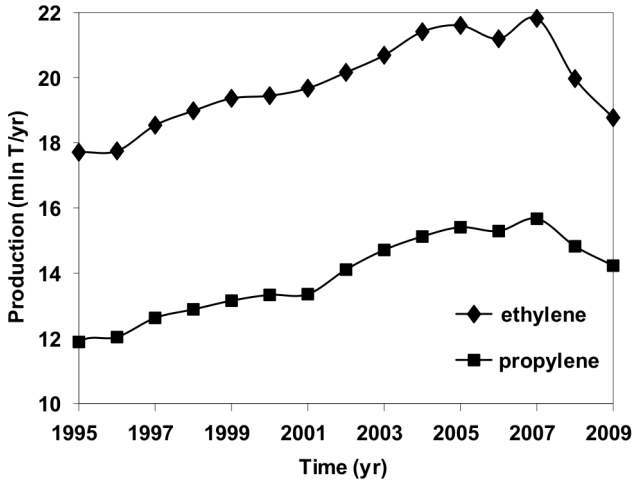

Figure 1. Production rates of both ethylene and propylene in Western Europe [1].

Although propylene demand in Europe is expected to grow slowly, global demand for propylene will grow from 69 mln tonnes in 2006 to 88 mln tonnes in 2011 at an average rate of about 5% [3]. This is faster than growth rates in demand of ethylene. Global ethylene demand is expected to grow from 110 mln tonnes in 2006 to 137 mln tonnes by 2011 at an average rate of 4.3% per year [3]. The demand of butylene is expected to grow annually by 1.3% [2].

Propylene and butylene yields from current production technologies are unlikely to be able to satisfy these demands. These olefins are currently produced from steam cracking of naphtha and from fluidized catalytic cracking (FCC) units [4]. Although these two routes are well developed, increasing the capacity of these processes is only possible to some extent.

Steam cracking of naphtha, although the major route for the production of light olefins, is becoming less attractive both environmentally and economically. It is a strongly endothermic process requiring substantial external heat input, accompanied with large amount of CO_2 emissions. During steam cracking, a hydrocarbon feedstock (naphtha) in presence of steam is decomposed to light olefins at high temperatures of 700–900 ^oC [4]. Steam cracking follows a radical chemistry route, the carbon radicals (primary or secondary) formed initially via C-H bond cleavage result in smaller primary radicals after subsequent β-cleavage. Every further β-cleavage of the primary radicals formed results in C_2 product. Steam cracking therefore maximizes ethylene yields, and both propylene and butylenes are formed at smaller levels. The greater increase in the demand of propylene as compared to ethylene, makes steam cracking less attractive route for the production of propylene.

Dehydrogenation of alkanes to olefins is conceptually a promising route for light olefin production. Alkanes are cheap feedstock as compared to crude oil, and through this reaction route (eq. 1) they are converted to olefins with the same carbon number.

$$C_3H_8 \leftrightarrow C_3H_6 + H_2 \quad \Delta H = 117 \text{ kJ. mol}^{-1} \qquad (1)$$

Catalytic dehydrogenation processes, were developed in the early 80's for light olefin production. However, commercially, these processes have made only limited breakthrough. The bottleneck of this route is the thermodynamic equilibrium leading to limited yields, and the strong tendency to coking and consequently catalyst deactivation, resulting in short life times of the catalyst [5-9]. The existing processes for the dehydrogenation of light paraffins such as Oleflex (UOP, Pt/Al_2O_3 catalyst) [6], Catofin (ABB and Lummus Crest, Cr catalyst) [7], STAR (Phillips Petroleum Company, Pt based catalyst) [8], and FDB-4 (Snamprogetti-Yarsintez, Chromium oxide) [9] typically include catalyst regeneration (*i.e.*, carbon burn-off) in combination with heat integration.

Continuously increasing global demand for light olefins has, therefore, spurred substantial interest in the development of alternative routes for light olefin production.

2 Alternative routes for light olefin production

2.1 Oxidative catalytic dehydrogenation of lower alkanes to olefins

Oxidative catalytic dehydrogenation of alkanes to olefins has been identified as a promising route to olefins. This is achieved via selective combustion of the hydrogen formed in the conversion of alkanes to olefins (eq. 2) [10].

$$C_3H_8 + ½\ O_2 \rightarrow C_3H_8 + H_2O \quad \Delta H = -126 \text{ kJ.mol}^{-1} \qquad (2)$$

The major advantages of oxidative dehydrogenation over conventional dehydrogenation is that it; (i) overcomes the thermodynamic equilibrium limitations in the

direct catalytic dehydrogenation process, (ii) minimizes the coke formation and the related catalyst deactivation due to the presence of oxygen and (iii) minimizes the external heat input, as the reaction in presence of oxygen is exothermic and can be run adiabatically and at lower temperatures [10-11]. Oxidative dehydrogenation of alkanes to olefins is still at a developmental stage and no commercial process is operative at the moment. Olefins are highly active and tend to further oxidize via the catalyst to CO_x. Development of catalysts that minimize combustion and maximize olefin yields is still the bottleneck [12]. Basically two categories of catalysts have been reported; (i) transition metal oxide catalysts with red-ox properties, and (ii) alkali and alkaline earth oxide catalysts with non red-ox properties.

2.1.1 Oxidative conversion of alkanes to olefins over oxide catalysts with red-ox properties

Conventional transition metal oxides with pronounced red-ox properties such as supported vanadia and molybdena were mostly attempted in literature for the oxidative dehydrogenation of alkanes [13-17]. These oxides operate via a Mars and van Krevelen 'red-ox' type mechanism where lattice oxygen promotes homolytic C-H bond abstraction from the alkane, creating alkyl radicals [14]. Further, the alkyl radicals undergo subsequent homogeneous radical chain reactions in gas phase. The hydroxyls formed on catalyst surface are then released to the gas phase as water, reducing the catalyst. Re-oxidation of the catalyst by gas phase oxygen completes the catalytic cycle and regenerates the catalyst. Alternatively, the lattice oxygen also takes part in combustion reactions. Strong olefin adsorption and subsequent oxidation to carbon oxides, especially at high alkane conversions, usually limit the yields of olefins over these catalysts. This behavior is typical for almost all the catalysts studied (see Figure 2) [15].

Cavani and Trifiro [13], in their review on oxidative dehydrogenation of ethane and propane, reported that maximum olefins yields achieved with these oxidic catalysts were below 30 mol%. These yields were too low and insufficient for commercialization. Modification of transition metal oxides with alkaline metals such as Li, Na and K, however, suppresses the CO_x formation and increases olefin selectivity [11, 18]. Lemonidou *et al*. [18] reported that for the oxidative dehydrogenation of propane, promotion of V/Al_2O_3 with Li improved selectivity to propylene from 29 mol% to 50 mol%.

In oxidative dehydrogenation reaction, therefore, the critical issue for catalyst development is to minimize olefin sorption and its further oxidation.

2.1.2 Oxidative conversion of alkanes to olefins over oxide catalysts with no formal "red-ox" properties

Recent studies on oxidic catalysts with no formal 'red-ox' properties have shown tremendous improvement in olefin yields. Basic alkali and alkaline earth oxides have been attempted as catalysts for the oxidative coupling of methane to ethylene [19-20] and the oxidative dehydrogenation of ethane to ethylene [21]. One of the most studied catalysts is the Li/MgO [21-34].

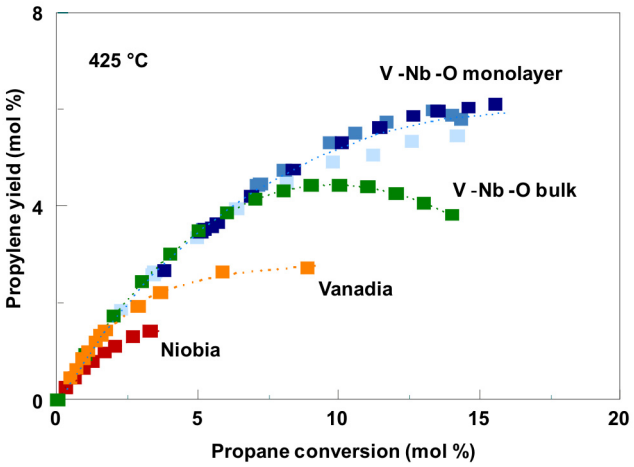

Figure 2. Conversion yield plots for a series of vanadia based catalysts at 425 ^{o}C [15].

It has been established through the work of Lunsford [23-27], on the oxidative coupling of methane, that [O^-] species in Li/MgO are responsible for catalytic activity. The existence of these species in MgO was mainly characterized using the electron paramagnetic resonance (EPR) technique [24-25]. Remarkably, [O^-] are reported to be very stable at high temperatures and can exist in the crystal lattice of oxides even in the absence of oxygen in the gas phase [28]. It has been suggested that the similar ionic radii of Li^+ (r_{Li+}=0.76 Å) and Mg^{2+} (r_{Mg2+}=0.72 Å) allows easy accommodation of Li^+ in the lattice of MgO [29]. Replacement of Mg^{2+} by Li^+ creates lattice defects, *i.e.*, oxygen vacancies (positive holes) (see scheme below). The proposed active site [Li^+O^-] is produced by a hole adjacent to a Li+ site trapping an oxygen atom [30-31].

$$2\ LiMg'\ O_O^x + V_O^{\cdot\cdot} + \tfrac{1}{2}O_2 \rightarrow 2\ LiMg'\ O_o^{\bullet} + O_O^x$$

Scheme 1. Proposed mode of formation of the [Li^+O^-] (LiMg' O_O•) active site in Li/MgO catalysts. A hole trapped at the O_2^- (O_O^x) is adjacent to Li+ sites (LiMg'). The Kroger-Vink notation has been used [30-31].

Unlike Li/MgO catalyst prepared by impregnation, recently used sol gel methods result in high surface area catalyst. The advantage of this method over the impregnation preparation route is that it allows the incorporation of Li in the magnesia under milder conditions (during sol-gel transformation); thus avoiding the need to calcine the catalyst at very high temperatures (causing sintering and loss of surface area) [32-33] for achieving Li incorporation. Thus, in the sol-gel synthesized Li/MgO, enhanced concentration of [Li^+O^-] defect sites lead to improved catalyst activity and selectivity (Figures 3&4) [32-33]. As Li/MgO catalyst has no formal red-ox properties, during oxidative conversion of propane both sol-gel and impregnated catalysts showed olefin selectivities which are almost independent of conversion (Figure 4).

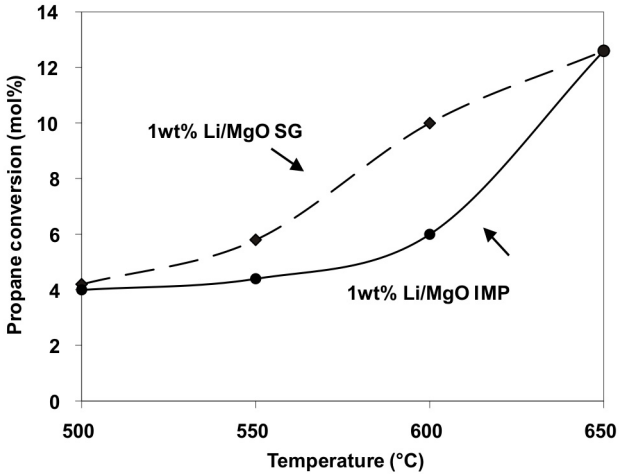

Figure 3. Conversion of propane as function of temperature over 1wt%Li/MgO obtained by sol-gel method and conventional impregnation. Reaction conditions: 10% propane, 8% oxygen, 2% CO_2 and 78% helium. GHSV = 120000h^{-1} [32].

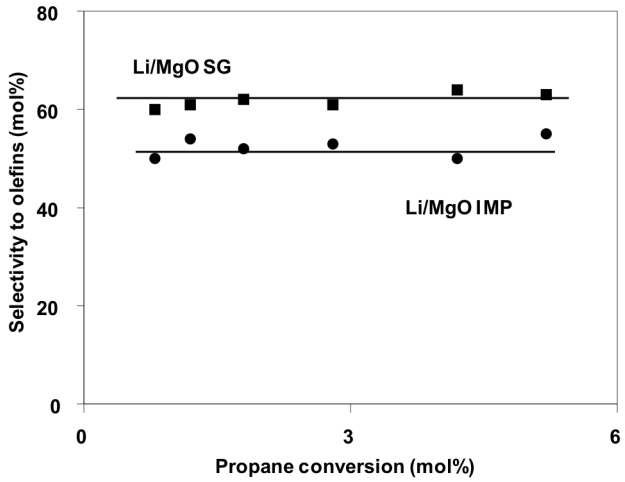

Figure 4. Selectivity to olefins as function of propane conversion for 1wt%Li/MgO catalyst obtained by sol-gel method and conventional impregnation. Reaction conditions: 10% propane, 8% oxygen and balance helium. T=550 ^{o}C. Different conversions achieved by varying GHSV [32].

Extensive work from the groups of Lunsford *et al*., Ross *et al*., and Seshan *et al*., have shown, in the case of Li/MgO catalysts, that the first step in the oxidative conversion of alkanes involves the homolytic scission of C-H bonds forming surface -OH groups and alkyl radicals (eq. 3) [20, 23-25]:

$$[O^-]_{(s)} + C_nH_{2n+2} \rightarrow [OH^-]_{(s)} + C_nH_{2n+1}\bullet \qquad (3)$$

The resulting radicals are released from the catalyst surface and subsequently initiate gas-phase chain propagation reactions to yield products [22]. Thus alkane to olefin conversion on this catalyst involves a route of heterogeneously-initiated homogeneous reactions. Burch and Crabb [34] showed that combination of heterogeneous (catalytic) and homogeneous (gas phase) reactions is necessary to obtain commercially acceptable yields of propene.

Oxygen in the gas phase plays a significant role in the regeneration of the catalyst by removing hydrogen from the surface [Li^+OH^-] species formed during the activation of the alkane. The regeneration reactions as proposed by Sinev [35] are summarized as:

$$O_2 + [OH\text{-}] \rightarrow [O^-] + HOO\bullet \quad (4)$$

$$HOO\bullet + [OH^-] \rightarrow [O^-] + H_2O_2 \quad (5)$$

$$H_2O_2 \rightarrow 2\bullet OH \quad (6)$$

$$\bullet OH + [OH^-] \rightarrow [O^-] + H_2O \quad (7)$$

However, a drawback of the Li/MgO catalyst is that the [Li^+O^-] active sites of the catalyst are susceptible for deactivation during reaction upon interaction with product CO_2. This poisoning effect of CO_2 on [Li^+O^-] active sites has been reported by Lunsford *et al*., Ross *et al*. and Seshan *et al*. [36-38] for the oxidative conversion of C_1-C_3 alkanes. During the oxidative coupling of methane, Lunsford *et al*. [37] reported that reaction of product CO_2 with [Li^+O^-] results in formation of $Li^+CO_3^-$ which is converted with time into the more stable Li_2CO_3. In situ FTIR spectra of Li/MgO during the oxidative coupling of methane indicated the presence of adsorbed CO_2 on the [O^-] sites ($O^-.CO_2$) in addition to the presence of stable Li_2CO_3 phase [38]. Similar observations were also made by Galuszka [39].

2.2 Oxidative conversion of alkanes at ambient conditions using cold plasma

Even in the presence of a strong hydrogen radical [H●] abstractor such as [Li^+O^-], C-H, C-C bond scission during the oxidative conversion of alkanes [13] requires high temperatures (T > 550 ^oC). To further facilitate radical generation at lower reaction temperatures, the development of more active catalysts is necessary.

The use of cold plasma, however, is an alternative way to achieve C-H and C-C bond activation at ambient temperatures. Plasma generated between two parallel electrodes by di-electric barrier discharge (DBD) consists of energetic electrons [40-41]. These electrons can activate hydrocarbon molecules, as a result of electron impact excitations. Ions and radicals are thus formed at much lower temperatures than in catalytic processes [41-42]. Recently we [43-44] reported on the oxidative dehydrogenation of propane, ethane and methane at ambient conditions in plasma micro reactor both in presence and absence of Li/MgO catalyst. The low reaction temperatures used in this system, favored the coupling of C-C bonds, hence products with higher carbon number than the reactant were observed as major products. In the plasma micro reactor, plasma induced propane activation as result of electron impact collisions (eq. 8).

$$C_3H_8 + e^- \rightarrow C_3H_7\bullet + H\bullet + e^- \quad (8)$$

Higher propane conversions were observed in the presence of oxygen and plasma. The electron impact dissociation of molecular oxygen yielding atomic oxygen in the ground $O(^3P)$ and excited $O(^3D)$ states has been reported in literature and is described in reaction equations 9 and 10 [45].

$$O_2 + e^- \rightarrow 2O(^3P) + e^- \quad (9)$$

$$O_2 + e^- \rightarrow O(^3P) + O(^1D) + e^- \quad (10)$$

The $O(^3P)$ species, present in the gas phase, are reported to cause C-H bond scission in alkanes *e.g.*, methane [46], ethane [47]. Similarly, in the case of propane this resulted in the formation of propyl and hydroxyl radicals as shown below:

$$O(^3P) + C_3H_8 \rightarrow [OH\bullet] + C_3H_7\bullet \quad (11)$$

In the presence of a layer of Li/MgO, the reactivity of micro-plasma towards propane was further improved (Figure 5). This was due to the larger permittivity of oxide layer (εMgO = 9.7) compared to Pyrex (ε = 4.8) [48]. The relative permittivity of a dielectric barrier can strongly determine the amount of charge that can be stored for a certain value of applied electric field [49]. The higher the number of charges transferred, the higher is the number of electron impact excitations. Hence, reactions 8 and 11 are strongly influenced by the number of charges transferred or accumulated on the dielectric surface.

Moreover, presence of Li/MgO catalyst resulted in higher selectivity to propylene than with MgO (Figure 6). Improved propylene selectivities suggest the consecutive interaction of propyl radicals generated by plasma at room temperature, with the $[Li^+O^-]$ sites of the catalyst, where the latter abstracts a second hydrogen atom from the propyl radical forming propylene. The existence of the $[Li^+O^-]$ defect sites at low temperatures has been investigated and confirmed, using EPR spectroscopy, by Lunsford and co-workers [23-27].

Alternatively, it was suggested [50-51] that the presence of plasma can also help to create new defect sites on the surface of Li/MgO. Nelson *et al*. [50] and later Knozinger *et al*. [51] reported, using EPR studies, that interaction between UV light and MgO particles can give rise to surface paramagnetic centers (trapped electrons, typically F-centers, [VO•]). Goodman *et al*. [28] suggested, during methane oxidative coupling, that these [VO•]-type defect sites are able to activate C-H bond in the alkane. Thus, the presence of [VO•]-type defect sites caused by the plasma may allow H● abstraction both from propane and propyl radicals, leading to enhanced activity and selectivity.

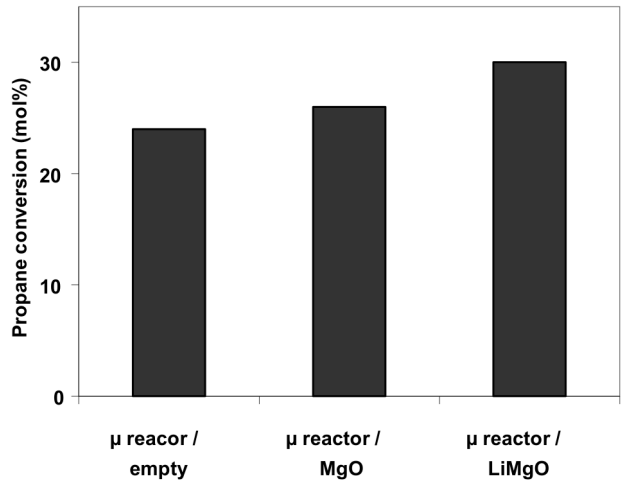

Figure 5. Propane conversion in micro reactor in the presence of plasma at RT (a) empty reactor, (b) reactor containing MgO, (c) reactor containing Li/MgO. Reaction conditions: 15ml/min of 10% propane, 1% oxygen and balance helium. 3 W plasma power was applied [41].

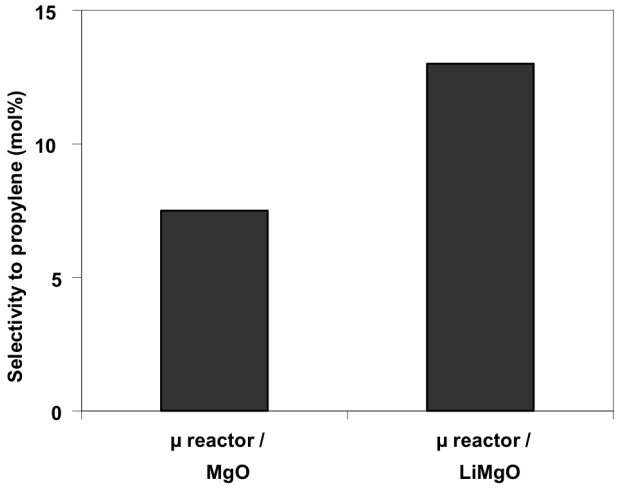

Figure 6. Selectivity to propylene for MgO and Li/MgO catalyst in a micro reactor in presence of plasma at RT. Comparison made at similar levels of propane conversion. Reaction conditions: 15ml/min of 10% propane, 1% oxygen and balance helium. 3 W plasma power was applied [41].

2.3 Oxidative catalytic cracking of naphtha

Oxidative cracking, in addition to C-H bond scission, also involves C-C bond splitting in the alkane resulting in olefins of lower carbon number than the feed. Catalytic oxidative cracking of naphtha is conceptually a potential alternative route to steam cracking for light olefin production. This alternative route aims, in the presence of both catalyst and oxygen, to: (i) lower reaction temperatures, thus minimize the energy consumption of the process, and (ii) increase olefin yields [52]. Figure 7 compares thermal cracking of n-butane to non catalyzed oxidative cracking of n-butane. Results clearly show the role of oxygen in promoting n-butane cracking and increasing yields to olefins at temperatures lower than in thermal cracking. In presence of catalyst, even higher yields of olefins are expected. Despite of numerous patents on oxidative catalytic cracking of naphtha, none of these processes have been commercialized. Research work on developing catalysts for the catalytic cracking of naphtha to light olefins started in the late 1960's. Typically two classes of catalysts have been tested for oxidative cracking; (i) basic catalysts (Li/MgO, CaO-SrO-Al_2O_3, WO_3-K_2O-Al_2O_3, KVO_3/corundum) and transition metal oxide catalysts (non-reducible Cr_2O_3/Al_2O_3, reducible V-oxides) [52].

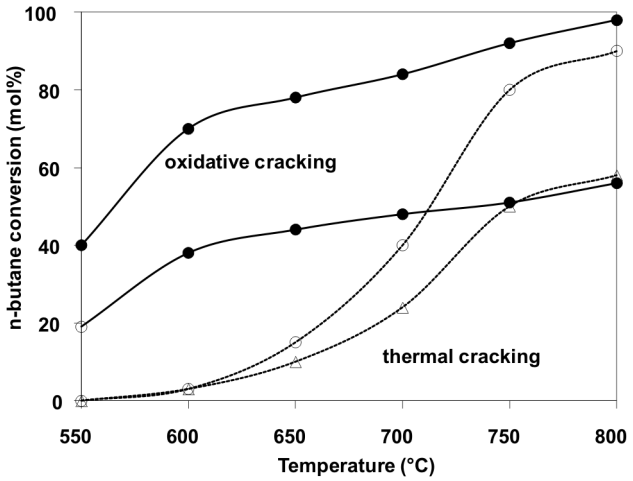

Figure 7. Effect of temperature on conversion of n-butane and yields to olefins for thermal and oxidative cracking of n-butane in an empty reactor. Oxidative cracking: conversion (●), yield of ethylene-plus-propylene (▲), thermal cracking: conversion (○), yield of ethylene-plus-propylene (Δ). Reaction conditions: n-butane/oxygen/nitrogen = 20/10/70 for oxidative cracking, and n-butane/nitrogen = 20/80 for thermal cracking. Residence time=4 s [52].

Research work in the last years elucidated that in addition to oxidative dehydrogenation of low alkanes (methane, ethane), Li/MgO is also a promising catalyst for the oxidative cracking of propane and butane [22]. The product distribution obtained during the oxidative conversion of propane over Li/MgO is given in Table 1.1. The presence of C_1-C_2 hydrocarbons in the products indicates that both C-H scission (oxidative dehydrogenation) and C-C bond splitting (oxidative cracking) occur over Li/MgO.

Table 1. Selectivity to different products observed during the oxidative dehydrogenation of propane over 1wt% Li/MgO SG catalyst. Reaction conditions: 10% propane, 8% oxygen, and balance helium, T = 550 °C. Propane conversion = 15 mol% [32].

Component	CO_x	CH_4	$C_2+C_2^=$	$C_3^=$
Selectivity (mol%)	15	10	30	45

Oxidative catalytic cracking over the basic catalysts, similar to oxidative dehydrogenation/cracking of alkanes over Li/MgO, is believed to follow a radical mechanism, initiated on the catalyst surface followed by radical chain reactions in the gas phase. During the oxidative cracking of n-butane [52], the basic metal oxides showed a significant catalytic activity, and the rare earth oxides showed both high activity and high ethylene-plus-propylene yields (Figure 8). Among the rare earth oxides tested, samarium oxide showed the highest activity and selectivity. However, non-stoichiometric rare earth oxides such as CeO_2, Pr_6O_{11} and Tb_4O_7 showed low cracking activity [52].

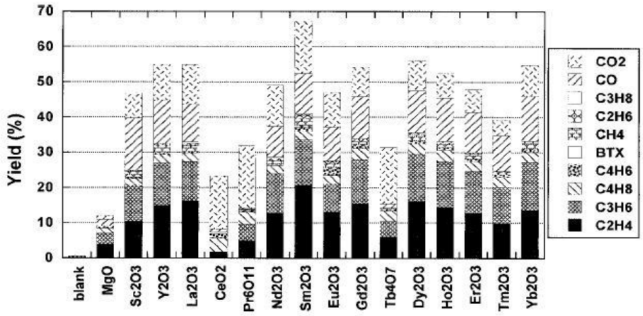

Figure 8. Oxidative cracking of n-butane over basic metal oxide catalysts. Reaction conditions: n-butane/oxygen/helium = 1.4/1.5/5.6/88.5 (ml/min NTP), W / F= 0.12 g.s/ml, T = 600 ^oC [52].

These oxides showed red-ox property, and oxygen was mostly used to form CO_x. CO_x formation was favored at a lower reaction temperature (< 600 ^oC) due to the high interaction between adsorbed radicals and active oxygen species on the catalyst surface. However, at a higher temperature (> 600 ^oC) lower selectivity to CO_x was observed mainly due to an increase in the rate of the desorption of adsorbed radical species from the catalyst surface. Modification of rare earth oxide catalysts (CeO_2, Pr_6O_{11}, Tb_4O_7) by alkali metals such as Li and K minimized the CO_x formation during oxidative cracking of n-butane (Figure 9).

The objective behind oxidative cracking over transitional metal oxides, was to promote oxidative cracking by supplying activation energy via internal combustion of part of the hydrocarbons. During the catalytic oxidative cracking of n-butane [53], at temperatures between 540-580 ^oC, MgO supported V_2O_5 exhibited high activity towards n-butane conversion. At 580 ^oC, 55 mol% selectivity to C_2-C_4 olefins was reported.

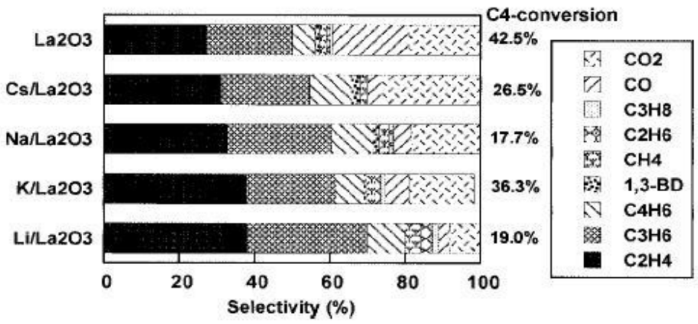

Figure 9. Changes in selectivity after modifying La_2CO_3 with alkali metals. Reaction conditions: 1.4/1.5/5.6/88.5 (ml/min NTP), molar ratio of alkali metal/La =1.0, W / F= 0.43 g.s/ml, T = 600 ^oC [52].

3 Scope and outline of the thesis

The present thesis discusses the catalytic oxidative cracking of n-hexane, as an alternative route to steam cracking for light olefin production. n-Hexane is studied as a model compound of naphtha. The objective of this thesis is to explore catalytic pathways to induce cracking of n-hexane, in the presence of oxygen, at temperatures lower than those utilized in steam cracking process, making the overall process less energy consuming. The ideal catalyst for this reaction should possess non-red-ox properties in order to minimize, in presence of oxygen, combustion reactions, and to maintain high selectivity to olefins. The catalyst studied here is the sol-gel synthesized Li/MgO. The catalyst has no red-ox properties, is basic in nature and has shown promising results for the oxidative conversion of propane. Interestingly, in addition to C-H bond scission, C-C bond cleavage in the propane has been observed as well, resulting in formation of light olefins as ethylene. These properties make the catalyst an appropriate choice for the oxidative cracking of n-hexane.

Chapter one of this thesis explores the performance of the sol-gel synthesized Li/MgO for the oxidative cracking of n-hexane. The influence of different reaction parameters; *i.e.*, temperature, O_2 concentrations in the feed are reported. Moreover, the chapter discusses catalyst stability and the effect of product CO_2 on the $[Li^+O^-]$ catalytic active sites. Further, in this chapter, in an attempt to improve catalyst performance, the effect of promotion of Li/MgO with low amounts of different red-ox oxides; *i.e.*, V_2O_5, Bi_2O_3 and MoO_3 are studied. This chapter is adapted from the following publication.

C. Boyadjian, L. Lefferts, K. Seshan, Appl. Catal. A 372 (2010) 167-174.

Despite of its promising performance for the oxidative cracking of n-hexane, the sol-gel synthesized Li/MgO catalyst suffers from the following two drawbacks; (i) the catalyst undergoes sintering when exposed to high temperature treatments (> 500 ^oC), due to Li_2CO_3 originally present in the catalyst, and (ii) during oxidative cracking reaction, catalyst undergoes deactivation due to the poisoning of the $[Li^+O^-]$ active sites by product CO_2. Chapter two addresses the positive effect introduced on both surface area and stability of Li/MgO upon promotion with Mo. Moreover, the chapter discusses kinetics and the

influence of varying Mo loading on both catalyst activity and selectivity, for the oxidative cracking of n-hexane. This chapter is adapted from the following publication.

C.Boyadjian, B. van der Veer, I. V. Babich, L. Lefferts, K. Seshan, Catal. Today, in press 2010.

Chapter three elucidates the correlation between the structural and catalytic properties of Li/MgO catalyst promoted with varying Mo loading. The physical and chemical changes induced in the catalyst when promoting with Mo are characterized with BET, XRF, XRD, XPS and Raman spectroscopy. Raman spectroscopy, a common technique for the characterization of supported molybdena systems, is used to identify the MoO_x species, as well as the solid solutions (molybdates) formed from interaction of Mo with Li/MgO system. The presence of these species/molybdates is then correlated to the high surface area and stability of the Mo promoted catalyst, as well as the activity and selectivity of the catalyst for the oxidative cracking of n-hexane. These aspects are discussed in the following manuscript.

C. Boyadjian, S. Crapanzano, I.V. Babich, B.L. Mojet, L. Lefferts, K. Seshan, J. Catal. (2010) submitted.

In an attempt to enhance C-H and C-C bond cleavage in n-hexane, catalytic oxidative cracking in the presence of plasma is investigated. Chapter four discusses the influence of plasma on both n-hexane conversions and selectivities to olefins during the oxidative conversion of n-hexane at temperatures 500 and 600 ^{o}C. In the presence of plasma, the role of surface chemistry, *i.e*., the contribution of Li/MgO catalyst in n-hexane conversion and controlling olefin distribution is discussed. This study on the integrated plasma-Li/MgO system is reported in the following manuscript.

C. Boyadjian, A. Agiral, J.G.E. Gardeniers, L. Lefferts, K. Seshan, Plasma Chem. Plasma Process. (2010) submitted.

The last chapter of the dissertation addresses the process design aspects of the oxidative catalytic cracking of n-hexane over the Li/MgO catalyst. In this chapter a technical feasibility study of the oxidative cracking of n-hexane is reported. Moreover, the technical and economical potential of the process in comparison to steam cracking is discussed. These process design aspects are discussed in the following manuscript.

C. Boyadjian, L. Lefferts, K. Seshan, A.G.J. van der Ham, H. van den Berg, Ind. Eng. Chem. Res. (2010) submitted.

References

[1] http://www.petrochemistry.net/capacity-and-production-propylene-and-derivatives.html.

[2] www.sriconsulting.com

[3]http://www.plastemart.com/upload/Literature/Global-ethylene-propylene-demand-capacity-to-change.asp

[4] T. Ren, M. Patel, K. Blok, Energy (2006) 425-451.

[5] S. Gussow, D.C. Spence, E.A. White, Oil & Gas J. 78 (49) (1980) 96-101.

[6] P.R. Cortelli, S.T. Bakas, M.F. Bentham, J.H. Gregor, C.R. Hamlin, L.F. Smith, Oleflex process – The proven route to olefins UOP, Des Plaines, III, 1992.

[7] D. Sanfilippo, Chemtech (1993) 35-41.

[8]H. Bolt, H. Zimmerman, in: M. Baerns, J. Whitelamp (Eds.), DGMK Proc, Kassel, 1993, 175-185.

[9] P.R. Sarathy, G.S. Suffridge, Hydrocarbon Processing 72 (1993) 89-92.

[10] F. Cavani, N. Ballarini, A. Cericola, Catal. Today 127 (2007) 113–131.

[11] T.C. Watling, G. Deo, K. Seshan, I.E. Wachs, J.A. Lercher, Catal. Today 28 (1-2) (1996) 139-145.

[12] L. Lefferts, K. Seshan, B. Mojet, J.G. van Ommen, Catal. Today 100 (2005) 63-69.

[13] F. Cavani and F. Trifiro, Catal. Today 24 (1995) 307-313.

[14] K.T. Nguyen, H.H. Kung, J. Catal. 122 (1990) 415-428.

[15] T.C. Watling, G. Deo, K. Seshan, I.E. Wachs and J.A. Lercher, Catal. Today, 28, (1996) 139-145.

[16] T. Iizuka, K. Ogasawara, K. Tanabe, Bull. Chem. Soc. Japan, 56 (1983) 2927-2931.

[17] M.A. Chaar, D.Patel, M.C. Kung, H.H. Kung, J. Catal., 109 (1988) 463-467.

[18] A.A. Lemonidou, L. Nalbandian, I.A. Vasalos, Cat. Today 61 (2000) 333-341.

[19] C.-H. Lin, K.D. Campbell, J.-X. Wang, J.H. Lunsford, J. Phys. Chem. 90 (4) (1986) 534-537.

[20] M. Baerns, J.R.H. Ross "Perspectives in Catalysis" J.M. Thomas, K.I Zamarev (eds) Blackwell, Oxford, (1992) 315.

[21] H.M. Swaan, A. Toebes, K. Seshan, L.G. van Ommen and J.R.H. Ross, Catal. Today 13 (1992) 201-208.

[22] L.Leveles, K. Seshan, J.A. Lercher, L. Lefferts, Catal., 218 (2003) 296-306.

[23] T. Ito, J.-X. Wang, C.-H. Lin, J.H. Lunsford, J. Am. Chem. Soc.107 (1985) 5062-5068.

[24] J. X. Wang, J. H. Lunsford, J. Phys. Chem. 90 (1986) 5883-5887.

[25] J.H. Lunsford, Langmuir 5 (1989) 12-16.

[26] E. Morales, J.H. Lunsford, J. Catal. 118 (1989) 255-265.

[27] K.-I. Aika, J.H. Lunsford, J. Phys. Chem. 82 (16) (1978) 1794-1800.

[28] M.C. Wu, C.M. Truong, K. Coulter, D. W. Goodman, J. Catal. 140 (2) (1993) 344-352.

[29] T. Berger, J. Schuh, M. Sterrer, O. Diwald, E. Knozinger, J. Catal., 247 (2007) 61-67.

[30] P. J. Gellings, H. J. M. Bouwmeester, Catal. Today 58 (2000) 1-153.

[31]C.R.A. Catlow, R. A. Jackson, J. M. Thomas, J. Phys. Chem. 94 (1990) 7889-7893.

[32] C. Trionfetti, I.V Babich, K. Seshan, L. Lefferts, Appl. Catal. A 310 (2006) 105-113.

[33] C. Trionfetti, I.V Babich, K. Seshan, L. Lefferts, Langmuir 24 (2008) 8220-8228.

[34] R. Burch, E. Crabb, Appl. Catal. A 100 (1993) 111-130.

[35] M.Y. Sinev, V.Y. Bychkov, Kinet. Katal. 34 (2) (1993) 309-313.

[36] S. Fuchs, L. Leveles, K. Seshan, L. Lefferts, A. Lemonidou, J.A Lercher, Top. Catal.15 (2-4) (2001) 169-174.

[37] M. Xu, C. Shi, X. Yang, M.P. Rosynek, J.H. Lunsford, J. Phys. Chem. 96 (15) (1992) 6395-6398.

[38] S.C. Bhumkar, L. L. Lobban, Ind. Eng. Chem. Res. 31 (1992) 1856-1864.

[39] J. Galuszka, Catal. Today 21 (1994) 321-331.

[40] U. Kogelschatz, Plasma Chem. and Plasma Proc. 23 (1) (2003) 1-46.

[41] A. Agiral, C. Trionfetti, L. Lefferts, K. Seshan, J.G.E. Gardeniers, Chem. Eng. Tech. 31 (8) (2008) 1116–1123.

[42] H. Kim, Plasma Proc. Polym 1 (2004) 91-110.

[43] C. Trionfetti, A. Agiral, ChemPhysChem. 9 (4) (2008) 533-537.

[44] C. Trionfetti, A. Agiral, J. Phys. Chem. 112 (11) (2008) 4267-4274.

[45] S.V. Kudryashov, G.S. Shchegoleva, E.E. Sirotkina, A.Yu. Ryabov, High Energy Chem. 34 (2) (2000) 112-115.

[46] T. Nozaki, A. Hattori, K. Okazaki, Catal. Today 98 (2004) 607-616.

[47] X. Zhang, A. Zhu, X. Li, W. Gong, Catal. Today 89 (2004) 97-102.

[48]http://clippercontrols.com/pages/dielectric-values.

[49] X. Xu, Thin Solid Films 390 (1-2) (2001) 237-242.

[50] R.L. Nelson, A.J. Tench, J. Chem. Phys. 40 (9) (1964) 2736-2737.

[51] M. Sterrer, O. Diwald, E. Knozinger, P.V. Sushko, A.L. Shluger, J. Phys. Chem. B 106 (2002)12478-12482.

[52] Y. Yoshimura, N. Kijima, T. Hayakawa, K. Murata, K. Suzuki, F. Mizukami, K. Matano, T. Konishi, T. Oikawa, M. Saito, T. Shiojima, K. Shiozawa, K. Wakui, G. Sawada, K. Sato, S. Matsuo, N. Yamaoka, Catal. Surv. Jpn. 4 (2) (2000) 157-167.

[53] A.A. Lemonidou, A.E. Stambouli, Appl. Cat. A 171 (1998) 325-332.

Chapter 1

Catalytic Oxidative Cracking of n-Hexane as a Route to Olefins

Catalytic oxidative cracking of naphtha is conceptually an alternative process to steam cracking. The performance of sol-gel synthesized Li/MgO in oxidative cracking of n-hexane as a model compound of naphtha, has been studied and compared to that of conventionally prepared catalyst. At a temperature as low as 575 ^{o}C, Li/MgO shows reasonable hexane conversions (28 mol%) and excellent selectivity to light olefins (60 mol%). It is proposed that hexane activation occurs on the catalyst surface via the [$Li^{+}O^{-}$] defect sites, where [O^{-}] active sites abstract hydrogen from a secondary carbon atom. The formed hexyl radical then in gas phase and in presence of molecular oxygen undergoes a complex radical chemistry resulting in a product mixture of C_1-C_5 hydrocarbons (paraffins, olefins) as well as combustion products. Presence of oxygen in the feed is crucial to prevent coking, and to regenerate the catalyst surface through reaction with adsorbed surface hydrogen atoms, thus maintaining catalyst activity. Oxygen also plays a significant role in accelerating radical chemistry in gas phase. Unlike steam cracking, catalytic oxidative cracking results in a relatively higher ratio of high olefins (butylenes + propylene) to ethylene. Thus presence of the catalyst provides a better control over product distribution. Promotion of Li/MgO with MoO_3 and Bi_2O_3 results in considerable improvements in catalyst activity and stability.

1.1 Introduction

Environmental regulations and attempts towards more energy efficient processes introduce new challenges for the petrochemical industry. Ethylene and propylene are building blocks for the chemical industry. The demand for these olefins is enormous and a growth rate of 4% is predicted for the coming years [1]. Higher growth rate for propylene demand compared to ethylene is expected in the future [1]. Olefin yields from current production technologies are unlikely to be able to satisfy these demands.

Steam cracking is the major route for the production of light olefins today. A hydrocarbon feedstock (ethane to naphtha) in presence of steam is cracked to light olefins at high temperatures of 700 – 900 ^{o}C. Steam cracking maximizes the yield of ethylene and ($C_4^=$+$C_3^=$) / $C_2^=$ ratios of typically 0.8 are observed [1]. Steam cracking is a highly endothermic reaction, requiring substantial external heat input. Coke deposition on the inner walls of the reactor tubes, inhibiting heat transfer, is also considered a significant issue.

Catalytic oxidative cracking is a potential alternative to steam cracking, because (i) oxidation is exothermic, (ii) the process can be carried out adiabatically and (iii) minimizes coke formation. Liu *et al.* [2] observed, for the non catalytic pyrolysis of hexane at 750 ^{o}C, that oxygen in the feed (i) accelerated reaction rates resulting in higher conversions of hexane (85 mol%) and (ii) gave reasonable olefin selectivities (59 mol% of light olefins) with ethylene produced as the major product. The presence of oxygen allowed the cracking process to run in an auto-thermal way, where the exothermic combustion of product hydrogen provided the heat required for cracking internally.

Liu *et al*. [3] also performed a comparative study of homogeneous gas phase versus heterogeneous catalytic oxidative cracking of hexane at a temperature of 700 ^{o}C. Amongst the catalysts tested, 0.25 wt% Li/MgO showed the best performance (64 mol% conversion of hexane, 67 mol% selectivity to olefins). However, the high temperature used in the study, resulted in the domination of gas phase reactions and presence of catalyst had no major influence on conversions of hexane and yields of olefins. In order to use catalysts efficiently, two things are required; (i) need for more active catalysts and (ii) possibility to operate at lower temperatures. Burch and Crabb [4] showed that, for the oxidative conversion of propane, combination of heterogeneous (catalytic) and homogeneous (gas phase) reactions is necessary to obtain commercially acceptable yields of propylene. In an earlier study in our laboratory, Leveles *et al*. [5] justified the use of a catalyst in oxidative dehydrogenation (ODH) of propane in order to have more control over the distribution of products and $C_3^=$ / $C_2^=$ ratios. Moreover, it was shown that in the presence of a catalyst the reaction temperatures can be decreased to 550 ^{o}C [5-6].

The development of an efficient oxidation catalyst, however, remains a challenge. The right catalyst should be able to selectively activate the alkane in the presence of the very reactive olefins, thus inhibiting the consecutive deep oxidation of the product olefins. Very little information is reported in literature regarding catalytic oxidative cracking of naphtha range hydrocarbons. Extensive studies have been reported on the development of an efficient catalyst for the oxidative dehydrogenation/cracking of propane/butane. Oxidic catalysts with red-ox properties were mostly attempted and showed limited yields of olefins (< 30 mol%) due to the re-adsorption of product olefins and their combustion on the catalyst surface [7-9]. Recent work in our laboratory [5-6] on oxidative conversion of propane clearly highlights non reducible alkali metal-based oxides such as Li-promoted magnesia (Li/MgO) as

promising catalysts. The results show (i) remarkably high olefin yields, as high as 50 mol%, (ii) low combustion yields (< 5 mol%), (iii) no aromatic products and (iv) higher selectivity to propylene than to ethylene. These promising results are due to both basic and non-red-ox properties of the Li/MgO catalyst which prevents further adsorption and hence combustion of the product olefin, respectively. These studies have shown, in agreement with earlier work on methane [10-11] that [Li^+O^-] type defect sites are responsible for catalytic activity. Oxidative cracking of propane follows a radical mechanism where the oxygen defect site on the catalyst surface selectively abstracts hydrogen from the propane. The resulting propyl radicals leave the catalyst surface and follow radical chain reactions in the gas phase. Oxygen has two functions in the mechanism. Firstly, oxygen plays a significant role in the regeneration of the catalyst by removing hydrogen from the surface [Li^+OH^-] species formed during the activation of the alkane. Secondly, oxygen enhances the concentration of chain propagator radicals such as HO_2● in the gas phase [6].

We showed earlier that nanoclusters of Li/MgO brought considerable improvement in activity for the oxidative conversion of propane [12]. Sol-gel method was applied for the synthesis of these nano clusters. The advantage of this method over the conventional impregnation preparation route is that it allows the incorporation of Li in the magnesia under milder conditions (during sol-gel transformation) thus avoiding the need to calcine the catalyst at very high temperatures (causing sintering and loss of surface area) for achieving incorporation of Li [12-13]. Li/MgO catalyst prepared with the sol gel method had (i) higher surface area, (ii) higher concentration of surface [Li^+O^-] sites and (iii) higher activity than the same catalyst prepared by conventional impregnation method.

In this chapter we explore catalytic oxidative cracking of hexane over the newly developed Li/MgO catalyst, and compare performance to that achieved with conventional Li/MgO catalyst. Further, we investigate the possible modification of Li/MgO with small amounts of red-ox promoters to enhance hydrogen abstraction, which is the rate limiting step in oxidative cracking, aiming at improving catalyst activity further and increasing total yields of olefins. V_2O_5, MoO_3 and Bi_2O_3 are selected as promoters. V/MgO and Mo/MgO based catalysts are extensively studied in literature for the oxidative dehydrogenation of C_2-C_4 paraffins [7-9, 14-20]. V/MgO catalysts show high dehydrogenation activity at relatively low temperatures (450 – 550 ^oC), however selectivities to olefins decrease with conversion due to the secondary combustion of olefins *via* the catalyst surface [9]. Mo/MgO based catalysts however, in comparison to V/MgO catalysts show lower activity but better selectivities to olefins [19-20]. It is reported [18] that oxidative dehydrogenation of C_2-C_4 paraffins over supported transition metal oxides proceeds *via* Mars and van Krevelen mechanism involving lattice oxygen. Bismuth based catalysts are reported in literature [21] as efficient catalysts for the oxidation of propylene to acrolein. Mechanistic studies [21] suggest propylene activation *via* H● abstractant by Bi_2O_3 and the consecutive reaction of the formed allyl radical. Moreover, Bi_2O_3 based catalysts have been repeatedly reported by Grasselli *et al.* [22-23] and Late *et al.* [24] as selective catalysts for consecutive hydrogen oxidation during the dehydrogenation of light paraffins.

1.2 Experimental

1.2.1 Materials

Commercially available $Mg(OCH_3)_2$ solution (Aldrich, 6-8wt% in methanol), methanol (Merck), $LiNO_3$ (Aldrich, assay ≥ 99.99%) and MgO (Merck) were used for preparation of Li/MgO catalysts. Ammonium meta-vanadate (Aldrich, 99.999%), ammonium molybdate (Aldrich, 99.98%) and bismuth (III) nitrate pentahydrate (Aldrich, 99.999%) were used as precursors for V_2O_5, MoO_3 and Bi_2O_3 respectively. Pure hexane (Fluka, GC assay ≥ 99.0%) was used for catalytic experiments.

1.2.2 Catalyst preparation

The conventional Li/MgO catalyst (Li/MgO IMP) was prepared by wet impregnation of MgO (Merck) with $LiNO_3$ solution, according to the method described in [5]. Sol-gel synthesized MgO and Li/MgO (Li/MgO SG) catalysts used in this study were prepared according to the method described in [12]. A methanol solution containing $Mg(OCH_3)_2$ (0.4 M) was mixed at room temperature with another methanol solution containing water (0.8 M) to form a sol. For Li/MgO the required amount of $LiNO_3$ was added to the solution to obtain ~1 wt% Li. The solution was allowed to stay for gelation for 24 h. The gel formed was dried at 50 °C in vacuum for 7 h, and calcined at 500 °C in air for 1 h. Modified V_2O_5-Li/MgO, MoO_3-Li/MgO and Bi_2O_3-Li/MgO were prepared by wet impregnation of the sol-gel synthesized Li/MgO using solutions of the metal precursors. The modified catalysts were then dried at 50 °C in vacuum for 7 h and calcined at 600 °C for 5 h. Similarly, both MoO_3-MgO and Bi_2O_3-MgO were prepared by the wet impregnation of the sol-gel synthesized MgO.

1.2.3 Sample characterization

BET surface area of the catalyst was determined with nitrogen physisorption using a Micro-metrics Tristar instrument. The samples were out-gassed in vacuum at 250 °C for 24 h prior to the analysis. Elemental composition of Li was determined with atomic absorption spectroscopy (AAS).The composition of Mo, Bi and V oxides were determined with X-ray fluorescence spectroscopy (XRF) (Phillips PW 1480 spectrometer). Results are presented in Table 1.1.

Table 1.1. Surface area (BET) and XRF data of the catalysts.

Catalyst	BET surface area (m^2/g)	Metal oxide loading (wt%)
MgO	176	–
MoO_3-MgO	144	0.5
Bi_2O_3-MgO	99	0.7
Li^a/MgO IMP	8	–
Li^a/MgO SG	76	–
MoO_3-Li^a/MgO	70	0.5
Bi_2O_3-Li^a/MgO	63	0.6
V_2O_5-Li^a/MgO	85	1.2

[a] Li content in all samples =0.86wt%

1.2.4 Catalytic tests

The catalytic tests were carried out at atmospheric pressure and isothermal conditions in a conventional fixed-bed reactor. An alumina reactor of 4 mm internal diameter was used. The catalyst bed (10 mm length) was packed between two quartz-wool plugs in the alumina reactor. Powder catalyst was pressed, crushed and sieved to the particle size of 0.4-0.6 mm before use. An alumina rod of 3 mm internal diameter was placed right below the catalytic bed to reduce the post catalytic volume in order to minimize homogenous gas phase reactions. A Chromel-Alumel thermocouple inside a quartz tube was inserted above the catalytic bed to record reaction temperature. The temperature of the furnace was controlled by another thermocouple placed outside the reactor tube within the isothermal zone of the tubular furnace.

Reactions were studied in the temperature range between 475 and 600 ^{o}C. Total feed of 100 ml/min was used. The feed consisted of 10 mol% of hexane vapor, 8 mol% of oxygen and balance helium (unless stated differently). Before each catalytic test, the catalysts were pretreated in 50%O_2/He (60 ml/min) for 1 h at a temperature of 625 ^{o}C. For analysis of the product mixture for every set of experimental conditions, samples were injected to both micro GCs every 5 min during a period of 5 h. In case of blank experiments, quartz inert (0.4-0.6 mm particle size) was used instead of the catalyst (10 mm bed length).

A schematic drawing of the experimental setup is shown in Figure 1.1. Mass-flow controllers (Brooks) were used to control the flow of gases. Two electrically actuated 4-port 1-position valves (Valco) were used to switch the reaction mixture to the by pass line to measure the composition of the feed. Dionex Dual Gradient P680 HPLC pump was used to dose liquid hexane with an accurate rate which was gasified in a cylindrical gasifier operated at a temperature of 130 ^{o}C. The temperature of all lines of the setup was kept constant at 130 ^{o}C to avoid condensation of hexane.

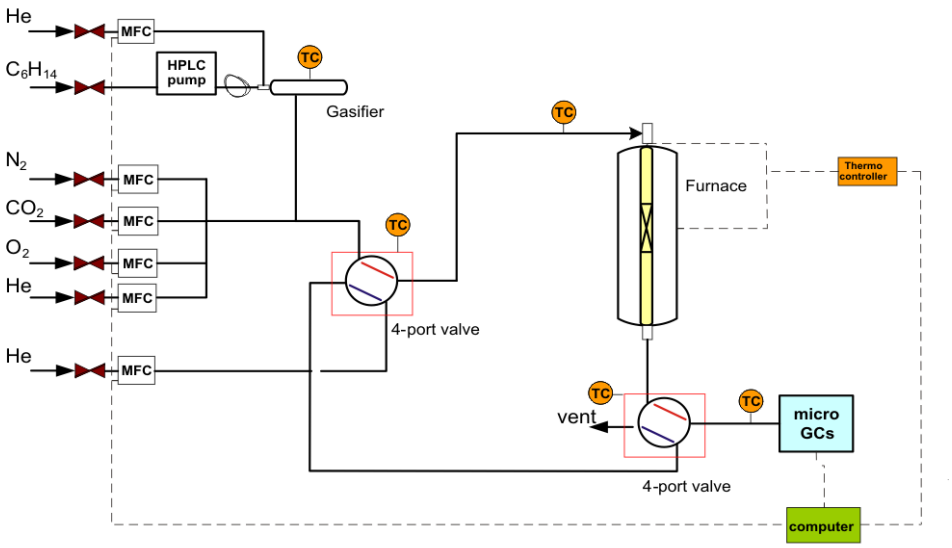

Figure 1.1. Schematic of the experimental setup.

The online analysis system consisted of two micro GCs (Varian CP4900). The first micro GC is a quad system consisting of four channels with four different columns. Column 1: Molsieve 5A Plot (He carrier gas) for the separation of O_2, N_2, CH_4 and CO, Column 2: PoraPlot Q for the separation of CO_2, C_2H_6, C_2H_4, H_2O, Column 3: Alumina KCl Plot at T = 80 °C for the separation of C_3 and C_4 hydrocarbons (paraffins and olefins), Column 4: Alumina KCl Plot T = 160 °C for the separation of C_5 hydrocarbons (paraffins and olefins). The second Micro GC is a dual system consisting of two channels of two different columns. Column 1: Molsieve 5A Plot (Ar carrier gas) for the separation of He and H_2, Column 2: CP-SIL 5CB for separation of C_6–C_8 hydrocarbons both paraffins and olefins. All channels used TCD detectors. This elaborate GC system allows full analysis of C_1-C_8 hydrocarbons both paraffins and olefins.

A gas mixture of known concentrations of C_1-C_6 hydrocarbons (paraffins, olefins) was used for the calibration of the micro GCs. Table 1.2 presents a typical analysis of product mixture.

Table 1.2. Typical analysis of product mixture of a catalytic experiment.

Component	Concentration (mol%)	Component	Concentration
Oxygen	2.828	iso-Pentane	0.023
CO	1.470	n-Pentane	0.0025
CO_2	2.303	3-methyl-1-Butene	0.010
Methane	0.288	trans-2-Pentene	0.010
Ethane	0.095	2-methyl-2-Butene	0.205
Ethylene	1.785	2-methyl-1-Butene	0.125
Propane	0.048	cis-2-Pentene	0.010
Propylene	1.330	Hexane	7.075
iso-Butane	0.038	Hydrogen	2.390
n-Butane	0.050	Water	6.575
1-Butene	0.425	Helium balance	72.900
cis-2-Butene	0.015		

Hexane conversions were calculated on a carbon mol basis; *i.e.,* (C_6^{in} moles – C_6^{out} moles) /C_6^{in} moles *100%. The carbon balance closed between 100 and 105%. Selectivity to individual products was also calculated based on the number of moles of carbon contained in the products, divided by the total number of moles of carbon in the product mixture excluding unconverted feed; *i.e.,* $(n_iC_i / \sum n_iC_i)$* 100%. Selectivity to both H_2 and H_2O was similarly calculated based on the number of moles of H contained in each divided by the total number of moles of hydrogen in the product mixture excluding unconverted feed; *i.e*., $(n_iH_i / \sum n_iH_i)$* 100% .

1.2.5 Temperature programmed desorption

In situ CO_2 TPD was performed after catalyst testing (or after catalyst pretreatment) from 100 ^oC to 950 ^oC with an increment of 10 ^oC/min, with He flow of 10 ml/min as a carrier gas. The catalyst sample (100 mg) was allowed to stay isothermally at 950 ^oC for half an hour.

The concentration of desorbed CO_2 was determined with the quad micro GC (PPQ column) every two minutes.

1.3 Results

1.3.1 Influence of temperature on the performance of Li/MgO

Table 1.3 shows results of the catalytic oxidative cracking of hexane in the temperature range 475 to 575 °C, both with the conventionally and the sol-gel synthesized Li/MgO. Both catalysts showed activity at temperatures as low as 475 °C, however, experiments with inert quartz (not shown here) showed measurable hexane conversions only at temperatures above 600 °C. Compared to the conventional catalyst, the sol-gel synthesized Li/MgO showed improved performance*, i.e.,* higher hexane conversions and better selectivities to C_2-C_4 olefins, at almost all temperatures. The sol-gel Li/MgO is further investigated in this paper for the oxidative cracking of hexane.

Table 1.3. Performance of Li/MgO catalysts during oxidative conversion of hexane. Reaction conditions: 100 ml/min, 10% hexane, 8% oxygen and balance helium, WHSV = 15.4 h^{-1}.

	475		525		575	
	Li/MgO		Li/MgO		Li/MgO	
Conversion (mol%)	(IMP)	(SG)	(IMP)	(SG)	(IMP)	(SG)
Hexane	3.8	4.2	9.9	11.2	24.5	28.4
Oxygen	24.4	23.6	49.4	42.7	92.2	65.2
Selectivity based on C mol%)						
CO	40.3	41.2	32.3	24.9	12.8	9.6
CO_2	49.7	41.3	35.7	27.2	24.2	15.0
CH_4	–	–	0.5	0.6	1.5	1.9
C_2H_4	1.9	2.2	5.3	9.5	18.4	23.2
C_3H_6	4.3	6.8	10.8	18.9	20.0	26.0
$C_4^{=}{}_s$ (butylenes)	3.8	5.8	10.4	12.2	12.2	11.5
C_2-C_4 paraffins	–	–	0.5	0.4	3.7	4.4
C_{5s} (paraffins and olefins)	–	2.8	4.5	6.4	7.2	8.5
$(C_4^{=} + C_3^{=}) / C_2^{=}$	4.3	5.7	4.0	3.3	1.8	1.6
Selectivity based on H (mol%)						
H_2	9.3	11.8	10.5	13.8	7.8	11.3
H_2O	85.6	78.8	70.3	55.3	49.5	31.2

Results in Table 1.3 show clearly the influence of temperature on product distribution. With the increase in temperature we observe dramatic decrease in the formation of both H_2O and CO_x and increase in the formation of (oxi-) cracking products (C_2H_4, C_3H_6 and C_4 olefins) as well as C_1-C_5 paraffins. Hydrogen varied only slightly with temperature and a maximum was observed at 525 °C. In addition, temperature influences the relative concentrations of olefins formed during the oxidative conversion of hexane. Ratio of $(C_4^{=}+C_3^{=})/C_2^{=}$ decreased with increasing temperature due to the consecutive cracking of C_3-C_4 olefins to ethylene. At 575 °C formation of more $C_4^{=}+C_3^{=}$ than $C_2^{=}$ can still be achieved.

(($C_4^=+C_3^=$) / $C_2^=$ (mol/mol) = 1.6). This ratio would be typically about 0.8 under steam cracking conditions [1, 25]. Since best selectivities were achieved at 575 ^oC and since above this temperature gas phase activation of hexane starts to be significant, we chose this as the optimal temperature for studying the influence of the catalyst. This is much lower than the temperature commonly used for naphtha steam cracking to generate olefins (>700 ^oC).

1.3.2 Role of catalyst in controlling product distribution

Catalytic oxidative cracking (COC) over Li/MgO SG catalyst shows a product distribution that is different from that of gas phase oxidative cracking (GOC) at the same temperature. As shown in Figure 1.2, GOC resulted in formation of higher amounts of C_6^+ products (most probably aromatics, they could not be separated by the GC columns used) than COC. With catalytic cracking we observe formation of more light olefins ($C_2^=$-$C_4^=$) as well as more C_5 hydrocarbons (mainly olefins). The catalyst provides for more olefin, than in the absence of catalyst. CO_x production from COC is still significantly higher as compared to GOC because of CO_2 production due to deep oxidation *via* the catalyst surface. Hence further improvement of catalyst selectivity is necessary. Further, at 575 ^oC, olefin selectivity was invariant with the hexane conversion level.

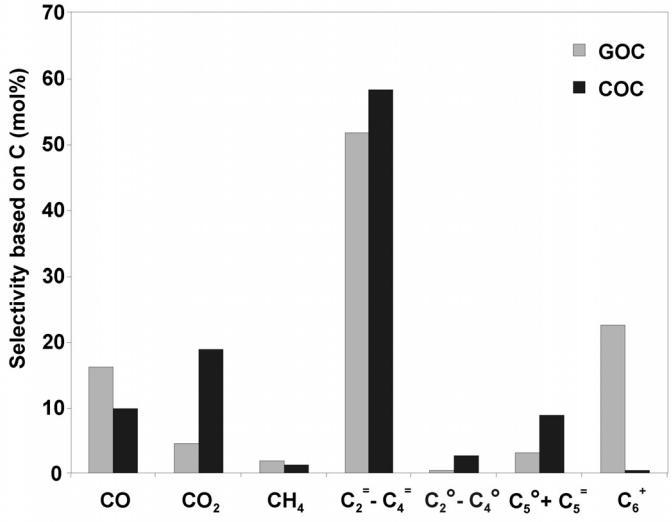

Figure 1.2. Gas phase oxidative cracking (GOC) vs. Catalytic oxidative cracking (COC) over Li/MgO SG. Conversion: 30 mol% hexane. Reaction conditions: 100 ml/min, 10% hexane, 20% oxygen and balance helium, T=575 ^oC.

Figure 1.3 shows that increase in hexane conversions from 15% to 45%, caused only marginal changes. High selectivities to olefins were maintained, with even slight decrease in selectivities to CO_x. Different levels of hexane conversion were achieved by varying weight-hourly-space velocity (WHSV).

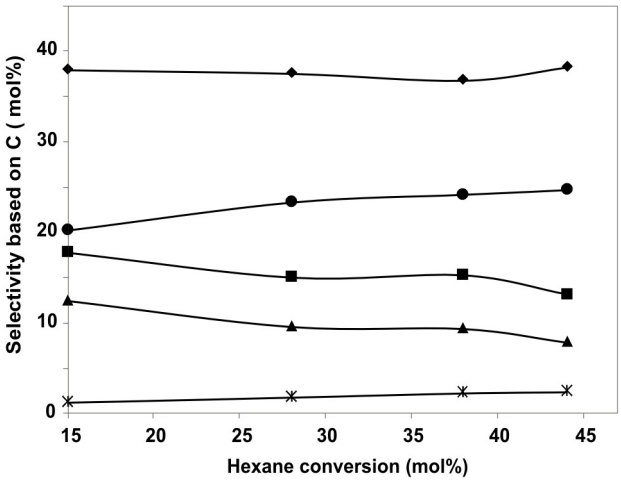

Figure 1.3. Selectivity to different products *vs.* hexane conversion with Li/MgO SG. (♦) ($C_3^=$ + $C_4^=$), (●) C_2H_4, (■) CO_2, (▲) CO, (*) CH_4. Reaction conditions: 100 ml/min, 10% hexane, 8% oxygen and balance helium. Different conversions achieved by varying WHSV from 5 to 102 h^{-1}.

1.3.3 Influence of oxygen concentrations in the feed

The influence of oxygen concentrations in the feed on both hexane conversions and selectivities to products has been as well investigated. Figure 1.4 shows that the increase in

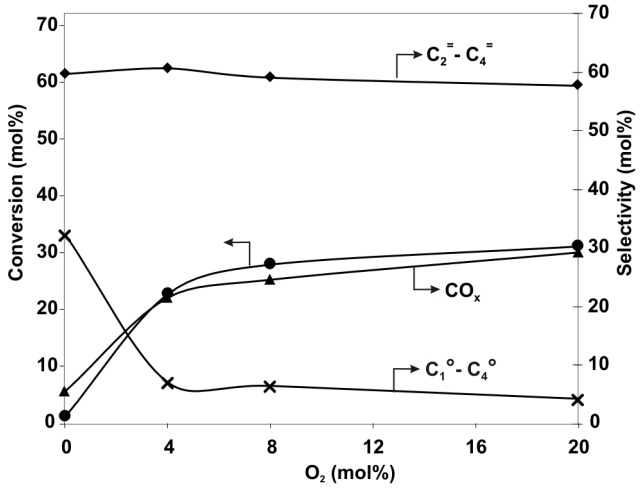

Figure 1.4. Influence of oxygen concentrations on hexane conversions as well selectivity to products; (●) hexane conversion, (▲) selectivity to CO_x, (♦) selectivity to light olefins ($C_2^=$-$C_4^=$), (x) selectivity to C_1-C_4 paraffins ($C_1°$-$C_4°$). Oxygen conversions = 69, 65 and 39 mol% at 4, 8 and 20 mol% O_2, respectively. Reaction conditions: 100 ml/min, 10% hexane and balance helium, T=575 °C, WHSV = 15.4 h^{-1}.

oxygen concentrations induced a significant increase in the conversion of hexane. In the absence of oxygen, hexane conversions were negligible. Increasing oxygen concentrations in the feed introduced only a slight decrease in selectivity to light olefins ($C_2^=$, $C_3^=$, $C_4^=_s$) *i.e.*, from 62 mol% to 60 mol%. In the low oxygen range (0-4%), increase in selectivity to CO_x was observed, at the expense of C_1-C_4 paraffins. For oxygen concentrations above 4 mol%, changes in the selectivities of CO, CO_2 and C_1-C_4 paraffins were only marginal.

Selectivities to products with varying oxygen concentrations were further investigated, keeping the hexane conversion constant by varying WHSV (Figure 1.5). At the higher oxygen concentrations (20 mol%) an increase in CO_x selectivity (22 to 38 mol%) accompanied by a slight decrease in selectivities to both olefins (63 to 54 mol%) and C_1-C_4 paraffins was observed. Generally, with increasing oxygen amounts in the feed there is a continuous increase in amount of CO_x produced, specifically an increase in CO_2 production (CO_2/CO > 1).

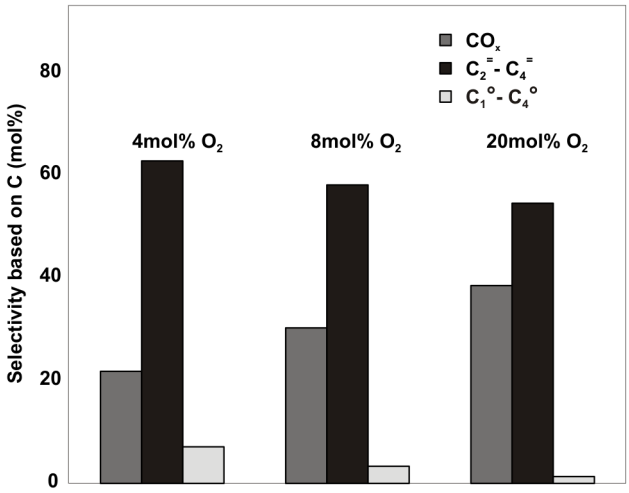

Figure 1.5. Influence of oxygen concentrations on selectivity to CO_x, C_2-C_4 olefins ($C_2^=$-$C_4^=$) and C_1-C_4 paraffins (C_1°-C_4°) at hexane conversion of 17 mol%. Oxygen conversions = 69, 41 and 24 mol% at 4, 8 and 20 mol% O_2, respectively. Reaction conditions: 100 ml/min, 10% hexane and balance helium, T=575 °C, WHSV = 15.4 – 44 h^{-1}.

1.3.4 Stability of Li/MgO SG catalyst

The activity of Li/MgO SG catalyst during a typical experiment is shown in Figure 1.6. Partial deactivation was observed within the first one hour of time on stream. After this the catalytic activity was almost stable.

Temperature programmed desorption of CO_2 was performed on the used Li/MgO SG (after test for 5 h) and compared to that of a fresh catalyst pretreated in oxygen at 625 °C (Figure 1.7). TPD of the fresh catalyst showed a typical CO_2 desorption peak of Li_2CO_3 at 860 °C [26-27]. The presence of Li_2CO_3 (formed with CO_2 from ambient) is an inherent property of Li/MgO [28]. TPD of the used catalyst however, showed a broad CO_2 desorption peak with a maximum at 690 °C followed by a second peak around 900 °C. The broad CO_2 desorption peak at 690 °C is most likely attributed to CO_2 adsorbed on [Li^+O^-] active sites [$Li^+CO_3^-$] [27, 29], and suggests that part of the adsorbed CO_2 is responsible for the observed

poisoning effect. The higher concentration of Li_2CO_3 observed in the used catalyst would possibly indicate that the surface carbonate phase, $[Li^+CO_3^-]$, further reacts with $[Li^+O^-]$ active sites, thus accelerating the segregation of Li from these active sites in the form of Li_2CO_3. Indeed, co-feeding 5 mol% of CO_2 in an experiment with fresh catalyst resulted in a steeper decrease in hexane conversions as shown in Figure 1.6. The negative influence of CO_2 on catalyst activity has been further confirmed by co-feeding up to 10 mol% of CO_2. CO_2 has a poisoning effect on the catalyst as indicated in Figure 1.6, addition of up to 10 mol% of CO_2 to the feed, introduced a decrease in initial hexane conversion from 40 to 20 mol%.

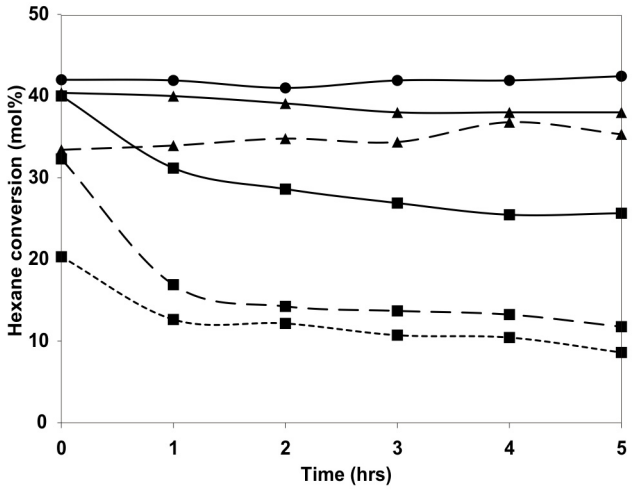

Figure 1.6. Hexane conversion as function of time-on-stream. (■) Li/MgO SG, (▲) MoO_3-Li/MgO, (●) Bi_2O_3-Li/MgO (solid lines) without CO_2 in the feed, (dashed lines) co-feeding 5 mol% of CO_2, (dotted line) co-feeding 10 mol% of CO_2. Reaction conditions: 100 ml/min, 10% hexane, 8% oxygen and balance helium, T=575 ^oC, WHSV = 15.4 h^{-1}.

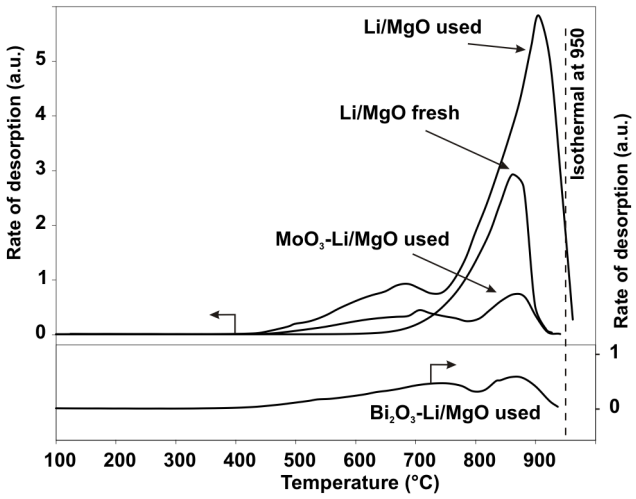

Figure 1.7. Temperature programmed desorption of CO_2 for fresh and used catalysts (TPD in situ after catalytic reaction, signals are normalized to the BET surface area). Temperature ramp 10 ^oC/min, He 10 ml/min.

1.3.5 Influence of post catalytic volume

Combining catalytic reaction with a post-catalytic thermal reaction (post catalytic void of 3.6 cm^3) introduced an increase in hexane conversions from 28 mol% to 33 mol% as well as slight improvement in selectivity to light olefins from 60 mol% to 63 mol%. Results are shown in Table 1.4.

Table 1.4. Influence of post catalytic volume. Reaction conditions: 100 ml/min, 10% hexane, 8% oxygen and balance helium, WHSV = 15.4 h^{-1}.

Conversion, mol%	Without post catalytic volume	With post catalytic volume
Hexane	28.4	33.6
Oxygen	65.2	65.5
Product selectivity, mol%		
CO_x	24.6	20.5
CH_4	1.9	2.3
C_2 - C_4 olefins	60.7	63.3
C_2 - C_4 paraffins	4.4	5.0
C_{5s} (paraffins and olefins)	8.5	8.9

1.3.6 Modification of Li/MgO catalyst

In order to improve catalyst activity further, hence yields of olefins, we modified Li/MgO SG with small amounts of red-ox promoters. Figure 1.8 shows yields of C_2-C_4 olefins at 575 ^oC with MoO_3, Bi_2O_3 and V_2O_5 promoted MgO and Li/MgO catalysts, initially and after time on stream.

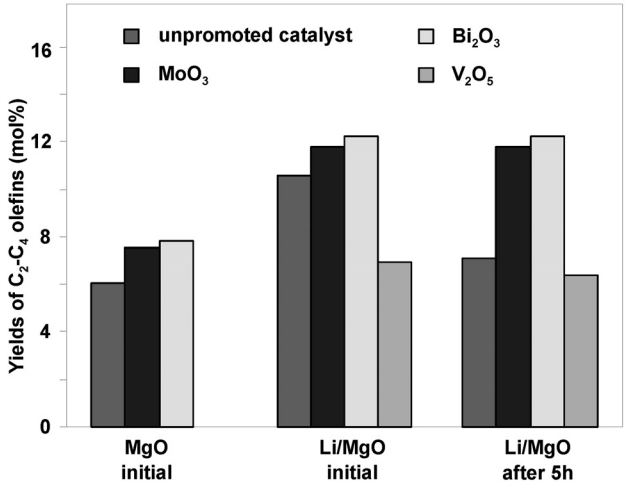

Figure 1.8. Yields of C_2-C_4 olefins for MgO, Li/MgO SG and MoO_3, Bi_2O_3, V_2O_5 promoted catalysts, initially (at minute 5) and after 5 h of time on stream. Initial hexane conversions (minute 5): 12%, 13%, 15%, for MgO, MoO_3-MgO, Bi_2O_3-MgO, respectively. 19%, 23%, 21%, 18% for Li/MgO SG, MoO_3-Li/MgO, Bi_2O_3-Li/MgO and V_2O_5-Li/MgO, respectively. Reaction conditions: 100 ml/min, 10% hexane, 8% oxygen and balance helium, T = 575 ^oC, WHSV = 154 h^{-1}.

As compared to Li/MgO both MoO_3-Li/MgO and Bi_2O_3-Li/MgO resulted in higher yields of light olefins. This improvement in the yields of olefins was more significant after five hours of reaction because Li/MgO catalyst lost activity with time (as shown in Figure 1.6). Moreover interestingly, addition of 0.5 wt% MoO_3 and 0.7 wt% Bi_2O_3 to MgO did as well result in better yields than MgO. Generally, in the MoO_3 and Bi_2O_5 promoted catalysts the observed higher yields of olefins, was result of enhancement in hexane conversions without any significant changes in selectivity to products. V_2O_5-Li/MgO however showed the minimum yields of olefins. Figure 1.9 shows the selectivities based on carbon to different products at 575 ^oC with the four catalysts; Li/MgO, MoO_3-Li/MgO, Bi_2O_3-Li/MgO and V_2O_5-Li/MgO at similar hexane conversion of 10 mol%. Similar hexane conversions were achieved by varying WHSV. V_2O_5-Li/MgO resulted in formation of more combustion products, while both MoO_3-Li/MgO and Bi_2O_3-Li/MgO showed similar selectivities as Li/MgO.

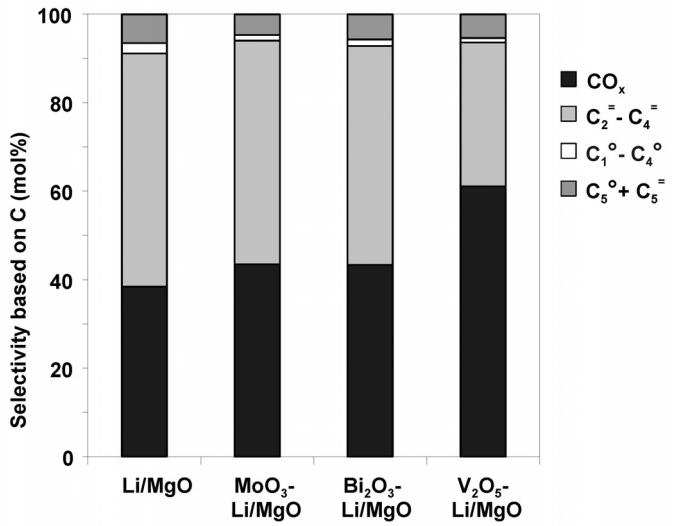

Figure 1.9. Selectivity to products based on C at hexane conversion of 10 mol%.
Oxygen conversions = 35 mol% (Li/MgO SG) , 37 mol% (MoO_3-Li/MgO), 44 mol% (Bi_2O_3-Li/MgO), and 70 mol% (V_2O_5-Li/MgO). Reaction conditions: 100 ml/min, 10% hexane, 8% oxygen and balance helium, T= 575 °C, WHSV = 154 – 385 h^{-1}.

Selectivities to products based on hydrogen (Figure 1.10) however, showed slight differences between Bi_2O_3-Li/MgO and MoO_3-Li/MgO. Bi_2O_3-Li/MgO resulted in formation of more water and less hydrogen than both Li/MgO and MoO_3-Li/MgO.

The stability of MoO_3 and Bi_2O_3 promoted Li/MgO has been as well investigated both with and without the presence of CO_2 in the feed. The promoted catalysts maintained complete activity. The presence of 5 mol% of CO_2 with MoO_3-Li/MgO did not influence catalyst activity unlike Li/MgO (Figure 1.6). Figure 1.7 shows the temperature programmed desorption of CO_2 for MoO_3-Li/MgO and Bi_2O_3-Li/MgO catalysts after testing in comparison to that of used Li/MgO. CO_2 desorption from the promoted catalysts showed the same trend as the unpromoted catalyst however with much smaller desorption peaks.

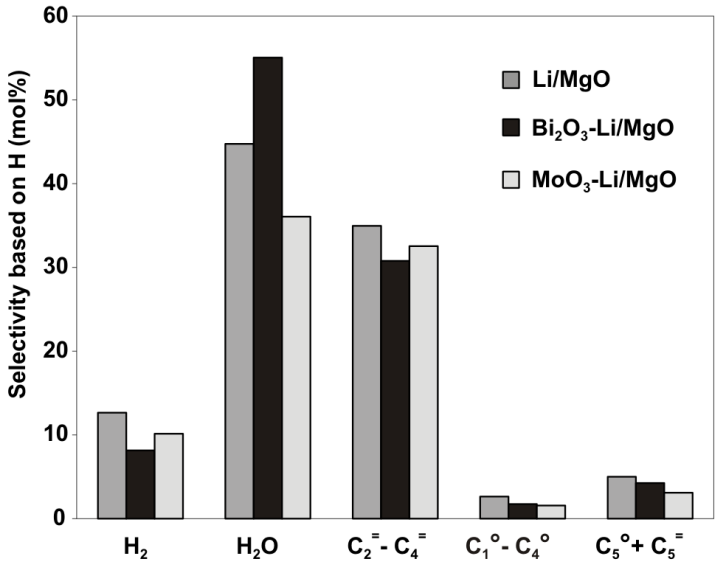

Figure 1.10. Selectivity to products based on H at hexane conversion of 10 mol%. Oxygen conversions = 35 mol% (Li/MgO SG) , 37 mol% (MoO_3-Li/MgO) and 44 mol% (Bi_2O_3-Li/MgO). Reaction conditions: 100 ml/min, 10% hexane, 8% oxygen and balance helium, T= 575 °C, WHSV = 154 – 385 h^{-1}.

1.4 Discussion

Li/MgO catalyst is active for oxidative cracking of hexane at temperatures as low as 475 °C. In the absence of the catalyst measurable hexane conversions were noticed only at T ≥ 600 °C. In the absence of catalyst, homogeneous activation occurs *via* hydrogen abstraction by gas phase diatomic oxygen, forming HO_2● radicals (eq. 1) [2, 30-31]).

$$C_6H_{14} + O_2 \rightarrow C_6H_{13}\bullet + HO_2\bullet \qquad (1)\ \text{(gas phase, homogeneous)}$$

At 575 °C hexane conversion was 25 mol% with the conventional catalyst and 28 mol% with the sol-gel synthesized Li/MgO (Table 1.3). Influence of the presence of catalyst Li/MgO on the activation of hexane is significant. As mentioned in the introduction, [Li^+O^-] type defect sites are responsible for catalytic activity of Li/MgO catalyst [10-13]. In the case of oxidative conversion of propane, we have shown earlier [6] that hydrocarbon activation occurs *via* a radical mechanism involving homolytic scission of C-H bonds. The oxygen of the [Li^+O^-] defect site on the catalyst surface selectively abstracts a hydrogen from propane, forming [Li^+OH^-] on the surface and releasing a propyl radical to the gas phase (eq. 2). As in the case of propane we propose that the first step in the activation of hexane is the abstraction of a hydrogen and formation of hexyl radicals (reaction 2). Further reactions of hexyl radicals take place in the gas phase.

$$C_6H_{14} + O^-_s \rightarrow C_6H_{13}\bullet + OH^-_s \qquad (2)\ \text{(catalytic, heterogeneous)}$$

The sol-gel synthesized Li/MgO showed improved performance at almost all temperatures. The relatively better performance of this catalyst as compared to the conventional catalyst is in agreement with results we have reported earlier during the ODH of propane [12-13]. This improvement is attributed to the higher concentration of $[Li^{+}O^{-}]$ sites in the sol-gel synthesized Li/MgO.

Generally, with the sol-gel synthesized Li/MgO, cracking reactions and olefin formation were more significant at T > 525 ^{o}C while at lower temperatures CO_x formation was more dominant. This improvement in selectivity to olefins with temperature is explained with the fact that the rates of radical chain propagation reactions increase with temperature, thus increasing the ratio of homogenous to heterogeneous reactions of these radicals [6]. At low temperatures radicals initiated on the catalyst surface most likely interact with unselective O^{2-} sites of MgO forming alkoxy species as precursors for CO_x. Reaction of hydrocarbon radicals with surface oxygen has been reported to lead to surface alkoxy species ($C_nH_{2n+1}O^{-}_s$) (eq. 3), and an electron trapped at an oxide ion vacancy (VO'') [10, 33]. Such species are reported for a variety of paraffins/olefins (ethane [8], C_1-C_4 paraffins [33], C_2-C_4 olefins [34]) during oxidation reactions. Alkoxide species are reactive and known to be intermediates in total oxidation pathways through consecutive attack by gas phase oxygen (reaction 4) [10, 31, 33]. In comparison to C_1-C_4 paraffins/olefins, the radical chemistry during oxidative cracking of hexane is expected to be even more complex because a variety of radicals are formed. However, we assume that deep oxidation reactions follow the same pathways as suggested earlier for lower paraffins [7, 10-11, 31].

$$C_nH_{2n+1}\bullet + O^{2-}_s \rightarrow C_nH_{2n+1}O^{-}_s + e^{-} \qquad (n \leq 6) \qquad (3)$$

$$C_nH_{2n+1}O^{-}_s + O_2 + e^{-} \rightarrow CO, CO_2, H_2O + O^{2-}_s \qquad (4)$$

At temperatures above 525 ^{o}C, desorption of radicals formed by hydrogen abstraction, is thermodynamically more favored than reaction with surface oxygen for alkoxide formation. This might be the reason that at higher temperatures, lower selectivities to CO_x (Table 1.3) are observed. Similarly with the increase in temperature, water concentrations decreased as result of decrease in extent of combustion reactions. Hydrogen formation showed a maximum at 525 ^{o}C, most probably due to the lower severity of cracking at this relatively low temperature while at the higher temperature (575 ^{o}C) cracking reactions and olefin formation were more dominant. Generally, during both oxidative dehydrogenation and cracking reactions occurring in gas phase in presence of molecular oxygen, possible pathways for H_2 formation are the termination reactions of H• radicals and/or addition reactions of alkyl and H• radicals [35].

Similar to results of our previous work on the oxidative conversion of propane [5-6, 12-13], during the oxidative conversion of hexane with Li/MgO olefin selectivity was almost invariant with the hexane conversion level (Figure 1.3). Moreover interestingly, selectivity to CO_x slightly decreased with hexane conversions, most probably due to the increase in ratio of homogenous gas phase to heterogeneous surface reactions. The concentration of surface initiated hexyl radicals will determine the extent of gas phase radical chemistry. Thus accelerated gas phase radical chemistry is expected at the higher hexane conversions, where oxygen is selectively involved in reactions with intermediate radicals resulting in formation of more of olefins and less CO_x. Typically for red-ox type catalysts, increasing conversion

leads to higher combustion and lower olefin selectivities [7-8]. Our results demonstrate that oxidative cracking of hexane over Li/MgO does not suffer from consecutive deep oxidation reactions, similar to ethane, propane and butane [5-6, 12-13].

Besides radical initiation, Li/MgO catalyst also contributes in controlling selectivity to olefins; *i.e.,* ratio of higher olefins to ethylene ($C_4^=$ + $C_3^=$/$C_2^=$). At 575 °C ratio of ($C_4^=$+$C_3^=$) / $C_2^=$ (mol/mol) is 1.6. This would be typically about 0.8 under steam cracking conditions [1, 25] mainly due to the severity of cracking at the elevated temperatures (> 700 ^oC). Moreover, thermal cracking of naphtha during steam cracking is unselective and variant types of radicals (primary, secondary) are initiated. However, at the presence of a strong hydrogen abstractant, in this case [O^-] site, there is preference for hydrogen abstraction from a secondary carbon atom forming secondary radicals. This preference is due to the relative stability of radical on a secondary carbon atom versus on a primary carbon atom. Previously, Sinev *et al*. [36] has shown the role of surface [O^-] sites (for example [Li^+O^-] in Li/MgO) as strong H● abstractants and their preference towards hydrogen abstraction from the secondary carbon atom of propane, thus leading to more dominant formation of iso-propyl radicals. Similarly, in the case of hexane the higher selectivity to C_3, C_4 olefins indicate involvement of the catalyst in the process and the related preference for hydrogen abstraction from a secondary carbon atom forming iso-hexyl radicals. β-scission of iso-hexyl radicals at this relatively mild cracking conditions (575 ^oC) will result in higher ratio of high olefins to ethylene. In addition, presence of the catalyst inhibits the formation of C_6^+ products unlike the case of gas phase oxidative cracking.

Oxygen in the feed has significant influence on hexane conversions. In the absence of oxygen, hexane conversions were negligible; this may be due to the fact that regeneration of active sites after one turn over (resulting in the formation of [Li^+OH^-]) is not possible. Consequently, a steep increase in conversion was observed when adding a low amount of oxygen, *via* regeneration of the sites responsible for radical formation (Figure 1.4). Additionally, with the presence of oxygen formation of a new type of chain propagator [HO_2•] radical is favored, enhancing activation of hexane in the gas phase with further increase in oxygen concentrations. Similar observations were earlier made by us [6] during the ODH of propane. Presence of oxygen in the feed is, thus crucial for the following reasons; (i) to prevent coke formation (catalyst in the absence of oxygen was completely covered with coke, hence presence of oxygen is crucial to prevent catalyst deactivation), (ii) to increase conversions hence increase olefin yields, through regeneration of active sites and (iii) to accelerate radical chain chemistry in the gas phase.

Nevertheless, optimum oxygen concentrations are necessary. Increasing oxygen concentrations slightly shifts product distribution towards formation of more CO_x. We speculate that this is mainly due to an increase in formation of intermediate oxygenates which further oxidize, either in gas phase or *via* the catalyst surface. As gas phase oxidative cracking, at similar conditions, gave more CO than CO_2 (Figure 1.2), our results indicate that even at these temperatures surface oxidation pathways still contribute significantly.

A drawback of Li/MgO catalyst however, is that it suffers from partial deactivation within the first one hour of time on stream. It is believed that CO_2 produced during reaction poisons the [Li^+O^-] active sites of the catalyst. It is reported in literature [6, 26-27, 29] that CO_2 produced during reaction, interacts with the active sites [Li^+O^-] of the catalyst forming surface intermediate carbonate phase [$Li^+CO_3^-$], which reacts further with [Li^+O^-] to form bulk Li_2CO_3 (eq. 6), deactivating the catalytic sites.

$$Li^+O^- + CO_2 \leftrightarrow Li^+CO_3^- + Li^+O^- \rightarrow Li_2CO_3 + \tfrac{1}{2} O_2 \qquad (6)$$

In situ CO_2 TPD results (Figure 1.7) of the used catalyst compared to the fresh pre-treated catalyst, confirmed the presence of both $Li^+CO_3^-$ and Li_2CO_3 phases. Thus, under our reaction conditions carbonates certainly exist, affecting catalyst activity.

The contribution of non-catalytic homogenous gas phase reactions in ODH of paraffins has been repeatedly discussed in literature [7, 30-32]. In our experiments combining catalytic reaction with post-catalytic homogenous reactions induced an increase in hexane conversion and olefin yield (Table 1.4). In both experiments (with and without post catalytic volume) similar oxygen conversions were observed. The formation of less CO_x in the experiment with post catalytic volume suggests that oxygen was selectively involved in accelerating the radical chemistry in gas phase in the post catalytic region, thus resulting in higher hexane conversions. The same trend was observed previously both by us [6] and Nguyen and Kung [32] in ODH of propane, Lemonidou and Stambouli [30] in ODH of n-butane as well as Sinev for ODH of C_3-C_4 paraffins [31]. The higher yields confirm that intermediate radicals desorb from the catalyst surface, initiating radical chain gas phase reaction in the post-catalytic volume. Under our conditions, the effect is positive, improving yields by about 20%.

Modification of Li/MgO with both MoO_3 and Bi_2O_3 resulted in higher yields of C_2-C_4 olefins than promotion with V_2O_5. V_2O_5 showed activity towards unselective combustion reactions of, most probably, intermediate radicals or product olefins. This performance of V_2O_5 is not surprising as it possesses strong red-ox properties resulting in high oxygen conversions and high selectivities to combustion products. V_2O_5 based catalysts have been repeatedly reported in literature as active yet unselective catalysts for ODH of lower hydrocarbons [7-9].

Mo/MgO catalysts however, were reported to be more selective than V/MgO catalysts. Mo doped V/MgO during the oxidative dehydrogenation of propane [20] and n-butane [19] showed better selectivities to olefins. It is believed that C-H bond scission from the alkane during oxidative dehydrogenation of C_2-C_4 paraffins over Mo oxides proceeds *via* Mars and van Krevelen mechanism involving lattice oxygen [18]. Bi_2O_3 is also reported in literature [21] as selective H● abstractant during oxidation of propylene to acrolein. The slight improvement in initial activity, thus initial yields of olefins (Figure 1.8), observed during the oxidative conversion of hexane in our experiments both with MoO_3 and Bi_2O_3 promoted catalysts as compared to the unpromoted ones (MgO, Li/MgO), might be attributed to activity of MoO_3 and Bi_2O_3 for C-H bond scission in hexane. The significantly higher yields of olefins at longer time on stream in the case of MoO_3-Li/MgO and Bi_2O_3-Li/MgO, is a result of the better stability of these catalysts as compared to Li/MgO. Based on the observations of CO_2 TPD experiments (Figure 1.7), we suggest that both MoO_3 and Bi_2O_3, being Lewis acidic, minimize CO_2 sorption (less formation of Li_2CO_3) and thus prevent poisoning of the $[Li^+O^-]$ active sites of the catalyst. MoO_3 promoted Li/MgO is selected for further characterization work and is currently under investigation. We will study the influence of varying loading of MoO_3 on the performance of Li/MgO during the oxidative cracking of hexane, as well as the effect of MoO_3 on the $[Li^+O^-]$ active sites.

The higher amounts of water formed with Bi_2O_3-Li/MgO in our experiments indicate enhanced hydrogen oxidation. This agrees well with results reported by both Grasselli *et al.* [22-23] and Late *et al.* [24] on the ability of Bi_2O_3 for selective hydrogen oxidation.

Generally, results obtained in this study show that catalytic oxidative cracking achieves the following advantages over the conventional steam cracking: (i) lowering reaction temperatures, (ii) increasing the ratio of (butylenes and propylene) to ethylene from 0.8 for steam cracking to 1.6 for oxidative cracking, and (iii) catalytic oxidative cracking is free of any coke formation. However, the formation of combustion products suggests further improvement in catalyst performance.

1.5 Conclusions

Li/MgO catalyst is active for oxidative cracking of hexane, shows minimal combustion, and gives excellent selectivity to olefins (60 mol%). Sol-gel synthesized Li/MgO shows better performance than the conventionally prepared catalyst due to the higher concentration of $[Li^+O^-]$ active sites in the latter. It is proposed that catalytic oxidative cracking of hexane is heterogeneously initiated at the $[Li^+O^-]$ active site of the catalyst. This occurs *via* homolytic C-H bond splitting and formation of radicals which undergo reactions in the homogeneous phase. Increasing hexane conversion does not have any detrimental effect on olefin selectivities, thus high olefin yields can be achieved. This behavior is similar to oxidative cracking of lower paraffins over Li/MgO.

Oxygen plays a significant role in regenerating the active sites and accelerating the radical chemistry. It also inhibits coke formation. Higher oxygen concentrations have a minor influence on olefin selectivity.

Active sites of the catalyst are susceptible for deactivation due to poisoning by product CO_2, which interacts with the $[Li^+O^-]$ sites forming stable Li_2CO_3. Both MoO_3 and Bi_2O_3 promoted Li/MgO, however, maintain activity and show considerably higher yields of C_2-C_4 olefins than Li/MgO during time on stream due to less formation of Li_2CO_3. Bi_2O_3 is selective in the consecutive oxidation of product hydrogen in the presence of olefins.

We conclude that in the oxidative cracking of hexane, Li/MgO shows a similar behavior as in oxidative dehydrogenation of propane; *i.e.,* heterogeneously initiated homogeneous reaction. Selectivities obtained (60 mol% of light olefins and 25 mol% of CO_x) are similar with those achieved during oxidative cracking of C_2-C_4 paraffins [6]. However, hexane is clearly more active than C_2-C_4 paraffins, consequently it is possible to operate at lower reaction temperatures, much lower than temperatures used in conventional steam cracking.

References

[1] T. Ren, M. Patel, K. Blok, Energy 31 (2006) 425-451

[2] X. Liu, W. Li, H. Xu, Y. Chen, React. Kinet. Catal. Lett. 81 (2) (2004) 203-209.

[3] X. Liu, W. Li, H. Zhu, Q. Ge, Y. Chen, H. Xu, Catal. Lett, 94 (1-2) (2004) 31-36.

[4] R. Burch, E. Crabb, Appl. Catal. A 100 (1993) 111-130.

[5] L. Leveles, K. Seshan, J.A Lercher, L. Lefferts, J. Catal. 218 (2003) 307-314.

[6] L. Leveles, K. Seshan, J.A. Lercher, L. Lefferts, J. Catal. 218 (2003) 296-306.

[7] F. Cavani, N. Ballarini, A. Cericola, Catal. Today 127 (2007) 113-131.

[8] F. Cavani, F. Trifiro, Catal. Today 24 (1995) 307-313.

[9] M.V. Landau, M.L. Kaliya, A. Gutman, L.O. Kogan, M. Herskowitz, P.F. van den Oosterkamp, Stud. Surf. Sci. Catal. 110 (1997) 315-326.

[10] T. Ito, J.-X. Wang, C.-H. Lin, J.H. Lunsford, J. Am. Chem. Soc.107 (1985) 5062-5068.

[11] C.-H. Lin, K.D Campbell, J.-X. Wang, J.H. Lunsford, J. Phys. Chem. 90 (4) (1986) 534-537.

[12] C. Trionfetti, I.V Babich, K. Seshan, L. Lefferts, Appl. Catal. A 310 (2006) 105-113.

[13] C. Trionfetti, I.V Babich, K. Seshan, L. Lefferts, Langmuir 24 (2008) 8220-8228.

[14] M.A. Chaar, D. Patel, M.C. Kung, H.H. Kung, J. Catal. 105 (1987) 483-498.

[15] M.A. Chaar, D. Patel, H.H. Kung, J. Catal. 109 (1988) 463-467.

[16] K.T. Nguyen, H.H. Kung, Ind. Eng. Chem. Res. 30 (1991) 352-361.

[17] D. Siew Hew Sam, V. Soenen, J.C. Volta, J. Catal. 123 (1990) 417-435.

[18] E. Heracleous, M. Machli, A. A. Lemonidou , I. A. Vasalos, J. Mol. Cat. A 232 (2005) 29-39.

[19] A. Dejoz, J.M. Lopez Nieto, F. Marquez, M.I. Vazquez, Appl. Cat. A 180 (1999) 83-94.

[20] J.D.Pless, B.B.Bardin, H.-S. Kim, D. Ko, M. T. Smith, R.R. Hammond, P.C.Stair, K.R. Poeppelmeier, J. Cat. 223 (2004) 419-431.

[21] S. Pudar, J. Oxgaard, K. Chenoweth, A.C.T. Van Duin, W. A. Goddard, J. Phys. Chem. C 111 (2007) 16405-16415.

[22] R.K. Grasselli, D.L. Stern, J. G. Tsikoyiannis, Appl. Catal. A 189 (1999) 1-8.

[23] J. G. Tsikoyiannis, D. L. Stern, R.K. Grasselli, J. Catal. 184 (1999) 77-86.

[24] L. Late, W. Thelin, E.A. Blekkan, Appl. Cat. A 262 (2004) 63-68.

[25] R.Le. Mao, S. Melancon, C. Gauthier-Campbell, P. Kletnieks, Catal. Lett. (73) (2-4) (2001) 181-186.

[26] S. Fuchs, L. Leveles, K. Seshan, L. Lefferts, A. Lemonidou, J.A Lercher, Top.Catal.15 (2-4) (2001) 169-174.

[27] M. Xu, C. Shi, X. Yang, M.P. Rosynek, J.H. Lunsford, J. Phys. Chem. 96 (15) (1992) 6395-6398.

[28] S.J. Korf, J.A. Roos, N.A. de Bruijn, J.G. van Ommen, J.R.H. Ross, Catal. Today 2 (1988) 535-545.

[29] S.C. Bhumkar, L. L. Lobban, Ind. Eng. Chem. Res. 31 (1992) 1856-1864.

[30] A.A. Lemonidou, A.E. Stambouli, Appl. Cat. A 171 (1998) 325-332.

[31] V.P. Vislovskiy, T.E. Suleimanov, M. Yu Sinev, Y.P Tulenin, L.Y. Margolis, V. Cortes Corberan, Catal. Today 61 (2000) 287-293.

[32] K.T. Nguyen, H.H Kung, J. Catal. 122 (1990) 415-428.

[33] K.-I. Aika, J.H. Lunsford, J. Phys. Chem. 81 (14) (1977) 1393-1398.

[34] K.-I. Aika , J.H. Lunsford, J. Phys. Chem. 82 (16) (1978) 1794-1800.

[35] C.A. Mims, R. Mauti, A.M.Dean, K.D.Rose, J. Phys. Chem. 98 (1994) 13357-13372.

[36] E. V. Kondratenko, M. Yu. Sinev, Appl. Catal. A 325 (2007) 353-361

Chapter 2

Oxidative Cracking of n-Hexane over MoO_3-Li/MgO

Li/MgO shows promise as catalyst for oxidative cracking of hexane. However, it suffers from low catalyst activity and slight deactivation. Aiming at higher yields of C_2-C_4 olefins during the oxidative cracking of hexane, modification of sol-gel Li/MgO with MoO_3 is reported. The influence of varying loadings of MoO_3 on performance of Li/MgO during the oxidative cracking of hexane has been studied. Catalyst with minimum MoO_3 loading (0.5 wt %) shows best yields to C_2-C_4 olefins. Promotion by MoO_3 maintains higher surface area upon calcination at T > 500 ^oC and improves catalyst stability significantly by minimizing surface carbonate formation.

2.1 Introduction

Catalytic oxidative cracking of naphtha is conceptually an alternative process to steam cracking. Co-feeding oxygen and presence of catalyst facilitate cracking to occur at lower temperatures, thus making the overall process less energy consuming. The development of an efficient catalyst, however, remains a challenge. The right catalyst should be able to selectively activate the paraffin in the presence of the very reactive olefins, thus inhibiting the consecutive deep oxidation of the product olefins. Very little information is reported in literature regarding catalytic oxidative cracking of naphtha range hydrocarbons. From this information available, typically three classes of catalysts have been tested for catalytic cracking of naphtha range hydrocarbons; acidic catalysts (Ag-mordenite/Al_2O_3, Cu/HZSM-5, steamed HZSM-5), basic catalysts (CaO-SrO-Al_2O_3, WO_3-K_2O-Al_2O_3, KVO_3/corundum) and transition metal oxide catalysts (Cr_2O_3/Al_2O_3, V-oxides) [1]. Modification of rare earth oxide catalysts (CeO_2, Pr_6O_{11}, Tb_4O_7) by alkali metals such as Li and K minimized the CO_x formation during oxidative cracking [1]. Recently, we reported [2] on the performance of Li/MgO catalyst for the oxidative cracking of hexane. The catalyst showed reasonable activity and very good selectivity to C_2-C_4 olefins (~ 60 mol%) at a temperature as low as 575 ºC, which is much lower than temperatures used in steam crackers (T ≥ 800 ^oC). Similar to what is reported in literature for oxidative conversion of lower paraffins (methane, ethane, propane) [3-9], in the case of hexane we proposed hexane activation on the [Li^+O^-] sites of Li/MgO. The hexyl radical formed then undergoes complex radical chemistry in gas phase in presence of molecular oxygen, forming the product mixture of C_1-C_5 products, including paraffins, olefins and combustion products.

A disadvantage of the Li/MgO is that the active sites of the catalyst are susceptible for deactivation during reaction upon interaction with product CO_2. Stability test of Li/MgO catalyst during oxidative cracking of hexane showed that it suffers from partial deactivation during the first hour of time on stream [2]. This poisoning effect of CO_2 on [Li^+O^-] active sites of Li/MgO has been repeatedly reported in literature [5, 10-11]. During the oxidative coupling of methane Lunsford and co-workers [10] reported that reaction of product CO_2 with [Li^+O^-] results with formation of [$Li^+CO_3^-$] which is most likely converted into the more stable Li_2CO_3 with time. *In situ* FTIR spectra of Li/MgO during the oxidative coupling of methane indicated the presence of adsorbed CO_2 ($O^-.CO_2$) in addition to the presence of stable Li_2CO_3 phase [11]. Similar observations were also made by Galuszka [12]. Li_2CO_3 is not only formed during reaction but is also an inherent property of the catalyst as a result of interaction of ambient CO_2 with Li_2O during the preparation of Li/MgO catalyst [7]. FTIR spectra of freshly prepared Li/MgO catalyst and calcined at 600 ^oC, showed bands attributed to presence of Li_2CO_3 in the catalyst [13].

Unlike in the case of oxidic catalysts with red-ox properties [6], sequential combustion of olefins over Li/MgO is less of a problem. This is due to the non red-ox nature of the catalyst and its lower oxidation capacity. Hence, olefin selectivity over Li/MgO is almost invariant with the hexane conversion levels [2]. Lower oxidation activity also implies that hexane conversions are lower. Therefore, we recently investigated the modification of Li/MgO with small amounts of red-ox promoters [2]. Our objective was to increase catalyst activity by possibly enhancing C-H bond scission in hexane, which is the rate-limiting step. Three promoters were investigated: V_2O_5, Bi_2O_3 and MoO_3. Both MoO_3 and Bi_2O_3 resulted in considerable improvements in the yields of C_2-C_4 olefins, while V_2O_5 resulted in formation of more combustion products [2]. Promotion of Li/MgO with Bi_2O_3 and MoO_3 oxides resulted in an increase in initial hexane conversions as expected and a significant improvement in the

yields of olefins. Moreover, the promoted catalysts were stable probably due to lower carbonate formation [2].

In this chapter we try to understand the role of MoO_3 in improving the yields of light olefins during oxidative cracking of hexane. Our objective is to verify whether MoO_3 enhances C-H bond scission in hexane and to investigate role of MoO_3 in minimizing the concentration of surface carbonates. Optimization of MoO_3 levels is reported.

2.2 Experimental

2.2.1 Materials

Commercially available $Mg(OCH_3)_2$ solution in methanol (Aldrich, 6-8 wt% in methanol), methanol (Merck) and $LiNO_3$ (Aldrich, assay ≥ 99.99%) were used for preparation of MgO and Li/MgO catalysts. Ammonium molybdate (Aldrich, 99.98%) was used as precursor for MoO_3. Pure hexane (Fluka, GC assay ≥ 99.0%) was used for catalytic experiments. MoO_3 (Aldrich, assay 99.99%) was used for TPD experiment.

2.2.2 Catalyst preparation

Sol-gel synthesized MgO and Li/MgO catalysts used in this study were prepared according to the method described in chapter 2. Modified MoO_3-Li/MgO catalysts were prepared by wet impregnation of the sol-gel synthesized Li/MgO using aqueous solution of the ammonium molybdate. The modified catalysts were then dried at 50 °C in vacuum for 7 h and calcined at 600 °C for 5 h with a heating rate of 5 °C/min. Under the conditions used for calcination (600 ^oC) ammonium molybdate completely decomposes to MoO_3. Similarly, MoO_3-MgO catalysts were prepared by the wet impregnation of the sol-gel synthesized MgO.

2.2.3 Sample characterization

BET surface area of the catalyst was determined with nitrogen physisorption using a Micro-metrics Tristar instrument. The samples were out-gassed in vacuum at 250 °C for 24 h prior to the analysis. X-ray diffraction patterns were recorded by a Philips PW 1830 diffractometer using Cu Kα radiation, λ=0.1544 nm. XRD patterns were measured in reflection geometry in the 2θ range between 35° and 50°. Elemental composition of Li was determined with atomic absorption spectroscopy (AAS). MoO_3 loadings were determined with X-ray fluorescence spectroscopy (XRF, Phillips PW 1480 spectrometer). Results are presented in Table 2.1. MoO_3 promoted samples are denoted as xMo-Li and xMo-MgO, where x is wt% of MoO_3.

2.2.4 Catalytic tests

The catalytic tests were carried out at atmospheric pressure and isothermal conditions in a fixed-bed reactor. An alumina tube reactor of 4 mm internal diameter was used. The

catalyst bed (10 mm length) was packed between two quartz-wool plugs in the alumina reactor. Powder catalyst was pressed, crushed and sieved to particle size of 0.4-0.6 mm before use. An alumina rod of 3 mm internal diameter was placed right below the catalytic bed to reduce the post catalytic volume in order to minimize homogenous gas phase reactions. A Chromel-Alumel thermocouple inside a quartz tube was inserted above the catalytic bed to record reaction temperature. The temperature of the furnace was controlled by a second thermocouple placed outside the reactor tube within the isothermal zone of the tubular furnace.

Table 2.1. Surface area (BET) and XRF data of the catalysts.

Catalyst[a]	BET surface area (m^2/g)	MoO_3 wt%	θ %[c]
Li/MgO[b]	106	-	-
0.2Mo-Li	36	0.2	5.2
0.5Mo-Li	70	0.5	6.1
3.6Mo-Li	76	3.6	41.0
7.1Mo-Li	82	7.1	78.2
MgO[b]	195	-	-
0.5Mo-MgO	144	0.5	3.0
3.3Mo-MgO	178	3.3	15.8
7.9Mo-MgO	189	7.9	38.1

[a] Li content in all samples is ~ 0.86wt%
[b] calcined at 500 °C
[c] theoretical surface coverage of Li/MgO by MoO_3 assuming monolayer

Reactions were studied in the temperature range between 475 and 575 °C. Feed (100 ml/min) consisted of 10 mol% of hexane vapor, 8 mol% of oxygen and balance helium. Before each catalytic test, the catalysts were pretreated in 50% O_2/He (60 ml/min) for 1 h at a temperature of 625 °C. For analysis of the product, samples were injected into two micro GCs every 5 min during a period of 5 h. A detailed description of the experimental setup is given elsewhere [2].

Hexane conversions were calculated on carbon mol basis; *i.e.,* (C_6^{in} moles – C_6^{out} moles) / C_6^{in} moles *100%. The carbon balance closed between 100 and 105%. Selectivity to individual products was also calculated based on the number of moles of carbon contained in the products, divided by the total number of moles of carbon in the product mixture excluding unconverted feed; *i.e.,* (n_iC_i / ∑ n_iC_i)* 100%.

2.2.5 Temperature programmed desorption

TPD experiments were performed in the same experimental setup used for catalyst testing. 100 mg of samples were used. Three sets of TPD experiments were conducted. (i) Fresh Li/MgO and MoO_3 promoted catalysts; the fresh catalysts were pretreated in O_2/He at 600

^{o}C for one hour to decompose any $MgCO_3$ present. After cooling the catalysts to 100 ^{o}C in He, TPD was conducted. (ii) Li/MgO; sample was pretreated in O_2/He at 600 °C for 1 h. It was then cooled to 575 ^{o}C and exposed to 50 ml/min of 10% CO_2/He for 1 h. After purging the catalyst in He and cooling down to 100 ^{o}C, TPD was conducted. (iii) MgO and MoO_3; samples were pretreated in O_2/He at 600 ^{o}C for 1 h. They were then exposed to 50 ml/min of 10% CO_2/He and simultaneously allowed to cool down to 100 °C. After purging the samples in He, TPD was conducted. In all experiments TPD was conducted from 100 to 950 ^{o}C (except with MoO_3 from 100 to 800 ^{o}C), with an increment of 10 ^{o}C/min, with He flow of 10 ml/min as a carrier gas. The catalyst sample was allowed to stay at the final temperature for half an hour. The concentration of desorbed CO_2 was determined with the quad micro GC (PPQ column) every 2 min.

2.3 Results

2.3.1 Effect of MoO_3 on BET surface area of the catalyst

Characteristics of the catalysts used in this study are shown in Table 2.1. 0.5 wt% MoO_3 promoted Li/MgO maintained higher surface area (70 m^2/g) upon calcination at 600 °C, than the unpromoted one (15 m^2/g). As shown in Figure 2.1, Li/MgO undergoes a dramatic decrease in surface area upon calcination at temperatures above 500 ^{o}C. This detrimental effect of temperature on surface area is not observed in the case of MgO. The effect of MoO_3 on surface area of Li/MgO was more pronounced for 0.5 wt% and higher MoO_3 loadings, as also shown in Table 2.1. In the presence of MoO_3 the high surface areas were retained after the high temperature heat treatment. In order to confirm the role of MoO_3 in maintaining higher surface area, we impregnated the sol-synthesized Li/MgO with water only and then calcined at 600 ^{o}C, mimicking the procedure of MoO_3 impregnation. The catalyst exhibited very low surface area (8 m^2/g).

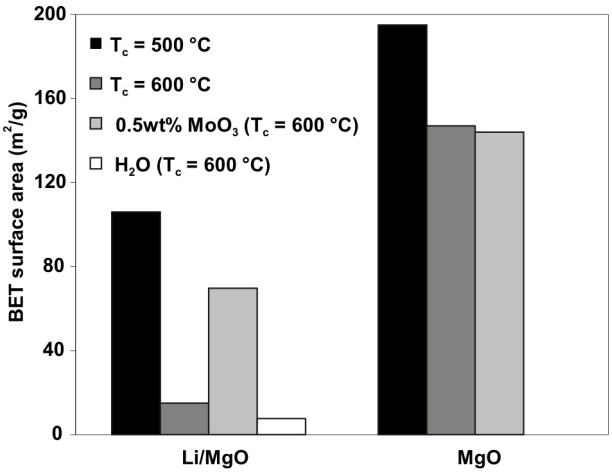

Figure 2.1. BET surface area of Li/MgO and MgO at different calcination temperatures before and after promotion with MoO_3.

Figure 2.2 presents XRD of Li/MgO and MoO_3 promoted catalysts. All catalysts exhibited peaks attributing to MgO. XRD of Mo containing samples did not show any additional peaks to indicate formation of new crystalline phases. Hence, we assume that Mo is present as MoO_3. However, the observed shift in the peak positions in the MoO_3 containing samples compared to Li/MgO might indicate formation of solid solutions between MoO_3 and Li-MgO support.

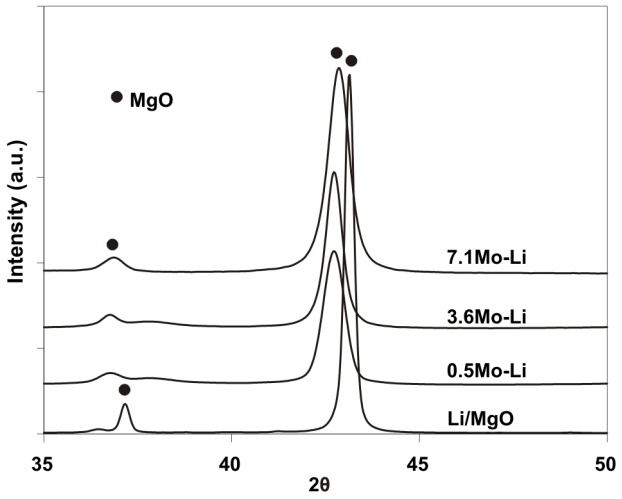

Figure 2.2. XRD of Li/MgO and MoO_3-Li/MgO catalysts.

2.3.2 Temperature programmed desorption

Temperature programmed desorption was performed for Li/MgO and MoO_3 promoted Li/MgO catalysts. Figure 2.3 presents results of these experiments. TPD of Li/MgO exhibited a CO_2 desorption peak at 860 ^oC which is typical for Li_2CO_3 [10]. The presence of Li_2CO_3 (formed with CO_2 from ambient) is an inherent property of Li/MgO [7, 14]. TPD of the MoO_3 promoted catalysts exhibited similar Li_2CO_3 peak, however with lower intensity. This peak continued to decrease with increasing MoO_3 loadings. This confirms the gradual decrease in the amount of Li_2CO_3 in Li/MgO with increasing MoO_3 loading. The small desorption peak observed at around 700 ^oC in both 0.2Mo-Li and 0.5Mo-Li catalysts, is attributed to desorption of adsorbed CO_2 from ambient on $[Li^+O^-]$ active sites $[Li^+CO_3^-]$ of Li/MgO. Li/MgO (see insert) also exhibited similar CO_2 desorption peak at around 650 ^oC. During TPD of CO_2 from Li/MgO, Lunsford and co-workers [10] attributed the CO_2 desorption peak at around 630 ^oC to CO_2 adsorbed on $[Li^+O^-]$ sites. In the high MoO_3 loaded sample (7.1Mo-Li), this was absent indicating the influence of MoO_3 on suppressing all types of carbonates. TPD of CO_2 of MoO_3 showed no significant CO_2 desorption peak, while TPD of MgO showed a broad desorption peak ($MgCO_3$ decomposition) of CO_2 between 100 and 600 ^oC with a maximum at 275 ^oC (see the insert).

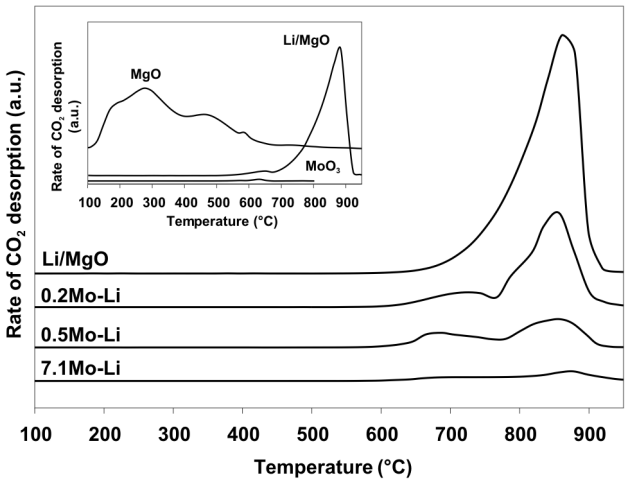

Figure 2.3. Temperature programmed desorption for Li/MgO and MoO_3-Li/MgO catalysts pretreated at 600 °C (Signals are normalized to the BET surface area). TPD of CO_2 for Li/MgO (100 mg), MgO (100 mg) and MoO_3 (100 mg) are included for comparison (see insert). Temperature rate 10 ^oC/min, helium flow 10 ml/min.

2.3.3 Catalytic tests

The influence of varying loadings of MoO_3 on the performance of Li/MgO during the oxidative cracking of hexane was investigated in the temperature range between 475 and 575 ^oC. These results are summarized in Table 2.2. Hexane conversions both initial and after 5 h of time on stream, are reported for each catalyst.

Table 2.2. Performance of Li/MgO and MoO_3-Li/MgO catalysts during oxidative cracking of hexane. Reaction conditions: 100 ml/min, 10% hexane, 8% oxygen and balance helium, WHSV = 15.4 h^{-1}.

	T (°C)	Conversion (mol%)		Selectivity based on C (mol%)[a]					Yields
		C_6H_{14}		O_2	CO_x	C_1^o-C_5^o	$C_2^=$ - $C_4^=$	C_6	$C_2^=$ - $C_4^=$
		Initial	After 5 h						After 5 h
Li/MgO	475	4.3	4.2	38.8	82.5	2.8	14.8	–	0.6
	525	20.3	11.8	42.7	52.1	7.3	40.6	–	4.8
	575	40.0	28.4	65.2	24.6	14.8	60.7	–	17.2
0.2Mo-Li	475	6.4	5.6	38.8	82.8	2.5	14.8	–	0.8
	525	19.7	16.8	77.5	54.9	6.4	38.7	–	6.1
	575	40.7	39.7	99.6	28.2	12.9	58.9	–	23.4
0.5Mo-Li	475	10.7	10.7	56.0	64.2	5.4	30.4	–	3.2
	525	23.2	22.1	76.3	46.9	5.9	47.1	–	9.0
	575	40.4	38.5	99.7	28.1	11.7	60.2	–	23.2
3.6Mo-Li	475	12.1	11.2	91.7	84.4	4.2	11.5	–	1.3
	525	16.6	16.5	99.6	63.8	3.4	32.9	–	5.4
	575	24.0	23.1	99.6	47.3	7.0	45.7	–	10.6
7.1Mo-Li	475	12.5	12.0	96.4	59.0	18.4	5.4	17.2	0.7
	525	13.5	13.0	99.6	61.2	5.9	11.7	21.2	1.5
	575	20.4	19.1	99.6	48.4	6.7	24.6	20.2	4.7

[a] Selectivities after 5 h of reaction

Li/MgO showed deactivation at almost all temperatures; however this was less significant in the case of the promoted catalysts. The addition of 0.5 wt% MoO_3 resulted in higher initial hexane conversions than Li/MgO at almost all temperatures. This was less significant at 575 ^oC due to complete oxygen consumption. In addition, both at 475 and 525 ^oC, the catalyst exhibited higher selectivities to C_2-C_4 olefins than the unpromoted Li/MgO. Both 3.6Mo-Li and 7.1Mo-Li catalysts exhibited higher initial conversions than Li/MgO at 475 ^oC.

However, at 525 and 575 ^oC these catalysts showed high activity for oxygen conversion but not for hexane. As compared to 0.5Mo-Li, catalysts with higher MoO_3 loading, 3.6Mo-Li and 7.1Mo-Li, resulted in low selectivity to C_2-C_4 olefins. This was mainly due to formation of more of combustion products, in addition to the formation of significant amounts of C_6 products in the case of 7.1Mo-Li catalyst. Thus at all temperatures, best yields were observed with 0.5Mo-Li catalyst. 0.2Mo-Li showed almost similar initial hexane conversions as Li/MgO, however, exhibiting better stability during time on stream.

Figure 2.4 shows the selectivities to different products at 575 ^oC for the catalysts Li/MgO, 0.5Mo-Li, 3.6Mo-Li and 7.1Mo-Li, at a similar hexane conversion of 10 mol%. Hexane conversions were maintained by varying WHSV. Both 3.6Mo-Li and 7.1Mo-Li catalysts resulted in formation of more of combustion products, while 0.5Mo-Li showed similar selectivities as Li/MgO. Significant formation of C_6 products was observed in the case of 7.1Mo-Li catalyst. The formation of C_6 products, mainly olefins, suggests the occurrence of dehydrogenation reactions in the case of 7.1Mo-Li catalyst.

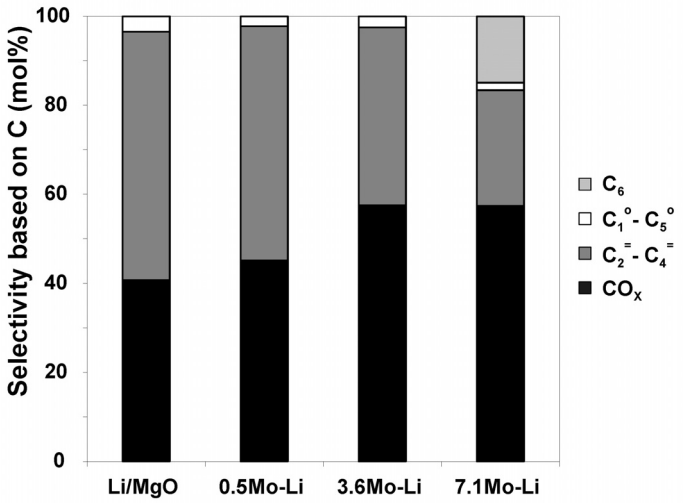

Figure 2.4. Selectivity to products based on C at hexane conversion of 10 mol%. Oxygen conversions = 35 mol% (Li/MgO) , 36 mol% (0.5 Mo-Li), 43 mol% (3.6 Mo-Li) and 53 mol% (7.1 Mo-Li). Reaction conditions: 100 ml/min total flow, 10% hexane, 8% oxygen and balance helium, T= 575 ^oC, WHSV = 154 – 385 h^{-1}.

In order to investigate further the role of MoO_3 on activity and to explore the ability of MoO_3 in C-H bond scission, we compared rates of hexane conversions of MoO_3-Li/MgO catalysts to those of MoO_3-MgO. Figure 2.5 shows rates of hexane conversion normalized to the surface area of each catalyst. Promotion of MgO with MoO_3 did not result in any

improvement in rates of hexane conversion. Moreover, in the case of Li/MgO we observed a decrease in rates of conversion with increasing MoO_3 loadings.

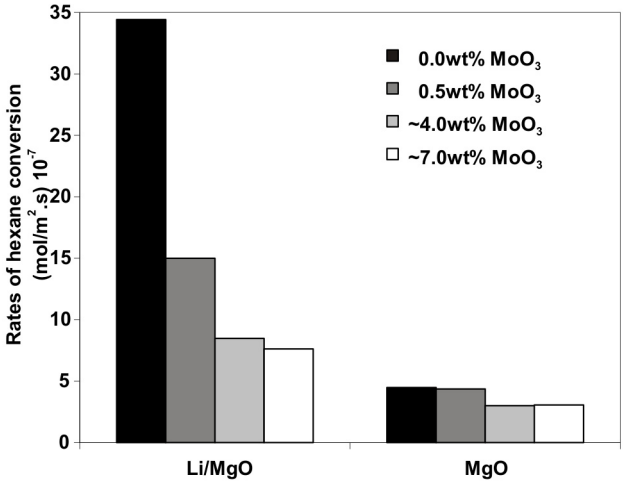

Figure 2.5. Rate of hexane conversion over Li/MgO and MgO before and after promotion with varying loadings of MoO_3 (all experiments were performed in oxygen available conditions). Reaction conditions: 100 ml/min, 10% hexane, 8% oxygen and balance helium, T=575 ^oC, WHSV = 154 h^{-1}.

2.4 Discussion

Oxidative cracking of hexane over Li/MgO, similar to oxidative coupling of methane [3] and oxidative dehydrogenation of lower paraffins over the same catalyst [4-8], is a heterogeneously initiated homogeneous reaction. We have proposed earlier [2] that hexane activation occurs on the catalyst surface *via* the $[Li^+O^-]$ defect sites, where $[O^-]$ abstracts hydrogen from a secondary carbon atom. However, we have also shown that active sites of the catalyst are susceptible for partial deactivation as result of interaction with product CO_2. We have reported earlier [2] that promotion of Li/MgO with small amounts of MoO_3 brings considerable improvement in the yield of C_2-C_4 olefins.

In order to further understand the function of MoO_3 in improving yields of olefins during the oxidative cracking of hexane, we investigated the influence of varying loadings of MoO_3 on the performance of Li/MgO. Amongst all catalysts, only 0.5Mo-Li brought considerable improvements. Li/MgO promoted with 0.5 wt% MoO_3 exhibited higher initial hexane conversions than the unpromoted catalyst. This led to better selectivities to C_2-C_4 olefins, especially at 475 and 525 ^oC, mainly due to increasing the ratio of homogeneous gas phase to heterogeneous surface reactions. We reported earlier that gas phase reactions are more selective while interaction of intermediate radicals with surface $[O^{2-}]$ sites of the catalyst leads to complete oxidation and CO_x formation [2]. However, increasing MoO_3 loadings, *i.e.,* above 0.5 wt%, influenced the performance of Li/MgO negatively, as result of unselective combustion reactions which competitively consumed the oxygen in the reactant mixture, limiting hexane conversions. We have reported earlier on the significance of oxygen in increasing rates of hexane conversions [2]. In addition to combustion reactions, in the case of 7.1Mo-Li activity for dehydrogenation reactions has been as well observed. Generally,

molybdenum based catalysts are extensively studied in literature for the oxidative dehydrogenation of C_2-C_4 paraffins [15-17]. Mo/MgO catalysts are reported as selective catalysts for dehydrogenation of propane and butane [18-19]. We suggest in the case of 7.1Mo-Li catalyst, the subsequent interaction of hexyl radicals with MoO_3, where the later abstracts a second hydrogen atom resulting in dehydrogenation.

Since promotion of MgO with comparable MoO_3 loadings as in Li/MgO, did not bring any considerable improvements in rates of hexane conversions (Figure 2.5), we suggest that in our catalysts MoO_3 does not enhance C-H bond scission in hexane. Yoon *et al.* [20] reported that catalyst with excess Mo on MgO exhibited reasonable activity during oxidative dehydrogenation of propane. Similarly, Oganowski *et al.* [21] reported for dehydrogenation of ethylbenzene to styrene over Mo-MgO catalysts, that catalysts containing excess of MoO_3 on $MgMoO_4$ are most active. Vrieland *et al.* [22] reported that optimum catalyst for non-oxidative dehydrogenation of butane to butadiene consists of 15-25 wt% of MoO_3. Most probably the MoO_3 loadings in our catalysts were too low for effective C-H bond scission in hexane.

In comparison to Li/MgO the improved initial hexane conversions with all catalysts at 475 ^oC, and at 525 ^oC with the 0.5Mo-Li catalyst (Table 2.2) is explained mainly by the higher surface area of the promoted catalyst. As shown in Figure 2.1, Li/MgO undergoes a detrimental decrease in surface area upon calcination at temperatures above 500 ^oC. Since this is not observed in MgO, we believe that sintering of Li/MgO is enhanced by the presence of Li_2CO_3. Li_2CO_3 makes the catalyst susceptible for sintering at calcination temperatures above 500 °C [23]. It was reported by Trionfetti *et al*. [7], that during the sol-gel synthesis of Li/MgO only 40% of Li incorporates into MgO and the rest stays behind as Li_2O which interacts with ambient CO_2 to form Li_2CO_3. BET N_2 physisorption results in Table 2.1 show that an optimum MoO_3 loading of 0.5 wt% is sufficient to maintain high surface area upon calcination at temperatures above 500 ^oC. The higher surface area of the MoO_3 promoted catalyst most likely is attributed to the role of MoO_3 in minimizing these carbonates. The gradual decrease in CO_2 desorption peak area due to Li_2CO_3 with the increase in MoO_3 loadings, as observed from TPD experiments (Figure 2.3), confirm the presence of less Li_2CO_3 in MoO_3 promoted catalysts. These results suggest the possible interaction of MoO_3 with Li_2CO_3. XRD (Figure 2.2) of MoO_3 promoted Li/MgO showed a shift in the peak positions compared to Li/MgO, which might indicate the formation of solid solutions between MoO_3 and Li-MgO support. However, no additional peaks indicating the presence of new phases were present. Raman spectroscopy and temperature programmed techniques will be useful to identify, as function of Mo loadings, the nature of interaction of Mo with the support, thus the phases present.

Further as reported earlier by us [2], the significantly higher yields of olefins after longer time on stream in the case of 0.5Mo-Li catalyst is result of the better stability of the catalyst in comparison to Li/MgO. This illustrates the role of MoO_3 in minimizing the adsorption of product CO_2 during reaction on $[Li^+O^-]$ sites of Li/MgO, thus preventing the poisoning of the active sites.

Our results indicate that during the oxidative cracking of hexane, a minimum loading of MoO_3 (~0.5 wt%) on Li/MgO is sufficient to modify the catalyst, maintaining both higher surface area and better stability, hence leading to improved yields of C_2-C_4 olefins. Despite of the improvement of Li/MgO catalyst by promotion with MoO_3, we speculate that MoO_3 blocks some of the $[Li^+O^-]$ active sites in Li/MgO. This suggestion is based on the observed

decrease in rates of hexane conversion normalized to surface area in the promoted catalyst as compared to the unpromoted one.

2.5 Conclusions

The influence of varying loadings of MoO_3 on the performance of Li/MgO in oxidative cracking of hexane has been studied. Catalyst with 0.5 wt% MoO_3 loading exhibits optimal yields of C_2-C_4 olefins. This is a result of improved hexane conversions both initially as well as after time on stream, and of improved selectivities to olefins. Increasing MoO_3 loadings influences yields of olefins negatively as result of increasing combustion, as well as increasing yields of C_6 products in the case of 7 wt% MoO_3. The results also indicate that, during oxidative cracking of hexane, promotion of Li/MgO with 0.7 wt% and lower MoO_3 loadings does not enhance C-H bond scission in hexane. Apparently these loadings are too low for the catalyst to act as an effective dehydrogenation catalyst.

We conclude that promotion of Li/MgO with a minimum loading of MoO_3 of around 0.5 wt% is sufficient to bring the following advantages; (i) minimize the amount of Li_2CO_3 originally present in Li/MgO, thus promoting the catalyst to maintain higher surface area upon calcination at 600 ^oC, and (ii) prevent the poisoning of the $[Li^+O^-]$ by product CO_2 during reaction, improving the stability of the catalyst.

References

[1] Y. Yoshimura, N. Kijima, T. Hayakawa, K. Murata, K. Suzuki, F. Mizukami, K. Matano, T. Konishi, T. Oikawa, M. Saito, T. Shiojima, K. Shiozawa, K. Wakui, G. Sawada, K. Sato, S. Matsuo, N. Yamaoka, Catal. Surv. Jpn. 4 (2) (2000) 157-167.

[2] C. Boyadjian, L. Lefferts, K. Seshan, Appl. Catal. A 372 (2010) 167-174.

[3] T. Ito, J.-X. Wang, C.-H. Lin, J.H. Lunsford, J. Am. Chem. Soc. 107 (1985) 5062-5068.

[4] L. Leveles, K. Seshan, J.A Lercher, L. Lefferts, J. Catal. 218 (2003) 307-314.

[5] S. Fuchs, L. Leveles, K. Seshan, L. Lefferts, A. Lemonidou, J.A Lercher, Top. Catal. 15 (2-4) (2001) 169-174.

[6] F. Cavani, F. Trifiro, Catal. Today 24 (1995) 307-313.

[7] C. Trionfetti, I.V Babich, K. Seshan, L. Lefferts, Appl. Catal. A 310 (2006) 105-113.

[8] C. Trionfetti, S. Crapanzano, I.V. Babich, K. Seshan, L. Lefferts, Catal. Today 145 (1-2) (2009) 19-26.

[9] L. Leveles, K. Seshan, J.A. Lercher, L. Lefferts, J. Catal. 218 (2003) 296-306.

[10] M. Xu, C. Shi, X. Yang, M.P. Rosynek, J.H. Lunsford, J. Phys. Chem. 96 (15) (1992) 6395-6398.

[11] S.C. Bhumkar, L. L. Lobban, Ind. Eng. Chem. Res. 31 (1992) 1856-1864.

[12] J. Galuszka, Catal. Today 21 (1994) 321-331

[13] J.L. Boldu, E. Munoz, X. Bokhimi, O. Novaro, T. Lopez, R. Gomez, Langmuir 15 (1999) 32-35.

[14] S.J. Korf, J.A. Roos, N.A. de Bruijn, J.G. van Ommen, J.R.H. Ross, Catal. Today 2 (1988) 535-545.

[15] F. Cavani, N. Ballarini, A. Cericola, Catal. Today 127 (2007) 113-131.

[16] E. Heracleous, A.F. Lee, I.A. Vasalos , A.A. Lemonidou, Catal. Lett. 88 (1-2) (2003) 47-53.

[17] J.M. Lopez Nieto, P. Botella, M.I Vazquez, A. Dejoz, Chem. Commun. 8 (17) (2002) 1906-1907.

[18] A. Dejoz, J.M. Lopez Nieto, F. Marquez, M.I. Vazquez, Appl. Catal. A 180 (1999) 83-94.

[19] J.D. Pless, B.B. Bardin, H.-S. Kim, D. Ko, M.T. Smith, R.R. Hammond, P.C. Stair, K.R. Poeppelmeier, J. Catal. 223 (2004) 419-431.

[20] Y. S. Yoon, W. Ueda, Y. Moro-oka, Catal. Lett. 35 (1995) 57-64.

[21] W. Oganowski, J. Hanuza, B. Jezowska-Trzebiatowska, J. Wrzyszcz, J. Catal. 39 (1975) 161.

[22] G.E. Vrieland, C.B. Murchison, Appl. Catal. A 134 (1996) 101-121.

[23] V. Perrichon, M.C. Durupty, Appl. Catal. 42 (1988) 217-227.

Chapter 3

Structure and Performance of Li/MgO Supported Molybdenum Oxide for the Oxidative Cracking of n-Hexane

Mo promoted Li/MgO is studied as catalyst for the oxidative cracking of n-hexane. Structural details are investigated with XRD, XPS, TPR and Raman spectroscopy. Mo/Li/MgO catalyst contains three types of molybdena containing phases i.e. (i) monomeric $Mg[MoO_4]$, $Li_2[MoO_4]$, in which Mo is tetrahedrally coordinated, (ii) polymeric species such as $Li_2Mo_4O_{13}$ in which Mo is octahedrally coordinated, and (iii) a dispersed amorphous lithium molybdate phase in which Mo is also octahedrally coordinated. The amorphous lithium molybdate species are proposed to enhance catalyst stability by hindering Li_2CO_3 formation from catalytically active $[Li^+O^-]$ sites during oxidative cracking reaction. However, higher Mo contents lead to phases that do not contribute to catalytic activity or form dispersed phases that enhance combustion. 0.3 wt% Mo promoted Li/MgO catalyst is efficient for the selective conversion of hexane to olefins, giving olefin yield up to 24%, and excellent stability with time on stream.

3.1 Introduction

Supported molybdena catalysts have been studied often for the oxidative dehydrogenation of light alkanes, *e.g.,* ethane, propane, and butane [1-12]. It has been suggested [5-6] that the oxidation of the C-H bond in the alkane proceeds *via* a Mars and van Krevelen red-ox mechanism with participation of molybdena lattice oxygen, followed by re-oxidation with gas phase oxygen. Various molybdenum oxide systems have been reported, *e.g.,* supported on MgO, ZrO_2, Al_2O_3, TiO_2 and SiO_2 [6, 9-10, 13-17]. Generally the performance of molybdena based catalysts is related to the extent of crystallinity and chemical structure of the oxidic molybdena species on the support, for *e.g.,* free MoO_3, monomeric MoO_4^{2-} or polymeric $Mo_6O_{19}^{2-}$, $Mo_7O_{24}^{-6}$ units [6, 9, 15]. Hence, structure-performance correlations for supported molybdena catalysts have been of continuous interest.

Mo/MgO is reported to be efficient and selective catalyst for the oxidative dehydrogenation of C_3-C_4 alkanes to corresponding olefins [7-8]. It is reported by Bare and co-workers [15-17] that, in the case of Mo/MgO catalysts, the structure of the molybdena species depends on the molybdenum coverage of the support. For sub monolayer coverages, dispersed species are observed. These consist of highly distorted octahedral molybdena species, *e.g.,* MoO_6, at low molybdenum loadings and regular octahedrally coordinated polymolybdate species, *e.g.,* $[Mo_7O_{24}]^{6-}$, at high molybdenum loadings [15]. For coverages exceeding the monolayer, crystalline magnesium molybdate ($MgMoO_4$), where Mo is tetrahedrally coordinated, is observed as dominant species. Raman spectroscopic studies [13, 15] showed that for the magnesium oxide supported catalysts surface molybdena species are sensitive to hydration. Upon exposure to water, octahedrally coordinated molybdenum species, transform to tetrahedrally coordinated MoO_4^{2-} species.

Generally, the activity of the Mo/MgO system for the oxidative dehydrogenation of low alkanes, depends on the Mo loading [11-12]. It has been reported by Yoon *et al.* [11] that excess of Mo (18 wt%) resulted in high propane conversion (22% conversion at 515 °C). Vrieland and Murchison [12] reported that catalyst with highest activity for non-oxidative dehydrogenation of butane to butadiene (50% of n-butane conversion) contained 17 wt% of Mo. Unfortunately, these catalysts cause significant amount of combustion during oxidative conversions. The high oxidation activity in these catalysts is due to their facile red-ox properties, where the cation undergoes a change in the oxidation state easily (*e.g.,* Mo^{6+} to Mo^{4+}). Thus for the oxidative dehydrogenation/cracking reactions, limiting oxygen activity is essential for minimizing combustion and improving olefin yields.

We have shown earlier that Li/MgO is a promising catalyst for the oxidative dehydrogenation/cracking of lower alkanes [22-25]. This catalyst has no formal red-ox character, *i.e.,* Li^+ and Mg^{2+} are not susceptible to oxidation state changes during above reactions, and together with its inherent strong Bronsted basicity, minimizes re-adsorption and sequential combustion of formed olefins [22-25]. It has been established through the work of Lunsford [19-21] on the oxidative coupling of methane that $[Li^+O^-]$ type defect sites are responsible for catalytic activity. The nucleophilic $[O^-]$ site is strong hydrogen abstractor and initiates alkane activation *via* homolytic scission of C-H bond in the alkane forming a radical. There is general agreement that this is the rate determining step [21, 23, 26]. The formed radical then undergoes a complex set of reactions in the gas phase in presence of oxygen forming alkenes, alkanes as well as combustion products, like H_2O and CO_x [22-26].

Recently we reported [27] on the oxidative cracking of hexane over Li/MgO catalyst. In general, combustion selectivities were lower for Li/MgO compared to other catalysts containing oxides with facile redox properties, *e.g.,* V_2O_5/MgO [27]. The low oxidation activity of the Li/MgO catalyst resulted in lower hexane conversions at typical reaction temperatures (500-600 ^oC) studied [27]. Further, Li/MgO catalysts deactivated during time on stream due to the poisoning effect of the product CO_2 on the [Li^+O^-] active catalytic sites [21, 23]. In order to improve performance of Li/MgO, promotion with low amounts of oxides were attempted [27]. Molybdena promoted Li/MgO showed the best olefin yields. Significantly, the presence of molybdena also prevented deactivation and catalyst stability was restored [27-28].

In this chapter, detailed characterization of the Mo/Li/MgO catalysts is attempted in order to identify the chemical structure of the different molybdena species (MoO_x) evolving on the surface of Li/MgO. Our objective is to correlate the presence of the different molybdena species and their influence on (i) hexane conversion, (ii) olefin *vs* combustion selectivity and (iii) deactivation. This is expected to help establish guidelines for developing an optimal catalyst for the oxidative cracking of hexane.

3.2 Experimental

3.2.1 Materials

$Mg(OCH_3)_2$ solution in methanol (Aldrich, 6-8 wt% in methanol), methanol (Merck) and $LiNO_3$ (Aldrich, assay ≥ 99.99%) were used for preparation of MgO and Li/MgO catalysts. Ammonium molybdate (Aldrich, 99.98%) was used as Mo precursor. Pure hexane (Fluka, GC assay ≥ 99.0%) was used for catalytic experiments. The reference compounds Li_2MoO_4 (Aldrich, assay ≥ 99.99%) and Li_2CO_3 (Aldrich, assay ≥ 99.0%) were used as received.

3.2.2 Catalyst preparation

MgO and Li/MgO catalysts used in this study were prepared according to the method described in chapter 2. Modified Mo/Li/MgO catalysts were prepared by wet impregnation of the sol-gel synthesized Li/MgO using aqueous solution of the ammonium molybdate. These were then dried at 50 °C in vacuum for 7 h and calcined at 600 ^oC for 5 h with a heating rate of 5 ^oC/min. Similarly, Mo/MgO catalysts were prepared with wet impregnation of the sol-gel synthesized MgO. Mo promoted samples are denoted as xMo/Li/MgO and xMo/MgO, where x is wt% of Mo.

3.2.3 Catalyst characterization

BET surface area of the catalyst was determined with nitrogen physisorption using a Micro-metrics Tristar instrument. X-ray diffraction patterns were recorded with a Philips PW 1830 diffractometer using Cu Kα radiation, λ=0.1544 nm. Elemental composition of the catalysts was determined with atomic absorption spectroscopy (AAS). Li content in all the catalysts

was 0.86 wt%. Mo loadings were determined with X-ray fluorescence spectroscopy (XRF, Phillips PW 1480 spectrometer).

Raman spectral measurements were conducted with a SENTERRA instrument equipped with a cooled CCD detector (-60 ^{o}C). The samples were excited with 785 nm red laser of 100 mW power. Spectra were recorded at room temperature from 100 to 1000 cm^{-1}, at a resolution of 3 cm^{-1} and a 5 min integration time. In the case of Raman measurements to characterize reduction-oxidation changes, samples were pretreated externally; *i.e.,* reduced in hydrogen at 700 ^{o}C and re-oxidized in air at 600 ^{o}C.

X-ray photoelectron spectra were recorded *ex-situ* on a Physical Electronics Quantera XPS system using a monochromatic Al Kα (1486.6 eV). Peak shape fitting was performed with Gaussian-Lorentzian sum function and Shirley background [29] subtraction with constraints applied to full width, half maximum (FWHM) values. All binding energies were referenced against C (1s) peak at 285.0 eV.

Reducibility of the catalysts was probed using a temperature programmed reduction unit equipped with thermal conductivity detector. 200 mg of catalyst sample was pretreated at 600 ^{o}C in 5%O_2/He (20 ml/min) for 1 h. Afterwards the sample was allowed to cool down to 100 ^{o}C in He. TPR was performed by heating the catalyst sample to 700 ^{o}C at a rate of 5 ^{o}C/min in 5%H_2/Ar flow (20 ml/min).

Pulse reduction-oxidation experiments were carried out in a quartz reactor (ID 2 mm) at atmospheric pressure. The catalyst was first reduced at 550 ^{o}C in 10% H_2/He (15 ml/min) for 1 h. After purging the sample in He for 30 min, pulses of 2% O_2/He (loop volume 300 µl) were sent through the catalytic bed. The O_2 signal (m/z=32) was monitored by on-line QMS (Omnistar). This allowed estimation of oxygen uptake by the catalyst with an error of ±5%.

3.2.4 Catalytic tests

The catalytic tests were carried out at atmospheric pressure and isothermal conditions in a fixed-bed reactor [27]. An alumina tube reactor of 4 mm internal diameter was used. Powder catalyst was pressed, crushed and sieved to particle size of 0.4-0.6 mm before use. An alumina rod of 3 mm internal diameter was placed right below the catalytic bed to reduce the post catalytic volume in order to minimize homogenous gas phase reactions. A Chromel-Alumel thermocouple inside a quartz tube was inserted above the catalytic bed to record reaction temperature. The temperature of the furnace was controlled by a second thermocouple placed outside the reactor tube within the isothermal zone of the tubular furnace.

Reactions were studied at 575 ^{o}C. Feed (100 ml/min) consisted of 10 mol% of hexane vapor, 8 mol% of O_2 and balance helium. Similar hexane conversions were achieved by varying WHSV. Before each catalytic test, the catalysts were pretreated at 625 ^{o}C in 50% O_2/He (60 ml/min) for 1 h. For analysis of the product, samples of outlet gas stream were injected into two micro GCs (Varian CP4900) every 5 min during a period of 5 h. The first micro GC was a quad system consisting of four channels for the separation of O_2, N_2, CH_4 CO, CO_2, H_2O, C_2-C_4 hydrocarbons (alkanes and olefins). The second micro GC was a dual system consisting of two channels for the separation of He, H_2 and C_6-C_8 hydrocarbons (alkanes and olefins).

Hexane conversions were calculated on carbon mol basis; *i.e.,* (C_6^{in} moles – C_6^{out} moles) / C_6^{in} moles x 100%. The carbon balance closed between 100 and 105 %. Selectivity to individual products was also calculated based on the number of moles of carbon contained in the products, divided by the total number of moles of carbon in the product mixture excluding unconverted feed; *i.e.,* (n_iC_i / ∑ n_iC_i) x 100%.

3.3 Results

3.3.1 Surface area and XRD

The characteristics of catalysts studied are presented in Table 3.1. It is observed that Li/MgO suffered a dramatic decrease in surface area upon calcination at 600 °C (15 m^2/g), while in the presence of Mo high surface areas (70 - 82 m^2/g) were retained. In case of MgO, the loss in surface area upon calcination at 600 °C was less severe. Nevertheless, promotion with ≥ 2.2 wt% of Mo, resulted in even higher surface areas than the unpromoted sample calcined at 600 °C (148 m^2/g).

The MoO_x surface coverages (θ) of Mo promoted catalysts shown in Table 3.1 were calculated based on the surface area of the catalyst and using 22 $Å^2$ as the mean surface area occupied by one Mo^{6+} oxide unit (MoO_3) [5]. Values indicated sub monolayer coverage for all samples studied.

Table 3.1. Properties of the catalysts.

Catalyst	BET surface area (m^2/g)	Mo loading (wt%)	θ[c] (%)
Li/MgO[a]	106	–	–
Li/MgO[b]	15	–	–
0.3Mo/Li/MgO[b]	70	0.3	7
2.4Mo/Li/MgO[b]	76	2.4	45
4.7Mo/Li/MgO[b]	82	4.7	86
MgO[a]	195	–	–
MgO[b]	148	–	–
0.3Mo/MgO[b]	144	0.4	3
2.2Mo/MgO[b]	178	2.2	17
5.3Mo/MgO[b]	189	5.3	42

[a] calcined at 500 °C
[b] calcined at 600 °C
[c] surface coverage of Li/MgO by MoO_x

Figure 3.1 presents the XRD patterns of the catalysts. All catalysts exhibited peaks which are characteristic for crystalline MgO. The absence of peaks corresponding to any other crystalline phases, confirms that MoO_x is present in a well dispersed form in agreement with the sub monolayer coverage. Also, no peaks corresponding to any crystalline Li phases, *e.g.,* Li_2CO_3, were observed. The observed shift in the MgO peak positions in the Mo containing

samples may be an indication for the formation of solid solutions between MoO_x and Li/MgO. This was further investigated by characterization of the catalysts with Raman spectroscopy.

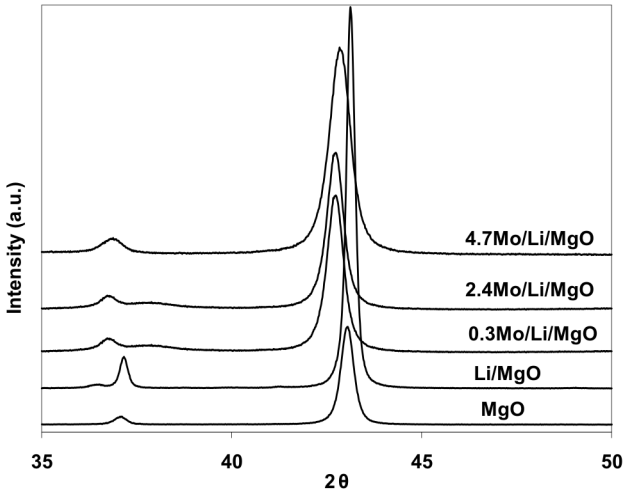

Figure 3.1. XRD patterns of Li/MgO and Mo/Li/MgO catalysts.

3.3.2 Temperature programmed reduction (TPR) and XPS

TPR profiles of Li/MgO and Mo/Li/MgO catalysts are presented in Figure 3.2.a. Li/MgO did not show any reduction up to 700 ^oC, which confirms the non red-ox nature of this catalyst. 0.3Mo/Li/MgO exhibited similar reduction behavior as Li/MgO. 2.4Mo/Li/MgO and 4.7Mo/Li/MgO catalysts exhibited clear reduction peaks at 535 ^oC and 600 ^oC, respectively.

Figure 3.2.b presents the TPR profiles of both Mo/Li/MgO and Mo/MgO systems at comparable Mo loadings. Both systems exhibited similar reduction profiles, however, in comparison to Mo/MgO, Mo/Li/MgO showed a higher degree of reduction. This could either be the result of a difference in MoO_x dispersion [30] or due to the presence of new phases in the Mo/Li/MgO system.

Figure 3.2.c shows the TPR profile of Li_2MoO_4 reference sample. Li_2MoO_4 showed a reduction peak at 685 ^oC.

Figures 3.3 and 3.4 show XPS spectra of fresh, used (after catalytic test at 575 ^oC) and reduced (after TPR, 700°C) (i) 2.4Mo/Li/MgO (Figure 3.3) and (ii) 4.7Mo/Li/MgO (Figure 3.4) catalysts, respectively. 0.3Mo/Li/MgO did not show clear XPS spectra and are not discussed here. In the fresh and tested samples of 2.4Mo/Li/MgO and 4.7Mo/Li/MgO a Mo 3d doublet located at 231.9 ($3d_{5/2}$) and 235.2 ($3d_{3/2}$) eV was observed. This corresponds to the Mo $3d_{5/2}$ – Mo $3d_{3/2}$ doublet of Mo^{6+} (232.6 and 235.8 eV) [31]. Since both fresh and tested catalysts showed similar XPS spectra, it is confirmed that after hexane cracking reactions, the molybdenum valence state in Mo/Li/MgO catalysts is regained.

XPS spectra of the two catalysts after TPR, showed the presence of an additional Mo 3d doublet located at 229.5 and 232.5 eV. This was more significant in the 4.7Mo/Li/MgO

catalyst and corresponds to the Mo $3d_{5/2}$ – Mo $3d_{3/2}$ doublet of Mo^{4+} (229.7, 232.9 eV) [31]. These results suggest that the reduction peak observed in TPR of both 2.4Mo/Li/MgO and 4.7Mo/Li/MgO catalysts (Figure 3.2.a) is possibly attributed to partial reduction of Mo^{6+} to Mo^{4+}. The presence of Mo^{6+} doublet in the reduced samples is not surprising as samples were exposed to ambient for *ex-situ* XPS measurement.

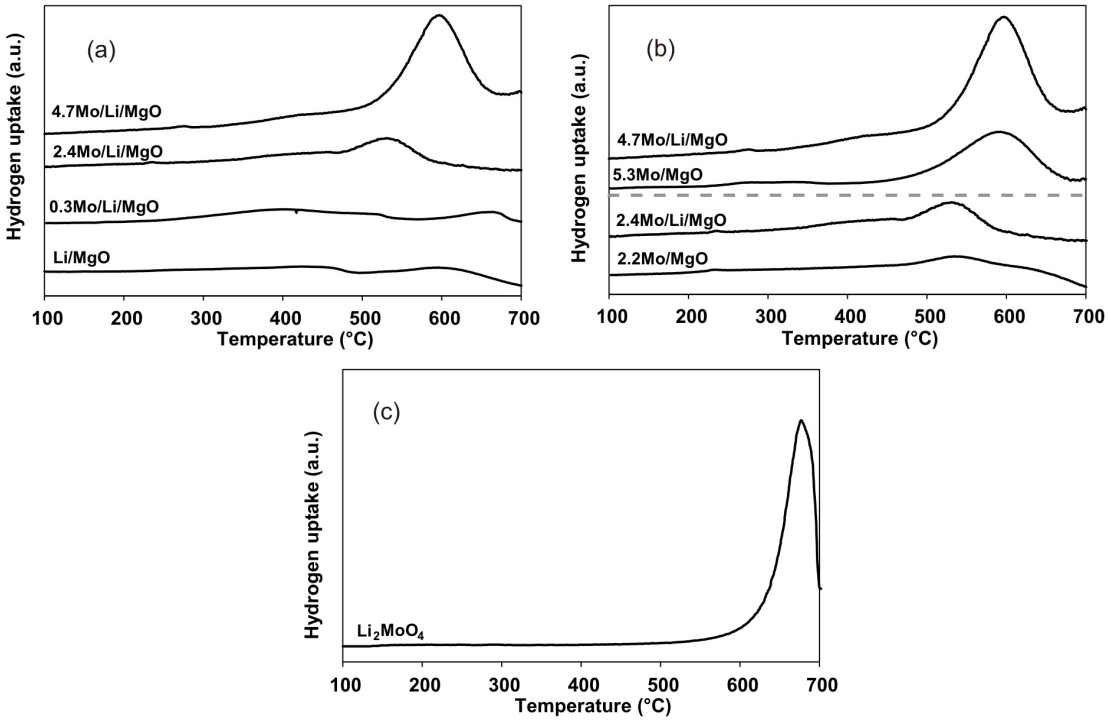

Figure 3.2. TPR profiles of Li/MgO as function of Mo loading (a), Mo/MgO in comparison to Mo/Li/MgO (b), and Li_2MoO_4 reference sample (d).

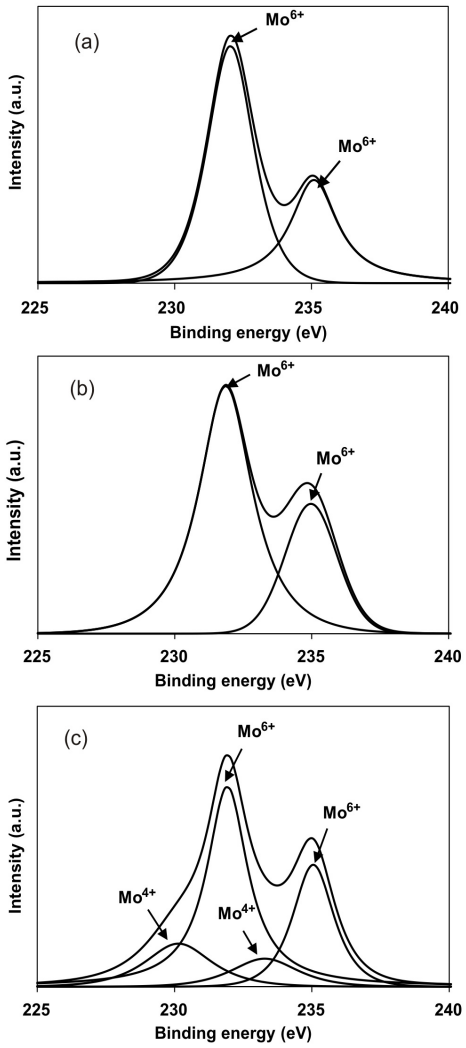

Figure 3.3. XPS spectra of 2.4Mo/Li/MgO catalyst; fresh (a), after catalytic test (b), and after TPR (c).

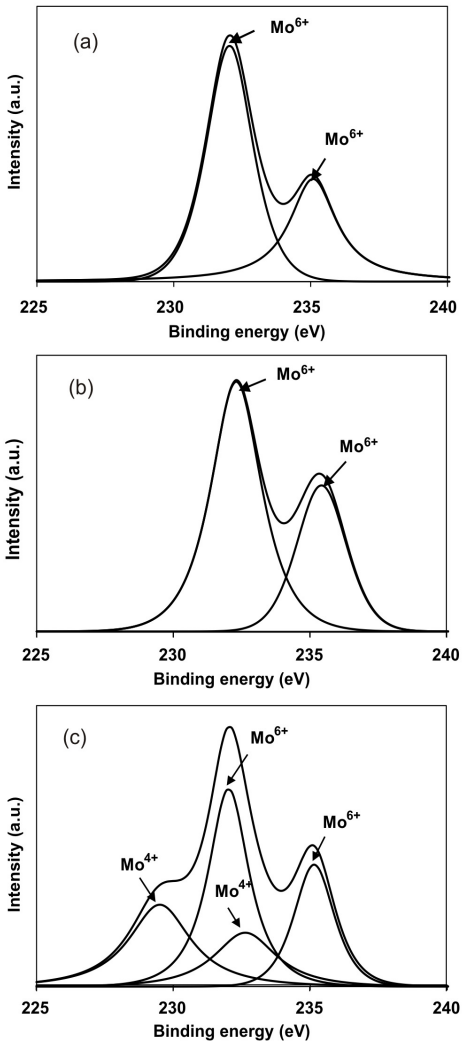

Figure 3.4. XPS spectra of 4.7Mo/Li/MgO catalyst; fresh (a), after catalytic test (b), and after TPR (c).

3.3.3 Raman spectroscopy

Figure 3.5 shows the Raman spectra of Li/MgO catalyst as a function of Mo loading. Reference data from literature are given in Table 3.2. The Raman band at 800 cm^{-1} is characteristic in all samples (Figure 3.5) and also appears in the Raman spectra of MgO in Figure 3.6. This band is not observed in any of the Raman spectra of MgO reported in literature [32]. Thus, the presence of such a band in our catalysts should relate to the sol-gel synthesized MgO support.

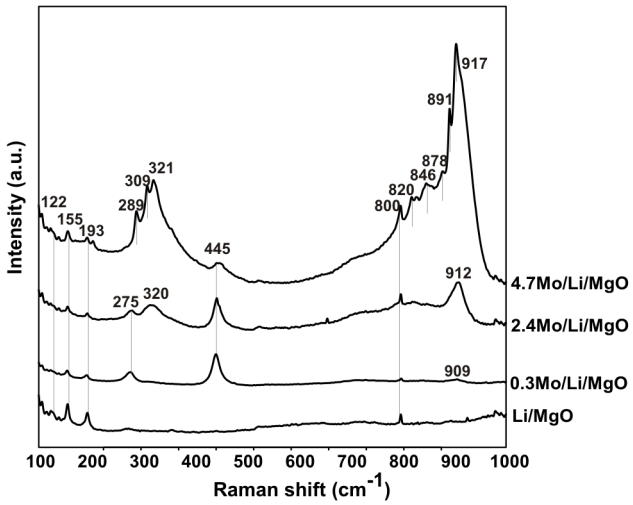

Figure 3.5. Raman spectra of molybdenum oxide supported on Li/MgO as a function of loading of Mo.

The Raman bands 122, 155, 193 cm^{-1} appearing in Li/MgO are characteristic for lattice vibrations in Li_2CO_3 (see Table 3.2). Raman spectra of the molybdenum containing catalysts showed significantly lower amounts of Li_2CO_3. These results are consistent with our previous findings [28] *via* temperature programmed desorption of CO_2, and confirm the role of Mo in lowering the amount of Li_2CO_3 in Li/MgO.

Upon promotion of Li/MgO with 0.3 wt% Mo, Raman bands at 275, 445, 909 cm^{-1} were observed. The Raman bands at 275 and 445 cm^{-1} appear only when Mo is present but surprisingly correspond to the lattice vibration and Mg-O stretching vibration in $Mg(OH)_2$, respectively [15]. With increasing Mo amount, the band at 909 cm^{-1} increased in intensity and shifted to 912 cm^{-1} and 917 cm^{-1} (shoulder) for 2.4Mo/Li/MgO and 4.7Mo/Li/MgO catalysts, respectively. The above characteristic changes are more clearly observed in the case of Mo/MgO catalysts shown in Figure 3.6. With increasing Mo amount, also here the band at 909 cm^{-1} increased in intensity and shifted to 912 and 917 cm^{-1}, for 2.2Mo/MgO and 5.3Mo/MgO, respectively, similar to the corresponding Mo/Li/MgO samples. These bands display close resemblance to those of Mo/MgO calcined at 600 ^{o}C and exposed to water saturated air as reported by Bare and co-workers (see Table 3.2) [15].

Table 3.2. Reference Raman data of Li_2CO_3 and 4.5wt%Mo/MgO.

	Raman shift (cm^{-1})	Compound	Vibration	Reference
Li_2CO_3[a]	122		lattice vibration	G. Li *et al.* [36]
	155		lattice vibration	
	193		lattice vibration	
	268		lattice vibration	
4.5wt%Mo/MgO[b]	275	$Mg(OH)_2$	lattice vibration	Bare *et al.* [15]
	320	MoO_4^{2-}	Mo-O_t bending	
	445	$Mg(OH)_2$	Mg-O stretching	
	870	MoO_4^{2-}	Mo-O_t asym	
	905	MoO_4^{2-}	Mo-O_t sym	

[a] our measurement

[b] calcined at 600 ^oC and exposed to water saturated air for 16 h [15]

In agreement with Bare and co-workers [15], we assign the Raman bands at 912, 874, 320 cm^{-1} in the 2.2Mo/MgO and the bands at 917, 874, 325 cm^{-1} in the 5.3Mo/MgO, to respectively the symmetric, asymmetric stretching and bending modes, of terminal Mo-O_t in tetrahedrally coordinated MoO_4^{2-} species.

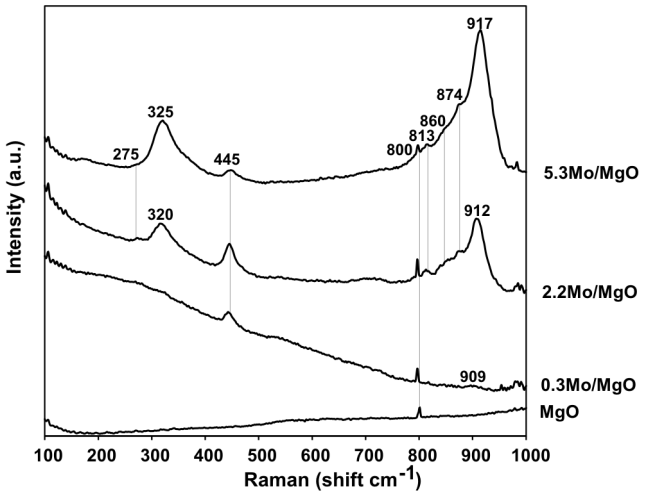

Figure 3.6. Raman spectra of molybdenum oxide supported on MgO as a function of loading of Mo.

Usually in Mo/MgO systems, a Raman band at 220 cm^{-1} is characteristic of heptamolybdates [15, 33]. The absence of this band in all the spectra (Figure 3.5 and 3.6), indicates the absence of well defined polymolybdate species in our systems. In the Raman spectra of 4.5 - 8.9 wt% Mo supported on MgO, calcined at 600 ^oC in dry air, Bare and co-workers [15] attributed Raman bands at 807 and 860 cm^{-1} to Mo-O-Mg vibrations. The

Raman band in our case at 813 cm^{-1} and the shoulder at 860 cm^{-1} in both 2.2Mo/MgO and 5.3Mo/MgO (Figure 3.6) is therefore probably due to Mo-O-Mg vibration.

Generally, the Raman spectra of Mo/Li/MgO catalysts showed close resemblance to that of Mo/MgO catalysts. Therefore, we conclude the presence of similar monomeric MoO_4^{2-} species in all Mo/Li/MgO catalysts. The catalyst with highest Mo loading, 4.7Mo/Li/MgO, however showed additional Raman bands at 289, 309, 820, 846, 878, 891 and 904 cm^{-1} (see Figure 3.5). These were absent in the corresponding 5.3Mo/MgO catalyst, and will be discussed later.

Further, to investigate the structural changes of Mo/Li/MgO catalysts during oxidative cracking reaction; *i.e.,* during reduction and oxidation, we studied the Raman spectra of the 4.7Mo/Li/MgO catalyst after reduction and then after subsequent oxidation. Figure 3.7 shows the Raman spectra of the fresh, reduced and re-oxidized 4.7Mo/Li/MgO catalyst as a typical example.

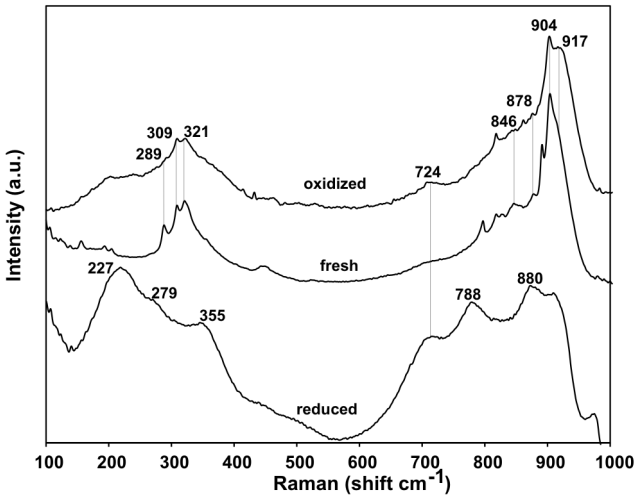

Figure 3.7. Raman spectra of fresh, reduced, and re-oxidized 4.7Mo/Li/MgO catalyst.

The reduced catalyst showed Raman bands at 227, 279, 355, 788 and 880 cm^{-1} which were absent in the fresh catalyst. Raman bands at 227 and 350cm^{-1} are typical for heptamolybdates [15, 33]. We assign these to the presence of heptamolybdate phase in the reduced catalyst. Raman bands in the range 750-860 cm^{-1} after reduction, have been reported to be due to $Mo^{5+,4+}$-O-Al group in the case of alumina supported MoO_3 catalysts [33]. Therefore, the Raman bands at 788 and 880 cm^{-1} (Figure 3.7), also in agreement with XPS results, are due to reduced Mo^{4+} species. Upon re-oxidation the sample retrieved almost all the original Raman bands as in the fresh catalyst.

3.3.4 Pulse reduction-oxidation

In order to investigate the red-ox properties of the Mo/Li/MgO catalysts, we performed reduction-oxidation experiments, in analogy to method used previously in our lab [34]. In this method the reduced catalyst (catalyst pretreated at 550 °C in H_2/He) is oxidized by pulsing oxygen containing stream over the catalyst. Typical MS response to the oxygen pulses is shown in Figure 3.8 for 0.3Mo/Li/MgO.

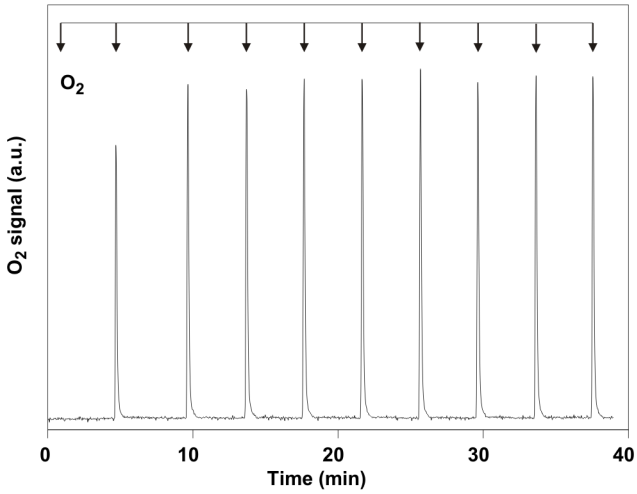

Figure 3.8. O_2 signal as monitored by the mass spectrometer during O_2 pulses over pretreated 0.3Mo/Li/MgO. Pretreatment: 10%H_2/He (15ml/min) at 550 ^oC for 1 h.

The complete first pulse, and part of the second pulse were consumed. Quantitative data from these pulse experiments are illustrated in Figure 3.9 for all catalysts. Oxygen consumption was higher for Li/MgO than MgO (no Mo present). This is in agreement with our earlier studies [34] and as suggested is due to regeneration of [Li^+OH^-] formed from the [Li^+O^-] sites during reduction. Further, the amount of oxygen consumption (mol O_2/m^2) increased with the increase in Mo loading. These results are not surprising, as molybdena species are reducible and contribute to the reduction-oxidation cycle. Similar results were also obtained with Mo/MgO samples.

Interestingly, results in Figure 3.9 clearly show that at a comparable Mo loading, the amount of oxygen uptake by reduced Mo/Li/MgO catalyst was much higher than that by Mo/MgO catalyst. These results are perfectly in line with TPR observations, in which Mo/Li/MgO showed a larger reduction peak in comparison to Mo/MgO, at a comparable Mo loading.

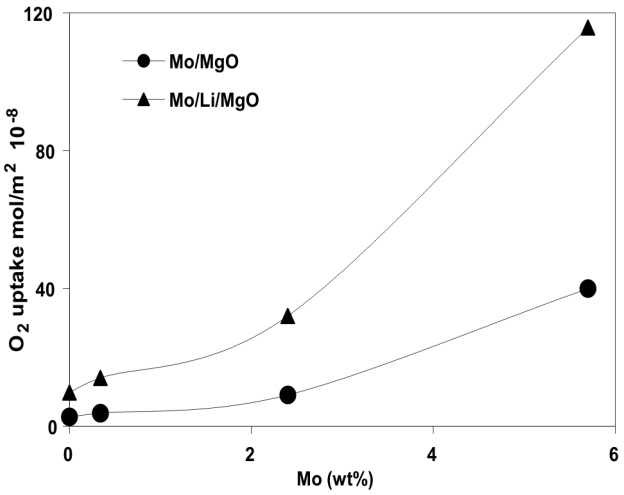

Figure 3.9. Amount of oxygen consumed during O_2 pulsing of the pretreated Mo/Li/MgO and Mo/MgO catalysts. Pretreatment: 10%H_2/He (15ml/min) at 550 ^oC for 1 h.

3.3.5 Catalytic tests

The influence of varying loadings of Mo on the performance of Li/MgO during the oxidative cracking of hexane was investigated at 575 ^oC. Figure 3.10 presents hexane conversions both initially and after 5 h of time on stream.

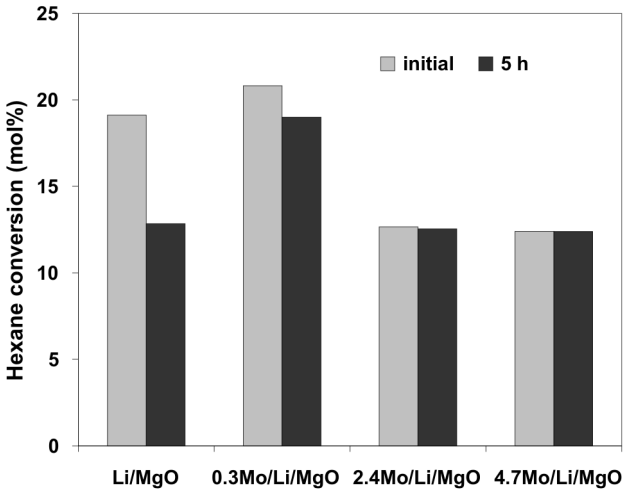

Figure 3.10. Hexane conversion over Li/MgO and Mo/Li/MgO catalysts, initially (at minute 5) and after 5 h of time on stream. Oxygen conversions (after 5h): 40 mol% (Li/MgO), 61 mol% (0.3Mo/Li/MgO), 55 mol% (2.4Mo/Li/MgO), 56 mol% (4.7Mo/Li/MgO). Reaction conditions: 100ml/min, 10% hexane, 8% oxygen and balance helium, T=575 ^oC, WHSV = 154 h^{-1}.

0.3Mo/Li/MgO catalyst resulted in similar initial hexane conversions as Li/MgO, however it exhibited better stability, hence significantly higher hexane conversions after 5 h time on stream. Both 2.4Mo/Li/MgO and 4.7Mo/Li/MgO catalysts were very stable, but exhibited lower initial hexane conversions than the unpromoted Li/MgO. Further, Figure 3.11 shows that an increase in Mo loading resulted in decreasing initial hexane conversion rates normalized to the surface area of the catalysts. Promotion of MgO with Mo, however, did not result in any significant changes in hexane conversions (Figure 3.12).

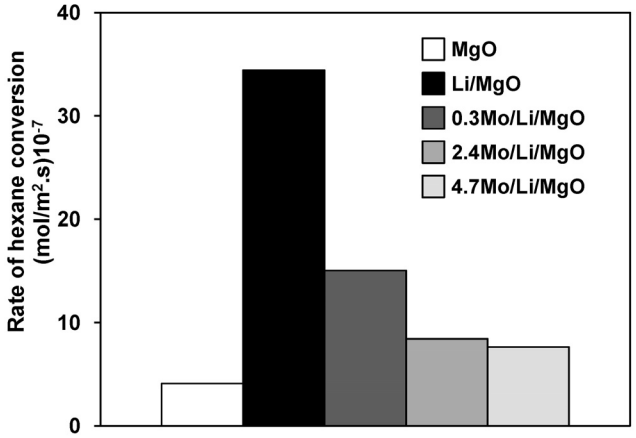

Figure 3.11. Rate of hexane conversion per unit surface area over MgO, Li/MgO and Mo/Li/MgO catalysts. Reaction conditions: 100 ml/min, 10% hexane, 8% oxygen and balance helium, T=575 ^{o}C, WHSV = 154 h^{-1}.

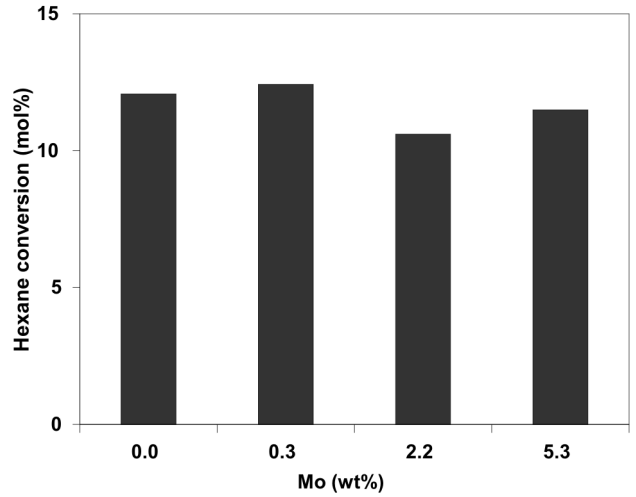

Figure 3.12. Hexane conversion over MgO as function of loading of Mo.
Oxygen conversions: 37 mol% (MgO), 35 mol% (0.3Mo/MgO), 21 mol% (2.2Mo/MgO) and 35 mol% (5.3Mo/MgO). Reaction conditions: 100 ml/min, 10% hexane, 8% oxygen and balance helium, T=575 ^{o}C, WHSV = 154 h^{-1}.

Figure 3.13 shows the selectivities to different products at 575 ^{o}C for all the catalysts at a similar hexane conversion of 10 mol%. 0.3Mo/Li/MgO showed similar selectivity pattern to that of Li/MgO, while both 2.4Mo/Li/MgO and 4.7Mo/Li/MgO catalysts resulted in formation of more combustion products. Significant formation of C_6 olefins were observed in the case of 4.7Mo/Li/MgO catalyst.

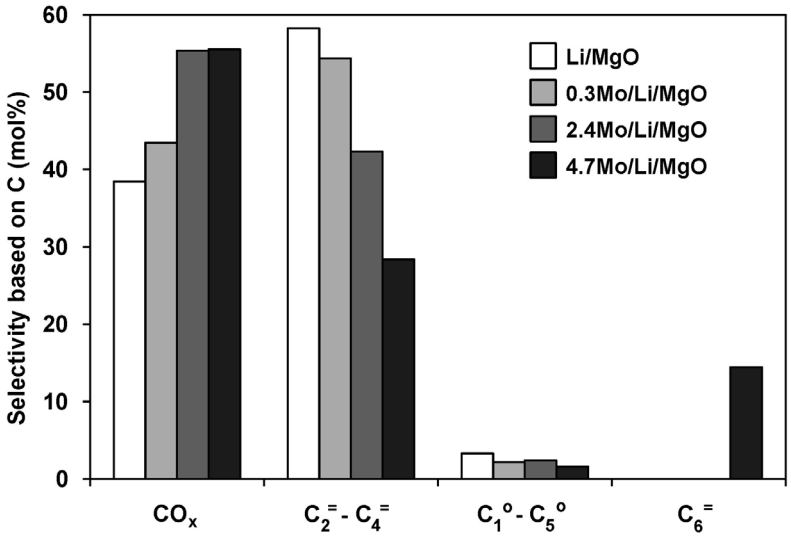

Figure 3.13. Selectivity to products based on C at hexane conversion of 10 mol%. Oxygen conversions = 35 mol% (Li/MgO) , 36 mol% (0.5 Mo/Li/MgO), 43 mol% (3.6 Mo/Li/MgO) and 53 mol% (7.1 Mo/Li/MgO). Reaction conditions: 100 ml/min total flow, 10% hexane, 8% oxygen and balance helium, T= 575 °C, WHSV = 154 – 385 h^{-1}.

Figure 3.14 shows the selectivities to C_2-C_4 olefins as function of hexane conversion. These results clearly indicate that the 0.3Mo/Li/MgO catalyst maintains the high olefin selectivity shown by Li/MgO.

3.4 Discussion

Results discussed so far indicate that promotion of Li/MgO with sub monolayer coverages of MoO_x introduces structural changes, which influence both physical properties and the performance of the catalyst in the oxidative cracking of hexane.

It is observed from XRD data that molybdenum is finely dispersed and no crystalline phases are observed (Figure 3.1). Molybdena precursor used, ammonium molybdate, decomposes to MoO_3 during catalyst pre-treatment at 600 ^{o}C. However, we do not detect any free MoO_3 in our samples. This is further confirmed from the TPR results of the Mo/Li/MgO catalysts (Figure 3.2.a). TPR of bulk and supported MoO_3 has been thoroughly investigated in literature [30, 35]. It is concluded that reduction of well dispersed supported MoO_3 is easier and occurs at lower temperatures than bulk MoO_3 crystals which reduce above 700 ^{o}C [35]. Thus, the relatively lower reduction temperature (535 ^{o}C, 600 ^{o}C) of the Mo/Li/MgO catalysts (Figure 3.2.a), and the absence of MoO_3 confirm the presence of other dispersed molybdena species. Our results are well in agreement with literature findings; in

supported molybdenum oxide systems with sub monolayer coverages the presence of dispersed molybdena anionic species such as MoO_4^{2-}, $Mo_6O_{19}^{2-}$, $Mo_7O_{24}^{-6}$ are commonly reported [6, 9-10, 15].

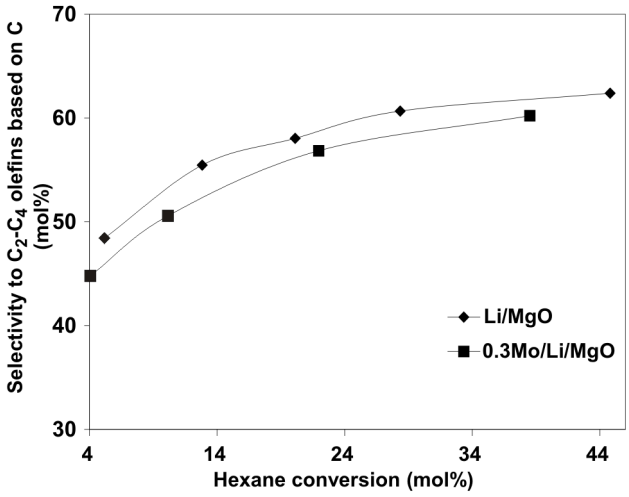

Figure 3.14. Selectivity to C_2-C_4 olefins as function of hexane conversion. Reaction conditions: 100ml/min, 10% hexane, 8% oxygen and balance helium, T=575 ^oC, WHSV = 5-154 h^{-1}.

From the Raman spectra in Figure 3.6, which show characteristic bands corresponding to tetrahedrally coordinated MoO_4^{2-} species, we conclude the presence of such molybdena species in our Mo/MgO catalysts. These are probably monomeric anions (Mg^{2+} $[MoO_4]^{2-}$) and are reported in literature both by Wachs and co-workers [13] and Bare and co-workers [15] for hydrated Mo/MgO samples.

In the case of Mo/Li/MgO catalysts, we as well observe the corresponding tetrahedrally coordinated MoO_4^{2-} species (Figure 3.5) which may involve $Mg^{2+}[MoO_4]^{2-}$ as well as $Li^+_2[MoO_4]^{2-}$. However, the appearance of additional Raman bands (compare Figures 3.5 and 3.6) in the 4.7Mo/Li/MgO catalyst, suggests the formation of other lithium-molybdenum phases. The formation of these phases becomes more significant with the increase in Mo loading and results in a continuous shift in the reduction temperature of Mo/Li/MgO catalysts (Figure 3.2.a).

To investigate the nature of these phases we subtracted the Raman spectra of the 4.7Mo/Li/MgO catalyst from the corresponding spectra of 5.3Mo/MgO catalyst. Figure 3.15 shows the difference spectrum. The majority of the bands appearing in the difference spectrum of 4.7Mo/Li/MgO catalyst (309, 321, 358, 820, 846, 878, 904 cm^{-1}) match those of Li_2MoO_4. The bands at 904, 820 and 321 cm^{-1} correspond to the symmetric, asymmetric stretching and bending modes of terminal Mo-O_t bond in Li_2MoO_4, respectively [37]. Thus, it is clear that, in the case of 4.7Mo/Li/MgO catalyst, part of the molybdenum is present as tetrahedrally coordinated in well defined Li_2MoO_4 phase.

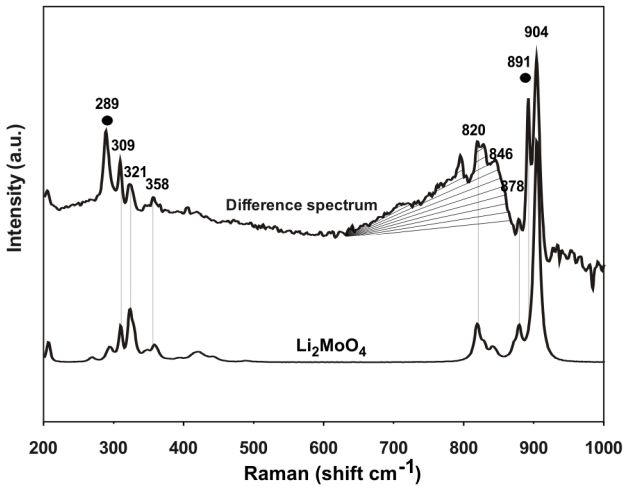

Figure 3.15. Raman spectra of Li_2MoO_4 , and difference spectrum of 4.7Mo/Li/MgO and 5.3Mo/MgO.

Additionally, the difference spectrum shows two sharp Raman bands at 289 and 891 cm^{-1}. The quasi-binary phase diagram of Li_2O and MoO_3 reported in literature [38], shows that in MoO_3 rich conditions ($MoO_3/Li_2O > 0.5$) at T > 600 ^oC the formation of $Li_2Mo_4O_{13}$ is favored. We also observe formation of such species by XRD (Figure 3.16) (see discussion below). We tentatively assign the Raman bands at 289 and 891 cm^{-1}, to bending and symmetric stretching modes of terminal Mo-O_t bond, respectively, in a well defined $Li_2Mo_4O_{13}$ phase. $Li_2Mo_4O_{13}$ is reported in literature [39] to have a regular derivative structure of V_6O_{13}, in which Mo is octahedrally coordinated. Although detected only in the catalyst with highest Mo loading (4.7Mo/Li/MgO), we propose the presence of such lithium molybdate species also in the low Mo containing samples. Due to the low concentration of Mo in these catalysts and thus small particles and less defined phases, the characteristic bands of these phases could not be detected.

Further, the difference spectrum of 4.7Mo/Li/MgO catalyst showed the presence of a broad Raman band in the 700 and 880 cm^{-1} range. It is reported in literature [15] that regular octahedral "MoO_6" groups exhibit Raman bands due to Mo-O_t symmetric stretching modes at a lower frequency (*e.g.,* Ba_2CaMoO_6, Mo-O_t sym band = 794 cm^{-1}) than regular tetrahedral "MoO_4" groups (*e.g.,* $MgMoO_4$, Mo-O_t sym band = 960 cm^{-1}). Thus, the broad Raman band in the range 700-880 cm^{-1} in the difference spectrum, could be the result of octahedrally coordinated molybdena species. The broadness of this band might imply the presence of a dispersed amorphous lithium molybdena phase. The new phase in the 4.7Mo/Li/MgO catalyst, thus, should correspond to dispersed amorphous molybdena species where Mo is octahedrally coordinated. This is in agreement with literature by Bare and co-workers [15-17], where Mo in dispersed molybdena species is usually octahedrally coordinated [15]. It is not possible to establish the exact composition of this phase with the current data.

Thus, the Mo/Li/MgO catalyst contains three types of molybdena containing phases *i.e.,* (i) monomeric $Mg[MoO_4]$ and $Li_2[MoO_4]$, in which Mo is tetrahedrally coordinated, (ii) polymeric species such as $Li_2Mo_4O_{13}$ in which Mo is octahedrally coordinated, and (iii) a

dispersed amorphous lithium molybdate phase in which Mo is also octahedrally coordinated. The importance of these phases on the catalyst performance is discussed below.

Conventionally, incorporation of Li into MgO to form the active site [Li^+O^-] is difficult and requires high temperature treatment (> 700 ^oC). Because of this, Li/MgO catalysts have (i) low surface areas due to sintering and (ii) lower activities. Unlike the conventional impregnation route, the sol-gel synthesis route allows incorporation of Li into MgO at milder temperatures (500 ^oC). This results in high surface area catalyst and enhanced [Li^+O^-] active sites [26]. However, even the sol-gel synthesized catalyst when exposed to high temperatures (> 500 °C) suffers a dramatic decrease in surface area (Table 3.1). Trionfetti *et al*. [24] reported that during the sol-gel preparation of Li/MgO, only ~40% of the lithium incorporates into the MgO lattice as [Li^+O^-] actives sites and the rest stays as Li_2O which through interaction with ambient CO_2 forms Li_2CO_3. Presence of Li_2CO_3 makes the catalyst susceptible for sintering upon exposure to high temperatures [40]. Li/MgO promoted with Mo, maintains the high surface area even after exposure to high temperature treatment (Table 3.1). Raman spectra (Figure 3.5) in the present work show that the presence of Mo reduces the amount of Li_2CO_3. We attribute the decrease in the amount of Li_2CO_3 in the Mo/Li/MgO catalysts, to the formation of mixed Li-Mo phases such as Li_2MoO_4, $Li_2Mo_4O_{13}$. During catalyst preparation at 600 ^oC, MoO_3 formed (as result of decomposition of ammonium molybdate) reacts with Li_2CO_3 in Li/MgO, forming Li_2MoO_4 and $Li_2Mo_4O_{13}$ phases according to [$yMoO_3 + xLi_2CO_3 \rightarrow Li_{2x}Mo_yO_{3y+1} + xCO_2$].

Indeed, the XRD pattern (Figure 3.16) of an equimolar mixture of Li_2CO_3 and $(NH_4)_2MoO_4$ calcined at conditions similar to that during catalyst preparation (600 ^oC for 5 h), results in characteristic peaks of Li_2MoO_4 and $Li_2Mo_4O_{13}$. The absence of characteristic peaks of MoO_3, confirms the high reactivity of MoO_3 with Li_2CO_3 in the catalyst, leading to the formation of the lithium molybdates. Decrease in the amounts of Li_2CO_3 in the presence of Mo makes it less susceptible to sintering. Thus the catalyst maintains the high surface area even after the high temperature treatment.

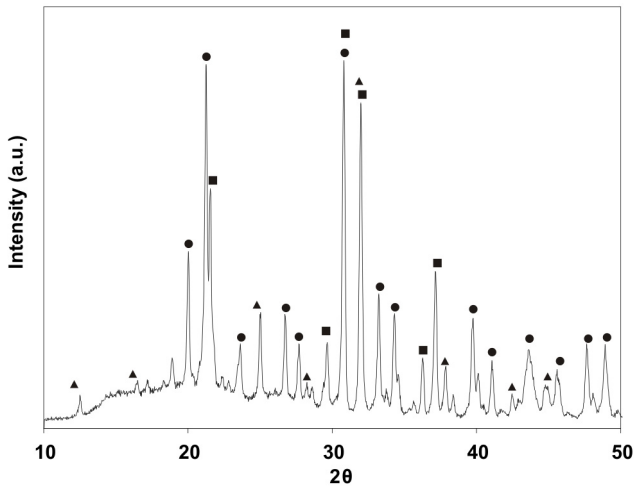

Figure 3.16. XRD patterns of an equimolar mixture of Li_2CO_3 and $(NH_4)_2MoO_4$ calcined at 600 ^oC. (●) Li_2MoO_4, (▲) $Li_2Mo_4O_{13}$, (■) Li_2CO_3.

Promotion of Li/MgO with Mo also improves stability of the catalyst during the oxidative cracking reaction (Figure 3.10). Recently, for the oxidative cracking of hexane over Li/MgO, we [27] proposed that reaction of product CO_2 with active catalytic sites [Li^+O^-] results in the formation of $Li^+CO_3^-$ which *via* reaction with another [Li^+O^-] site is converted into the more stable Li_2CO_3. The former [$Li^+CO_3^-$] can revert back to [Li^+O^-] *via* CO_2 desorption. Formation of Li_2CO_3 leads to irreversible loss of the [Li^+O^-] site because Li_2CO_3 is very stable at reaction temperatures (decomposes only above 700 ^oC [21]).

The catalyst stability of the Mo/Li/MgO catalysts can be related to the presence of surface Li-Mo-O species. We propose that these species are formed from the interaction of surface [Li^+O^-] active sites with MoO_3. Such interaction decreases the number of Li sites and makes the availability of free neighbouring lithium oxide sites less probable. Consequently, Li_2CO_3 formation is hindered, since the latter requires carbon dioxide reacting with two lithium sites [$Li_2O + CO_2 \rightarrow Li_2CO_3$], preferably in the vicinity of each other.

Thus interaction of MoO_3 with [Li^+O^-] sites has two effects; (i) reduction of the number of [Li^+O^-] active sites, thus decreasing catalytic activity, and (ii) hindering the formation of Li_2CO_3, thus improving stability.

As expected, for the Mo promoted catalysts, hexane conversion rates decrease with increase in Mo loading (Figure 3.11) due to higher loss of [Li^+O^-] sites by reaction with MoO_3. Since the [Li^+O^-] are isolated sites on MgO, their reaction with MoO_3 is expected to lead to a dispersed amorphous phase, similar to the one observed in our case.

Increase in Mo loading results in the formation of more combustion products (Figure 3.13). This indicates, as expected, an increasing red-ox activity in the Mo/Li/MgO catalysts with higher Mo amounts. Further, compared to Mo/MgO, Mo/Li/MgO catalysts exhibit even higher degree of reduction at the reaction temperature (575 ^oC) (Figures 2.b and 9).

It is well established in literature that crystalline molybdena phases are more difficult to reduce than dispersed phases [30, 35]. Li_2MoO_4 shows reduction at 685 °C (Figure 3.2.c). Based on TPR and literature [30, 35], we expect that both Li_2MoO_4 and $Li_2Mo_4O_{13}$ molybdates in the Mo/Li/MgO catalysts are red-ox stable at the reaction temperature (575 ^oC). The higher degree of reduction of the Mo/Li/MgO catalysts relative to Mo/MgO, is thus attributed to the presence of surface dispersed amorphous lithium molybdate which we observe in Raman spectra. It is expected that during oxidative cracking at 575 ^oC with the presence of oxygen in the feed, these species unselectively interact with intermediate radicals/olefins enhancing combustion. XPS results (Figures 3.3 and 3.4), indicate that the valence state of Mo in the fresh catalyst and after catalytic run is the same. Since oxygen was always present during reaction (oxygen conversion < 60%), we suggest that this amorphous lithium molybdate can undergo reduction with hydrocarbons followed by re-oxidation with oxygen as in a Mars and van-Krevelen mechanism. This is further confirmed from the Raman spectra of reduced and re-oxidized samples (Figure 3.7), which show that during oxidative cracking at 575 ^oC any structural changes as result of reduction are reversible upon subsequent oxidation.

Based on kinetic results of hexane conversion over the Mo/Li/MgO catalysts (Figure 3.10) we suggest that the irreducible molybdates (Li_2MoO_4, $Li_2Mo_4O_{13}$) formed in Li/MgO are inactive for C-H bond scission in the hexane. In studies by Vrieland and Murchison [12] on the oxidative dehydrogenation of butane to butadiene, characterization by Raman and XANES indicated that both (i) octahedral polymolybdates and (ii) crystalline $MgMoO_4$ are the

species responsible for catalytic activity at Mo loadings (15–25 wt%) corresponding to maximum activity. Interestingly, our results indicate that monomeric MoO_4^{2-} species are inactive, hence their presence in both Mo/MgO ($Mg^{2+}[MoO_4]^{2-}$) (Figure 3.12) and Mo/Li/MgO catalysts ($Li^{+}_2[MoO_4]^{2-}$, $Mg^{2+}[MoO_4]^{2-}$) (Figure 3.10) do not introduce any improvements in the hexane conversions.

Thus promotion of Li/MgO with Mo need to be kept at sufficient low levels to protect $[Li^{+}O^{-}]$ active sites from irreversible deactivation, as higher Mo contents lead to phases that do not contribute to catalytic activity or form dispersed phases that enhance combustion. The lowest Mo containing catalyst, 0.3Mo/Li/MgO, seems optimal because there is sufficient Mo for stabilization of catalyst activity during reaction. The catalyst exhibits similar activity (Figure 3.10) and selectivity to olefins (Figure 3.13) as Li/MgO. Moreover, it preserves the non-red-ox nature of Li/MgO; hence at the high hexane conversions the high olefin selectivities are maintained as clearly indicated from Figure 3.14.

3.5 Conclusions

Mo/Li/MgO catalysts show the presence of three types of molybdena containing phases *i.e.,* (i) monomeric $Mg[MoO_4]$ and $Li_2[MoO_4]$, in which Mo is tetrahedrally coordinated, (ii) polymeric species such as $Li_2Mo_4O_{13}$ in which Mo is octahedrally coordinated, and (iii) a dispersed amorphous lithium molybdate in which Mo is also octahedrally coordinated. These molybdates are inactive for C-H bond scission and hexane activation, yet bring considerable improvements in the catalyst. Formation of Li_2MoO_4 and $Li_2Mo_4O_{13}$ phases from reaction of MoO_3 with Li_2CO_3 during catalyst preparation reduces the amount of Li_2CO_3 originally present in Li/MgO. Thus, Mo promoted Li/MgO maintains the high surface area when exposed to high temperature treatment.

The amorphous lithium molybdate species are proposed to enhance catalyst stability. It is proposed that these species are formed from the interaction of MoO_3 with the $[Li^{+}O^{-}]$ catalytic active sites on the surface of Li/MgO, hence hindering the formation of Li_2CO_3. However, such interaction also results in loss of some of the $[Li^{+}O^{-}]$ active sites in Li/MgO. Thus increase in Mo loadings results in decrease in hexane conversions. Moreover, it is established that these amorphous lithium molybdates are highly reducible and responsible for secondary combustion reactions during oxidative cracking reaction.

Promotion of Li/MgO with low Mo loadings is sufficient to bring considerable improvements in both surface area and stability of the catalyst. Moreover, the catalyst exhibits similar activity for hexane conversion and selectivity to olefins as the unpromoted Li/MgO.

References

[1] M.C.Abello, M.F.Gomez, O. Ferretti, Appl. Catal. A 207 (2001) 421-431.

[2] M.C.Abello, M.F.Gomez, L.E.Cadus,Catal. Lett. 53 (1998) 185-192.

[3] L.E.Cadus, M.C.Abello, M.F.Gomez, J.B.Rivarola, Ind. Eng. Chem.Res. 35 (1996) 14-18.

[4] W. Ueda, K.H. Lee, Y.-S. Yoon, Y. Moro-oka, Catal. Today 44 (1998) 199-203.

[5] E. Heracleous, M. Machli, A.A. Lemonidou, I.A. Vasalos, J. Mol. Catal A: Chemical 232 (2005) 29-39.

[6] G. Tsilomelekis, A. Christodoulakis, S. Boghosian, Catal. Today 127 (2007) 139-147.

[7] A. Dejoz, J.M. Lopez Nieto, F. Marquez, M.I. Vazquez, Appl. Catal. A 180 (1999) 83-94.

[8] J.D.Pless, B.B.Bardin, H.-S. Kim, D. Ko, M. T. Smith, R.R. Hammond, P.C. Stair, K.R. Poeppelmeier, J. Catal. 223 (2004) 419-431.

[9] A. Christodoulakis, E. Heracleous, A.A. Lemonidou, S. Boghosian, J. Catal. 242 (2006) 16-25.

[10] A. Christodoulakis, S. Boghosian, J. Catal. 260 (2008) 178-187.

[11] Y. S. Yoon, W. Ueda, Y. Moro-oka, Catal. Lett. 35 (1995) 57-64.

[12] G.E. Vrieland, C.B. Murchison, Appl. Catal. A 134 (1996) 101-121.

[13] D.S.Kim, K. Segawa, T. Soeya, I. E. Wachs, J. Catal. 136 (1992) 539-553.

[14] M.A.Vuurman, I.E.Wachs, J. Phys. Chem, 96 (1992) (12) 5008-5016.

[15] S.-C. Chang, M.A.Leugers, S. Bare, J. Phys. Chem. 96 (1992) 10358-10365.

[16] S.R.Bare, G.E. Mitchell, J.J. Maj, G.E. Vrieland, J.L. Gland, J. Phys. Chem. 97 (1993) (22) 6048-6053.

[17] S.R.Bare, Langmuir 14 (1998) (6) 1500-1504.

[18] F. Cavani, F. Trifiro, Catal. Today 24 (1995) 307-313.

[19] T. Ito, J.-X. Wang, C.-H. Lin, J.H. Lunsford, J. Am. Chem. Soc.107 (1985) 5062-5068.

[20] E. Morales, J.H. Lunsford, J. Catal. 118 (1989) 255-265.

[21] M. Xu, C. Shi, X. Yang, M.P. Rosynek, J.H. Lunsford, J. Phys. Chem. 96 (15) (1992) 6395-6398.

[22] L. Leveles, K. Seshan, J.A Lercher, L. Lefferts, J. Catal. 218 (2003) 307-314.

[23] L. Leveles, K. Seshan, J.A. Lercher, L. Lefferts, J. Catal. 218 (2003) 296-306.

[24] C. Trionfetti, I.V Babich, K. Seshan, L. Lefferts, Appl. Catal. A 310 (2006) 105-113.

[25] C. Trionfetti, I.V Babich, K. Seshan, L. Lefferts, Langmuir 24 (2008) 8220-8228.

[26] M. Yu. Sinev, J. Catal. 216 (2003) 468-476.

[27] C. Boyadjian, L. Lefferts, K. Seshan, Appl. Catal. A 372 (2010) 167-174.

[28] C. Boyadjian, B.van der Veer, I.V. Babich, L. Lefferts, K. Seshan, Catal. Today (article in press 2010).

[29] J. F. Moulder, W. F. Stickle, P. E. Sobol, K. D. Bomben, Handbook of X-ray Photoelectron Spectroscopy, Perkin-Elmer Corporation, Eden Prairie, 1992, p. 572.

[30] P. Arnoldy, J.C. De Jonge, J.A. Moulijn, J.Phys.Chem. 89 (1985) (21) 4517-4526.

[31] E.-K. Lee, K.-D. Jung, O.-S. Joo, Y.-G. Shul, Appl. Catal. A 268 (2004) 83-88.

[32] M.A. Ulla, R. Spretz, E. Lombardo, W. Daniell, H. Knozinger, Appl. Catal. B 29 (2001) 217-229.

[33] E. Payen, J. Grimblot,S. Kasztelan, J.Phys.Chem 91 (1987) (27) 6642-6648.

[34] C. Trionfetti, S. Crapanzano, I.V.Babich, K.Seshan, L. Lefferts, Catal. Today 145 (2009) 19-26.

[35] J.R. Regalbuto, J.-W. Ha, Catal. Lett. 29 (1994) 189-207.

[36] G. Li, H. Li, Y. Mo, L. Chen, X. Huang, J. Pow. Sources 104 (2002) 190-194.

[37] A. Erdoheyli, K. Fodor, R. Nemeth, A. Hancz, A. Oszko, J. Catal. 199 (2001) 328-337.

[38] M. Moser, D. Klimm, S. Ganschow, A. Kwasniewski, K. Jacobs, Cryst. Res. Technol. 43(4) (2008) 350-354.

[39] B.M. Gatehouse, B.K. Miskin, J. Solid State Chem. 15 (1975) 274-282.

[40] V. Perrichon, M.C. Durupty, Appl. Catal. 42 (1988) 217-227.

Chapter 4

Oxidative Cracking of n-Hexane - Influence of Plasma and Catalyst on Reaction Pathways

An integrated plasma-Li/MgO system is efficient for the oxidative conversion of hexane. In comparison to the Li/MgO catalytic system, it brings considerable improvements in the yields of light olefins ($C_2^=$-$C_5^=$) at relatively low temperatures indicating synergy from combination of plasma and catalyst. The study on the influence of temperature on the performance of the integrated plasma-Li/MgO system shows dominancy of plasma chemistry at the lower temperature (500 ^oC), while contribution from the catalyst both in hexane activation and in enhancing olefin formation becomes significant at the higher temperature (600 ^oC). At 500 ^oC significant amount of acetylene formation is observed. This is minimized at 600 ^oC at oxygen depleting condition.

4.1 Introduction

Catalytic oxidative cracking of naphtha is conceptually a potential alternative process to steam cracking. Both the presence of oxygen and catalyst are beneficial for facilitating cracking reactions at lower temperatures. Reactions in presence of oxygen are exothermic, thus internally provide heat for endothermic cracking reactions (C-C, C-H bond cleavage). Presence of catalyst stimulates C-C, C-H bond scission in the alkane and induces cracking at lower temperatures than in the homogeneous phase. The development of an efficient oxidation catalyst that minimizes combustion, however, remains a challenge. Recent studies on oxidic catalysts with no facile red-ox properties have shown tremendous increase in olefin yields [1-2]. Among these is the Li/MgO catalyst, which has been extensively studied in literature for the oxidative conversion of alkanes; oxidative coupling of methane [3-4] and oxidative dehydrogenation/cracking of ethane [5-6], propane and butane [7-11]. Unlike in the case of oxidic catalysts with red-ox properties [12], sequential combustion of olefins over Li/MgO occurs to a minimal extent, resulting in an olefin selectivity which is almost invariant with the alkane conversion levels. Recently, we [13] reported on the performance of Li/MgO catalyst for the oxidative conversion/cracking of hexane. The catalyst showed very good selectivity to C_2-C_4 olefins (60 mol %) at a temperature as low as 575 ^oC, which is much lower than temperatures used in steam crackers (T ≥ 800 ^oC). Similar to what is reported in literature and our earlier studies for oxidative conversion of lower alkanes (methane [3], ethane [4-5], propane and butane [6-11]), we proposed hexane activation *via* the $[Li^+O^-]$ sites of Li/MgO abstracting H•. The hexyl radical formed then undergoes complex radical chemistry in gas phase in presence of molecular oxygen, forming the product mixture of C_1-C_5 products, including olefins, paraffins and combustion (CO_x) products.

Li/MgO has no cations with variable valency and unlike catalysts with red-ox properties ($Mn^{2+,3+}$, $Co^{2+,3+}$), has lower oxidation activity. This results in relatively low hexane conversions during the oxidative cracking of hexane [13]. Kinetic results from the oxidative conversion of alkanes over the Li/MgO show that C-H bond splitting is the rate limiting step in these reactions [9]. Even in the presence of strong H• abstractor, *e.g.*, $[Li^+O^-]$, high temperatures ≥ 550 ^oC are still required to induce this step.

In an attempt to enhance the H• abstraction in the alkane, we recently [14-15] investigated the oxidative conversion of propane, ethane and methane at ambient conditions in presence of plasma in a micro-reactor both in presence and absence of Li/MgO catalyst. Indeed, in these experiments plasma induced alkane activation and alkyl radicals were formed at ambient conditions as result of electron impact collisions caused by plasma. In the case of propane plasma experiments, higher conversions were observed in the presence of Li/MgO catalyst as compared to empty micro-reactor. This is due to enhanced plasma efficiency as result of increase in permittivity of the system, leading to increase in electron density, hence electron impact collisions [15]. The presence of Li/MgO catalyst also resulted in enhanced selectivity to propylene. Propyl radicals, generated from propane *via* activation by plasma, interact with the $[Li^+O^-]$ sites of the catalyst, where the latter abstracts a second hydrogen atom from the propyl radical forming propylene [15].

Further, we [16-17] recently investigated the influence of plasma on the gas phase oxidative conversion of n-hexane in the temperature range 400 to 600 ^oC. Introduction of plasma induced both hexane and oxygen activation *via* electron-impact dissociative excitations. In order to understand plasma chemistry initiated by electron impact processes, the average electron energy was determined using the Boltzmann distribution. At the lower

temperatures (400, 500 ^{o}C) coupling of formed radicals was observed leading to formation of C_6^+ hydrocarbons. At the higher temperature (600 ^{o}C), however, cracking and lower olefins ($C_2^=$-$C_4^=$) formation became more significant. It was established that the presence of oxygen introduces new routes for hexane conversion, involving gas phase activation of oxygen by plasma. Optimum olefins yields were obtained at 8 mol% of oxygen, as increasing oxygen concentrations above this resulted in enhanced CO_x formation.

Although application of non-thermal plasma (plasma at ambient conditions) is more commonly reported, integrated plasma-catalytic systems at elevated temperatures, so-called plasma/catalysis have also been of continuous interest, especially for decomposition of hydrocarbons [18-19]. In particular, decomposition of methane to hydrogen and carbon has been investigated [20-21]. Nozaki *et al*. [21], investigated steam reforming of methane using plasma with a Ni/SiO_2 catalyst. A strong synergistic effect and hence significant improvement in the methane conversion was observed at 400 ^{o}C. Similarly, the presence of catalyst downstream to plasma, during the oxidative conversion of methane [22], improved selectivities to ethylene.

In analogy to such systems, in this chapter the performance of an integrated plasma-Li/MgO system for the oxidative conversion of hexane is reported. Our objective is to further enhance the yields of olefins, compared to those achieved in the plasma reactor in the absence of the catalyst. The influence of plasma on the selectivities to various products in relation to the chemistry on the surface; *i.e*., the role of Li/MgO catalyst in hexane activation and controlling olefin formation, is discussed.

4.2 Experimental

4.2.1 Materials and methods

Commercially available $Mg(OCH_3)_2$ solution in methanol (Aldrich, 6-8 wt% in methanol), CH_3OH (Merck), $LiNO_3$ (Aldrich, assay ≥ 99.99%) were used for preparation of Li/MgO catalysts. Sol-gel synthesized Li/MgO catalyst used in this study was prepared according to the method described in chapter 2.

BET surface area of the catalyst was determined with nitrogen physisorption using a Micro-metrics Tristar instrument. The samples were out-gassed in vacuum at 250 °C for 24 h prior to the analysis. BET surface area of the catalyst was 82 m^2/g. The elemental composition of the catalyst was determined with atomic absorption spectroscopy (AAS). Li content in the catalyst was 0.86 wt%.

4.2.2 Catalytic measurements

Measurements with the integrated plasma-Li/MgO system were carried out at atmospheric pressure and isothermal conditions in a fixed-bed reactor as in Figure 4.1. A quartz reactor of 4 mm internal diameter was used. The reactor was equipped with an internal stainless steel wire (ID 1.5 mm) as high voltage electrode and an external aluminum foil as ground electrode. Plasma was generated between the high voltage wire electrode and the grounded aluminum foil around the quartz tube using 6 kV peak AC voltage. The power supply had an

output of 10 Watts maximum. The power absorbed by the plasma was calculated to be ~3 Watts (180 J/min). This was evaluated using the corresponding V-Q Lessajous figures, obtained using an oscilloscope [19]. Light emission from the discharge was collected through a collimating lens placed at a 90° angle to the outside of the reactor. An optical fiber was used to transmit the light to an optical emission spectrometer (HR 4000, Ocean Optics).

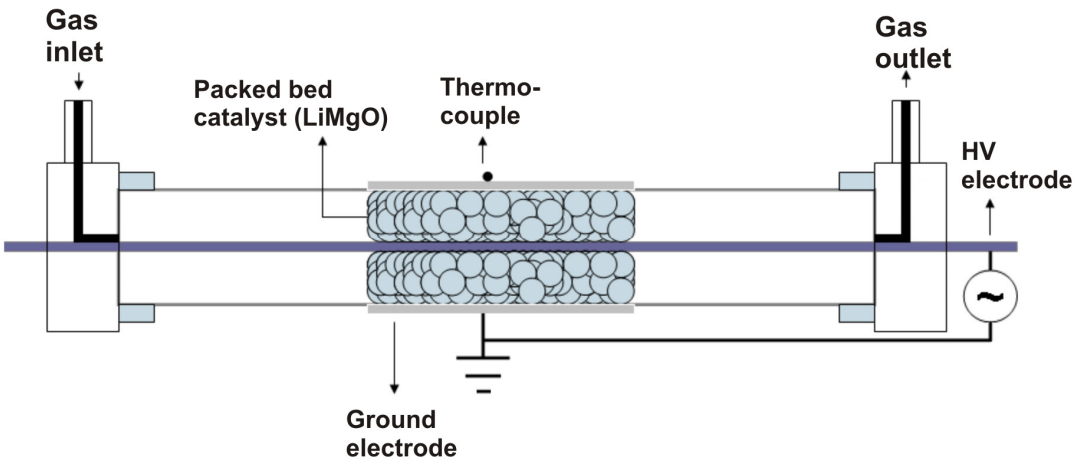

Figure 4.1. Schematic drawing of catalytic plasma reactor.

Catalyst or quartz particles (depending on the experiment) were packed between two quartz-wool plugs in the quartz reactor according to configuration in Figure 4.2.a. For gas phase non-catalytic reactions, an empty reactor according to configurations in Figures 4.2.b and 4.2.c were used. A different reactor configuration with Li/MgO downstream to plasma (Figure 4.2.d) was as well investigated. Powder catalyst was pressed, crushed and sieved to particle size range of 0.4-0.6 mm before use. Reactions were studied at both 500 and 600 °C. The reactor was heated using an electrical furnace. The temperature of the furnace was controlled by a thermocouple placed outside the reactor tube within the isothermal zone of the tubular furnace. Total gas feed of 100 ml/min was used. This consisted of 10 mol% of hexane vapor, 8 mol% of oxygen and balance helium. Before each catalytic test, the catalyst was pretreated in 50% O_2/He (60 ml/min) for 1 h at a temperature of 650 °C. For analysis of the product mixture two online micro GCs were utilized. The experimental setup used for catalyst testing and analysis details are described in chapter 2.

Hexane conversions were calculated on carbon mol basis; *i.e.,* (C_6^{in} moles – C_6^{out} moles) / C_6^{in} moles x100%. The carbon balance closed between 100 and 110%. Selectivity to individual products was also calculated based on the number of moles of carbon contained in the products.

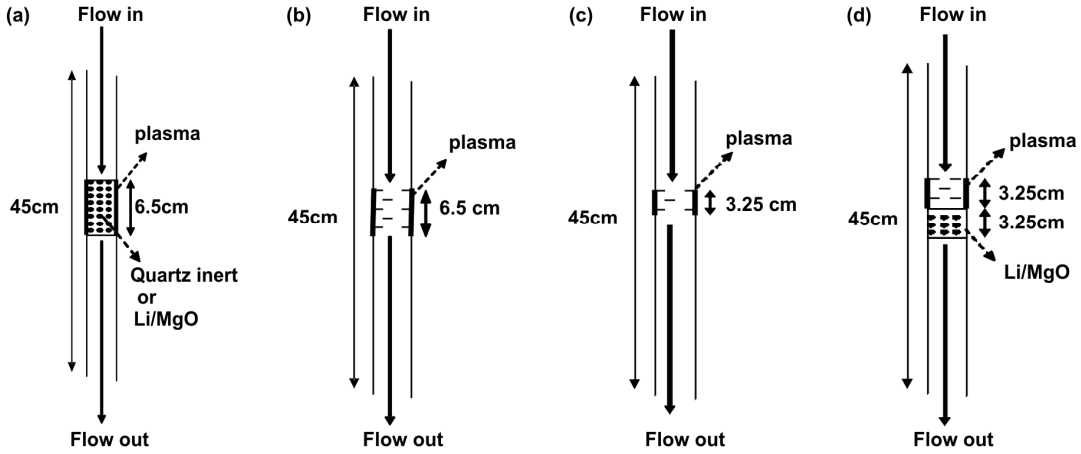

Figure 4.2. Reactor configurations used; Plasma applied to Li/MgO (P_Li/MgO) or quartz (P_Quartz) (a), plasma applied to empty reactor (P_ER) (b & c), and Li/MgO downstream to plasma zone (PB_Li/MgO) (d).

4.3 Results and discussion

Figure 4.3 shows hexane conversions from the oxidative conversion of hexane both at 500 and 600 ^{o}C, (i) in an empty reactor in the absence and presence of plasma and (ii) with Li/MgO catalyst without plasma.

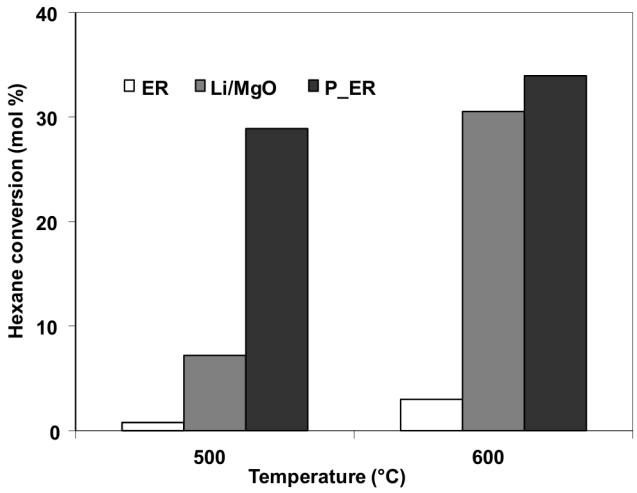

Figure 4.3. Hexane conversions (i) in an empty reactor, (ii) with Li/MgO and (iii) in a plasma reactor. Oxygen conversions (mol%): At 500 ^{o}C; 4 (ER), 56 (Li/MgO), 71 (P_ER) and at 600 ^{o}C; 10 (ER), 100 (Li/MgO), 100 mol% (P_ER). Reaction conditions: 100 ml/min, 10% hexane, 8% oxygen and balance helium, WHSV= 3.08 h^{-1}.

At both temperatures hexane conversions in the empty reactor were almost negligible. The introduction of the catalyst however, resulted in a considerable improvement in hexane conversions. Significantly, the application of plasma enhanced hexane conversions at both temperatures. Thus, results of hexane conversions in Figure 4.3 elucidate the significant influence of both Li/MgO catalyst and plasma on hexane activation. Temperature has also a clear effect on hexane conversions but was more significant in the case of the Li/MgO catalyst. Details of the oxidative conversion of hexane in the presence of both (i) plasma and (ii) Li/MgO catalyst at 500 and 600 ^{o}C are presented in sections below.

4.3.1 Oxidative cracking of hexane in the presence of plasma

During the oxidative conversion of hexane, we [16-17] showed that the role of plasma was to induce both hexane and oxygen conversions *via* electron impact excitations. The average electron energy for the 'hexane + oxygen + helium' system, solving the Boltzmann distribution [17], was calculated to be 4.3 eV. This is sufficient to induce C-C (bond energy 3.17 eV) and C-H (bond energy 3.97 eV) bond scission in the hexane, and the fraction of electrons with higher energy can also cause dissociation of molecular oxygen (~6 eV). The dramatic improvement observed [16-17] in hexane conversions with the introduction of oxygen in the system, confirmed the existence of new routes for hexane conversion, involving gas phase activation of oxygen by plasma. Thus, in the presence of plasma the following hexane dissociation routes were proposed [16-17] (ii) C-C, C-H bond scission by electron-impact excitation of hexane molecules (eq. 1-4) and (iii) C-H bond scission by collision of hexane molecules with O(^{3}P) oxygen atoms (eq. 5) formed from electron impact excitations of molecular oxygen (eq. 6-7). Moreover, we [16-17] previously showed the reaction of molecular oxygen with hexyl radicals forming HOO● radicals (eq. 8). The latter act as chain propagators and increase the radical concentration during oxidative conversion.

$$C_6H_{14} + e^- \rightarrow C_6H_{13}\bullet + H\bullet + e^- \quad (1)$$

$$C_6H_{14} + e^- \rightarrow C_5H_{11}\bullet + CH_3\bullet + e^- \quad (2)$$

$$C_6H_{14} + e^- \rightarrow C_4H_9\bullet + C_2H_5\bullet + e^- \quad (3)$$

$$C_6H_{14} + e^- \rightarrow C_3H_7\bullet + C_3H_7\bullet + e^- \quad (4)$$

$$C_6H_{14} + O(^3P) \rightarrow C_6H_{13}\bullet + OH\bullet \quad (5)$$

$$O_2 + e^- \rightarrow 2O(^3P) + e^- \quad (6)$$

$$O_2 + e^- \rightarrow O(^3P) + O(^1D) + e^- \quad (7)$$

$$O_2 + C_6H_{13}\bullet \rightarrow C_6H_{12} + HOO\bullet \quad (8)$$

Optical emission spectrum of a C_6H_{14}-He mixture in plasma (Figure 4.4) confirms the influence of plasma on hexane activation. Features of the electronic excitation of the CH● radical corresponding to the $A^2\Delta \rightarrow X^2\pi$ transition at 431.15nm and bands corresponding to

H● radicals (656.05nm) (Hα, Balmer series) and helium (587.61 and 667.78 nm) were observed. The existence of CH and H bands in the optical emission spectrum of C_6H_{14}-He mixture indicate the decomposition of hexane in plasma *via* C-H and C-C bond cleavage.

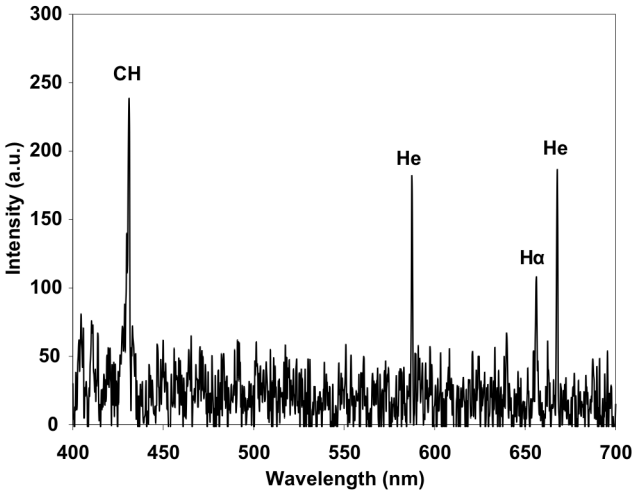

Figure 4.4. Optical emission spectrum for a gas mixture of 10% hexane in helium in the presence of plasma at 3W and at ambient conditions.

CH● radicals in the presence of plasma are generally formed, as proposed in literature by Kado *et al.* [23], through the extensive dehydrogenation of methyl radicals *via* multiple electron impact excitations (eq. 9-10) and/or from the coupling of atomic C and H radical (eq. 11) formed through extensive dissociation of methane (eq. 12).

$$CH_3\bullet + e^- \rightarrow CH_2\bullet + H\bullet + e^- \quad (9)$$

$$CH_2\bullet + e^- \rightarrow CH\bullet + H\bullet + e^- \quad (10)$$

$$C + H\bullet \rightarrow CH\bullet \quad (11)$$

$$CH_4 + e^- \rightarrow C + 4H\bullet + e^- \quad (12)$$

CH● radicals further follow predominantly two reactions; (i) Dimerization of CH● radicals lead to formation of C_2H_2 (eq. 13) and (ii) reaction with oxygen lead to CO_2 (eq. 14). Experiments studying the influence of oxygen concentrations during oxidative conversion of hexane in the plasma reactor, showed dramatic decrease in C_2H_2 formation with addition of oxygen in the feed [17]. Alternatively, CH● radicals can react with other radicals to form olefins (eq. 15). Since carbon balance in our experiments were relatively good (±10%) and experiments were carried out in the presence of oxygen, it is less likely that CH● is converted to coke.

$$CH\bullet + CH\bullet \rightarrow C_2H_2 \qquad (13)$$

$$2CH\bullet + 2.5O_2 \rightarrow 2CO_2 + H_2O \qquad (14)$$

$$CH\bullet + C_nH_{2n+1}\bullet \rightarrow C_{n+1}H_{2n+2} \quad n = 1\text{-}5 \qquad (15)$$

Figure 4.5 presents the selectivities to various products obtained from oxidative conversion of hexane in the plasma empty reactor.

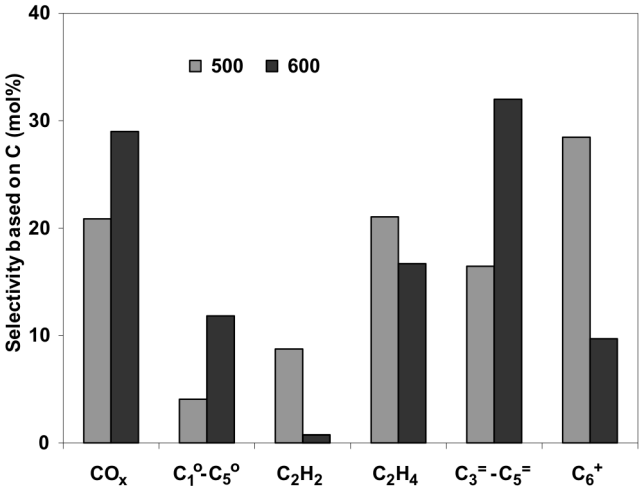

Figure 4.5. Effect of temperature on the product distribution from oxidative conversion of hexane in the presence of plasma. Hexane conversions: 29 mol% (500 ^oC) and 31 mol% (600 ^oC). Reaction conditions: 100 ml/min, 10% hexane, 8% oxygen and balance helium.

Temperature has a clear influence on the product distribution. At 500 ^oC, significant formation of C_6^+ products was observed. These products were not precisely identified at molecular level due to limitation of the micro GCs, but their presence indicates the coupling of the C_1-C_5 radicals subsequent to their formation from dissociation of hexane (eq. 16). At 600 °C, however, the formation of less C_6^+ products and more C_3-C_5 olefins was observed. This indicates that at this temperature coupling reactions of C_1-C_5 radicals occur to a lesser extent. C-C bond formation is exothermic hence favored at the lower temperatures. In agreement, during the oxidative conversion of methane, ethane and propane in a plasma-micro reactor [14-15], coupling reactions and formation of hydrocarbons with carbon numbers higher than the feed were observed at lower temperatures.

$$C_xH_{2x+1}\bullet + C_yH_{2y+1}\bullet \rightarrow C_nH_{2n+2} \qquad x,y = 1\text{-}5 \ , \ n = \geq 6 \qquad (16)$$

At 500 ^oC, significant formation of acetylene and ethylene and lower amounts of C_3-C_5 olefins was observed (Figure 4.5), *i.e.,* (C_2H_2 + C_2H_4) > ($C_3^=$-$C_5^=$). Acetylene formation is strong evidence of plasma chemistry. Two routes for formation of acetylene have been proposed in

literature [16, 20, 32]. In addition to dimerization of CH● radicals discussed above, acytelene is also formed through the extensive dehydrogenation of ethane (eq. 17).

$$C_2H_6 \rightarrow C_2H_4 \rightarrow C_2H_2 \qquad (17)$$

At 600 ^oC, however, a higher ratio of ($C_3^=$- $C_5^=$) / (C_2H_2 +C_2H_4) was observed than at 500 ^oC. This indicates that at this temperature the reaction of C_1-C_5 radicals with molecular oxygen to olefins is more favored (eq. 18).

$$C_nH_{2n+1}\bullet + O_2 \rightarrow C_nH_{2n} + HOO\bullet \quad n = 1\text{-}5 \qquad (18)$$

4.3.2 Oxidative cracking of hexane over Li/MgO catalyst

In the case of Li/MgO catalyst, [Li^+O^-] defect sites are responsible for catalytic activity [3-4, 8-11]. Oxidative conversion of hexane, thus, involves hexane activation *via* homolytic scission of C-H bond on the [Li^+O^-] sites, forming a hexyl radical (eq. 19) [13].

$$C_6H_{14} + Li^+O^- \rightarrow C_6H_{13}\bullet + Li^+OH^- \qquad (19)$$

Figure 4.6 shows the product distribution obtained from the oxidative conversion of hexane over Li/MgO catalyst at 500 and 600 ^oC.

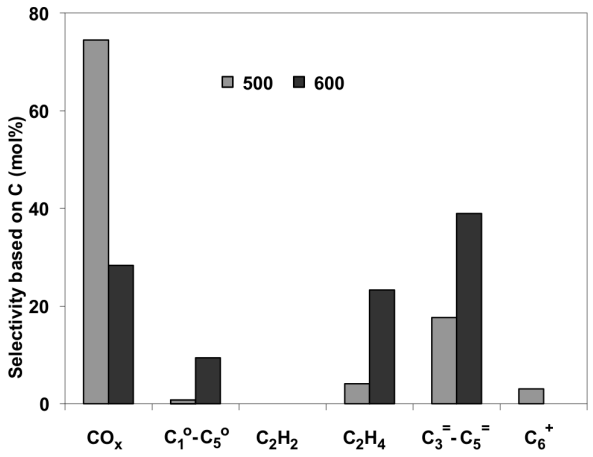

Figure 4.6. Effect of temperature on the product distribution from oxidative conversion of hexane over Li/MgO catalyst. Hexane conversions: 7 mol% (500 ^oC) and 31 mol% (600 ^oC). Reaction conditions: 100 ml/min, 10% hexane, 8% oxygen and balance helium, WHSV = 3.08 h^{-1}.

At 500 ^{o}C Li/MgO catalyst showed high selectivity to combustion products (75 mol %) and only 21 mol% of total olefins ($C_2^{=}$-$C_5^{=}$). In the oxidative conversion of lower alkanes/alkenes over MgO, the interaction of hydrocarbons with O^{2-} sites of MgO forming surface alkoxides as precursors for CO_x, has been reported by Aika and Lunsford [24-25]. Similarly, in the oxidative conversion of hexane over Li/MgO, the high selectivity to combustion products, especially at the low temperature (500 ^{o}C), has been shown by us [13] to be due to the adsorption of the intermediate radicals on O^{2-} sites of MgO, and their consecutive transformation to CO_x *via* molecular oxygen. At the higher temperature (600 ºC), however, cracking and olefin formation were more favored (62 mol% of $C_2^{=}$-$C_5^{=}$ and 28 mol% of CO_x). This is due to the high temperatures favoring desorption of radicals formed by hydrogen abstraction, and limiting reaction with surface oxygen for alkoxide formation.

Unlike in the presence of plasma, C_2H_2 or C_6^{+} products were not observed here. Both at 500°C and 600 °C selectivities to C_3-C_5 olefins were higher than those to C_2H_4 ($C_3^{=}$-$C_5^{=}$ > $C_2^{=}$) which is an indication of role for Li/MgO in cracking and olefin distribution, as homogeneous cracking would yield higher amounts of ethylene than higher olefins ($C_3^{=}$-$C_5^{=}$). In the oxidative conversion of hexane over Li/MgO, we proposed, based on experimental results [13] and similar to propositions by Sinev [26], the preference of the [O^{-}] sites of Li/MgO for hydrogen abstraction from a secondary carbon atom in hexane. This increases the probability of formation of iso-hexyl radicals. β-scission of iso-hexyl radicals yields preferentially more of C_3-C_5 olefins than ethylene.

Oxidative conversion of hexane in the situations discussed so far *i.e.,* (i) in the presence of plasma without catalyst and (ii) in the presence of Li/MgO catalyst without plasma, however, yields even at the higher temperature (600 °C) limited C_2-C_5 olefins (~18 mol%) due to formation of CO_x (~9 mol%). [$Li^{+}O^{-}$] sites have a strong affinity for H● abstraction, and since presence of plasma (i) enhances formation of hydrocarbon radicals and (ii) abstraction of H● from a hydrocarbon radical leads to olefins, combination of plasma with Li/MgO may be useful. In an attempt to further increase olefin yields, *i.e.,* enhance both hexane conversions and selectivities to total olefins ($C_2^{=}$-$C_5^{=}$), the integrated plasma-Li/MgO system is studied for the oxidative conversion of hexane.

4.3.3 Integrated plasma-Li/MgO for the oxidative cracking of hexane

Figure 4.7 shows hexane conversions in an empty reactor and with Li/MgO catalyst both in the absence (ER, Li/MgO) and the presence of plasma (P_ER, P_Li/MgO). Results of experiments with quartz inert particles are also included for comparison.

At 500 ^{o}C the integrated plasma-Li/MgO system resulted in higher hexane conversions than the cumulative conversions achieved with plasma and Li/MgO separately, showing synergy. This effect was not observed at 600 ^{o}C, due to depletion of oxygen (O_2 conversion = 100%) from reaction stream limiting hexane conversions

In order to explain the influence observed we will discuss two propositions: (i) Firstly, it concerns the presence of new [O^{-}] defect sites in the Li/MgO catalyst created by UV light generated from plasma. Knozinger and co-workers [27-29], reported, using EPR studies, the role of UV light in inducing ionization of low-coordinated surface oxygen anions $(O_{LC}^{2})^{-}$ in MgO, forming a localized surface hole state [O^{-}] and a surface-trapped electron (eq. 20).

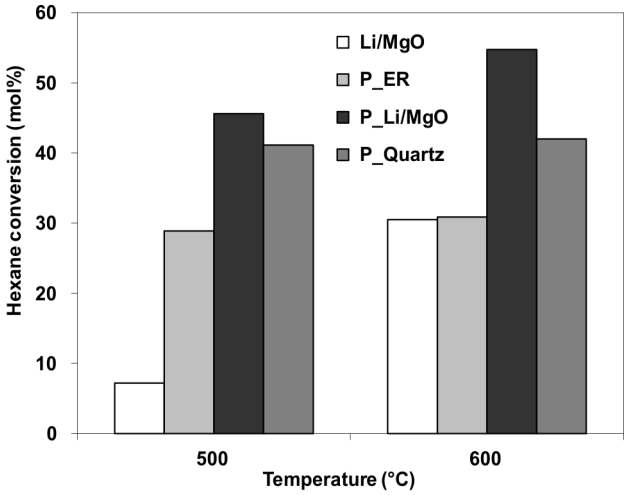

Figure 4.7. Hexane conversions with the systems; (i) Li/MgO, (ii) P_ER, (iii) P_Li/MgO, and (iv) P_Quartz. Oxygen conversion (mol %): At 500 ^{o}C; 56 (Li/MgO), 71 (P_ER), 75 (P_Li/MgO), and 68 (P_Quartz) and at 600 ^{o}C; 100 (Li/MgO), 100 (P_ER), 100 (P_Li/MgO) and 97 (P_Quartz). Reaction conditions: 100 ml/min, 10% hexane, 8% oxygen and balance helium, WHSV= 3.08h^{-1}.

$$O_{LC}^{2-} + h\nu \rightarrow O_{LC}^{-} + e^{-} \qquad (20)$$

These [O^{-}] defect sites created by the plasma, similar to the [$Li^{+}O^{-}$] sites, can also enhance H● abstraction from hexane forming hexyl radicals. (ii) Secondly, we explain the synergistic effect by the accelerated gas phase radical chemistry due to the higher permittivity of Li/MgO (dielectric constant of MgO = 9.7 [30]) in comparison to that of plasma (dielectric constant of plasma < 1 [31]) in the empty reactor. The relative permittivity of a dielectric barrier can strongly determine the amount of charge that can be stored for a certain value of applied electric field [32]. The higher the number of charges transferred, the higher is the number of electron impact excitations of hexane molecules [33]. The presence of Li/MgO particles would also, additionally, influence the strength of the electric field. Kang *et al.* [34] studied the influence of the ferroelectric pellets on the discharge characteristics of dielectric barrier discharges (DBD). They reported that the presence of ferroelectric pellets in plasma can create a non-uniform stronger electric field. This effect created by the packing material, can result in an increase in the average electron energy. Consequently, the number of electron impact dissociations of hexane molecules increases resulting in improved hexane conversions.

Table 4.1 shows the influence of plasma on the selectivities to various products during the oxidative conversion of hexane over the Li/MgO catalyst. At both temperatures, application of plasma improved the product distribution resulting in a considerable increase in the formation of total olefins ($C_2^{=}$-$C_5^{=}$) and a decrease in formation of CO_x. In accordance to our earlier suggestions of alkoxides as precursors to combustion [13], it is possible that in the P_Li/MgO system, the presence of new [O^{-}] defect sites created from the photo-excitation of the O^{2-} sites of MgO, minimizes the unselective interaction of radicals with the latter for alkoxide formation, thus minimizing combustion.

Table 4.1. Selectivity to various products with Li/MgO in the absence and the presence of plasma. Reaction conditions: 100 ml/min, 10% hexane, 8% oxygen and balance helium, WHSV = 3.08 h^{-1}.

T (°C)	Li/MgO	P_Li/MgO	Li/MgO	P_Li/MgO
	500		600	
Selectivity (mol%)				
CO_x	75.0	30.5	28.4	19.0
$C_1°$-$C_5°$	0.8	5.1	9.3	16.9
C_2H_2	–	16.7	–	0.4
$C_2^{=}$- $C_5^{=}$	21.2	43.9	62.3	63.7
C_6^{+}	3.0	3.8	–	–

Results discussed above indicate that combination of plasma and Li/MgO catalyst during the oxidative conversion of hexane is advantageous resulting in significantly higher hexane conversions and higher selectivities to olefins. However, it is crucial to investigate the contribution of the catalyst surface in both hexane activation and olefin formation when plasma chemistry is occurring.

At 500 °C, the similarity in hexane conversions with both the catalyst and quartz systems (Figure 4.7) indicates less significant contribution from the catalyst in hexane conversion at this temperature. The higher conversions achieved with the presence of a dielectric material (Li/MgO catalyst and quartz inert) compared to the plasma reactor (P_ER), is thus due to accelerated gas phase chemistry as result of increase in both permittivity and electron energy with the introduction of the packing material. However at 600 °C, hexane conversion from the P_Li/MgO was significantly higher than that from P_Quartz system. This indicates that at this temperature there is more contribution from the catalytic defect sites ($[O^-]$) in hexane activation.

Figure 4.8 presents the product distribution from the oxidative conversion of hexane at 500 °C in the systems: (i) plasma empty reactor (P_ER), (ii) plasma- Li/MgO (P_Li/MgO) and (iii) plasma-quartz inert (P_Quartz).

Compared to both P_ER and P_Quartz systems, P_Li/MgO resulted in less formation of C_6^+ products, and more of combustion products. This is mainly explained, as discussed earlier, by the unselective interaction of intermediate radicals with the O^{2-} sites of MgO, enhancing combustion and minimizing coupling reactions. Both the catalyst and quartz systems resulted in significantly higher C_2H_2 formation than the empty reactor. It is reported by Kado *et al.* [23] that extent of C_2H_2 formation depends on the concentration of CH radicals; thus depends on the extent of dissociation and dehydrogenation reactions *via* electron impacts. In agreement, the high selectivities to C_2H_2 observed for both catalyst and quartz systems are due to the increase in extent of electron impact excitations as result of increase in permittivity and electron energy with the introduction of the packing material.

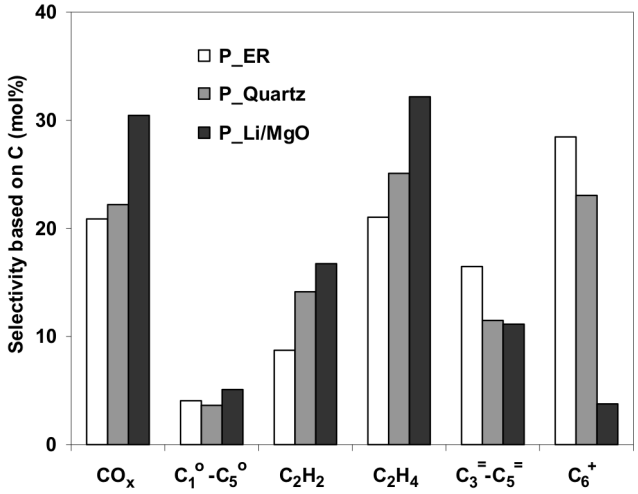

Figure 4.8. Product distribution of oxidative conversion of hexane at 500 ^oC, with (i) P_ER (ii) P_Quartz and (iii) P_Li/MgO systems. Reaction conditions: 100 ml/min, 10% hexane, 8% oxygen and balance helium, WHSV =3.08 h^{-1}.

The olefin distribution, *i.e.*, (C_2H_2+C_2H_4) > ($C_3^=$-$C_5^=$) for the above three systems (Figure 4.8) strongly suggests that at this temperature plasma chemistry is more dominant. Further, to gain insight on the contribution of Li/MgO catalyst in hexane activation and in controlling olefin formation, a different reactor configuration with Li/MgO downstream to plasma (Figure 4.1.d) was investigated and compared to gas phase non-catalytic reactions in an empty reactor as in Figure 4.2.c. Results of experiments with this reactor configuration at 500 °C (Table 4.2) confirm the low contribution of the catalyst in hexane activation and in olefin formation. At this temperature the catalyst downstream to plasma (PB_Li/MgO) showed slightly lower hexane conversion due to quenching and similar selectivity to C_2-C_5 olefins, compared to the plasma reactor in absence of the catalyst (P_ER) (Figure 4.2.c). Thus, at 500 °C, plasma chemistry is more dominant, where hexane activation in gas phase *via* electron impact excitations and collisions with O(^{3}P) atoms (eq. 1-7) is a more significant pathway.

Table 4.2. Influence of catalyst downstream to plasma zone.
Reaction conditions: 100 ml/min, 10% hexane, 8% oxygen and balance helium, WHSV =5.1 h^{-1}, T = 500 ^oC.

	P_ER	PB_Li/MgO
Conversion (mol%)		
C_6H_{14}	23.2	20.3
O_2	72.1	92.3
Selectivity (mol%)		
CO_x	20.0	54.7
C_1^o-C_5^o	2.3	3.6
C_2H_2	5.3	10.5
$C_2^=$- $C_5^=$	30.1	31.2
C_6^+	42.3	–

Figure 4.9 presents the product distribution at 600 °C of the three systems: i) plasma empty reactor (P_ER), (ii) plasma- Li/MgO (P_Li/MgO) and (iii) plasma-quartz inert (P_Quartz). Similar as in P_ER, acetylene formation in the P_Li/MgO system was minimal mainly due to complete oxygen consumption (O_2 conversion = 100%). In the quartz system, as oxygen was not completely consumed (O_2 conversion = 97 mol %), C_2H_2 formation was still observed.

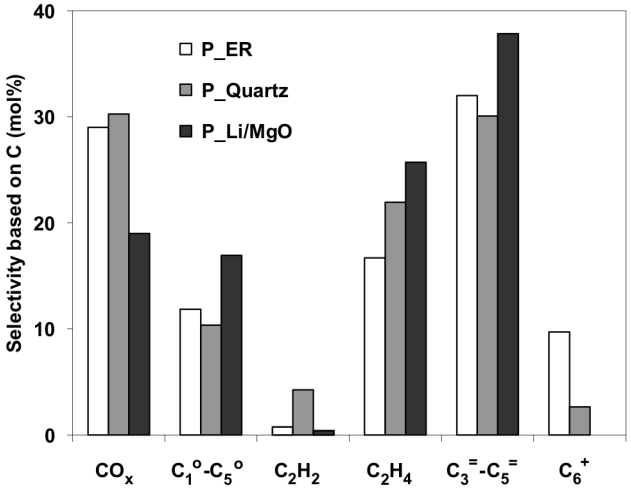

Figure 4.9. Product distribution of oxidative conversion of hexane at 600 °C, with (i) P_ER, (ii) P_Quartz and (iii) P_Li/MgO systems. Reaction conditions: 100 ml/min, 10% hexane, 8% oxygen and balance helium, WHSV =3.08 h^{-1}.

Generally at this temperature more of C_3-C_5 olefins than ethylene was observed with all the systems, *i.e.,* ($C_3^=$-$C_5^=$) > C_2H_4. The P_Li/MgO system, however, resulted in considerably higher formation of C_3-C_5 olefins (38 mol%) than P_ER (32 mol%) and P_Quartz systems (30 mol%). This indicates the role of the Li/MgO in enhancing C_3-C_5 olefin formation.

Further, experiments with Li/MgO downstream to plasma (PB_Li/MgO) at 600 °C (Table 4.3) showed higher hexane conversion and significantly higher C_2-C_5 olefins (64 mol%) than with the P_ER (48 mol%). The higher selectivity to olefins suggests consecutive interaction of alkyl radicals formed in the plasma with the active sites of Li/MgO, abstracting a second hydrogen atom from the alkyl radical forming an olefin.

Table 4.3. Influence of catalyst downstream to plasma zone.
Reaction conditions: 100 ml/min, 10% hexane, 8% oxygen and balance helium, WHSV =5.1 h-1, T = 600 ^{o}C.

	P_ER	PB_Li/MgO
Conversion (mol%)		
C_6H_{14}	30.5	38.0
O_2	99.4	99.3
Selectivity (mol%)		
CO_x	27.7	26.1
C_1^{o}-C_5^{o}	7.2	8.1
C_2H_2	1.3	1.0
$C_2^{=}$- $C_5^{=}$	48.2	64.8
C_6^{+}	15.6	–

Thus at 600 ^{o}C, even in presence of plasma, the surface chemistry of Li/MgO becomes significant; *i.e.,* (i) hexane activation *via* the [$Li^{+}O^{-}$] defect sites, forming iso-hexyl radicals, which through β-scission yield C_3-C_5 olefins, and (ii) consecutive interaction of intermediate radicals with the [O^{-}] defect sites of the catalyst leading to more olefin formation. A simplified mechanism for hexane cracking *via* [O^{-}] sites of Li/MgO at 600 ^{o}C is illustrated in scheme 5.1.

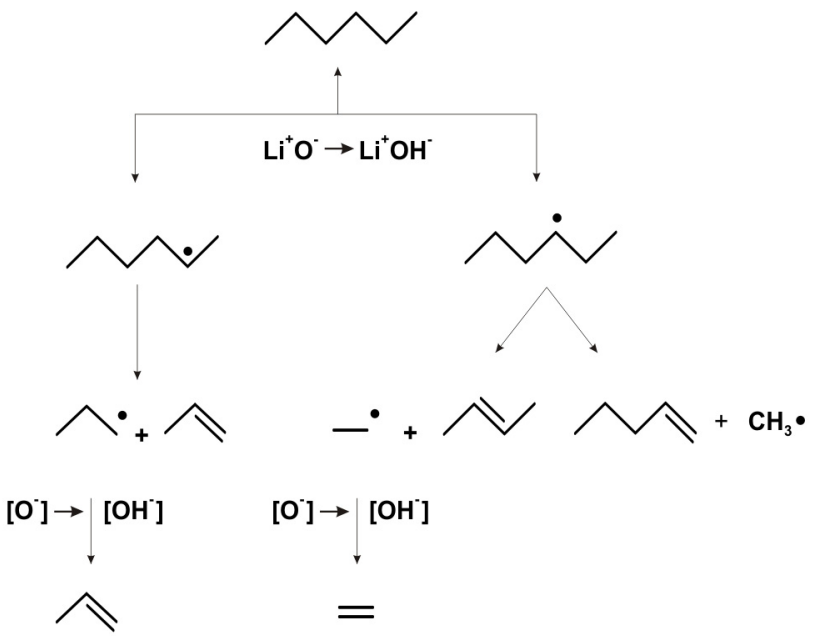

Scheme 4.1. Mechanism of hexane cracking *via* [O^{-}] sites of Li/MgO at 600 ^{o}C.

4.3.4 Optimal reactor configuration

The integrated plasma-Li/MgO system is the optimal reactor configuration with the highest yields of C_2-C_5 olefins, as shown in Figure 4.10. The introduction of the catalyst in the plasma system results in an increase in both electron density and energy; thus the number of electron impact excitations increases, leading to improved hexane conversions. Moreover UV light from plasma creates new [O^-] defect sites on the catalyst surface, enhancing activity and minimizing combustion reactions.

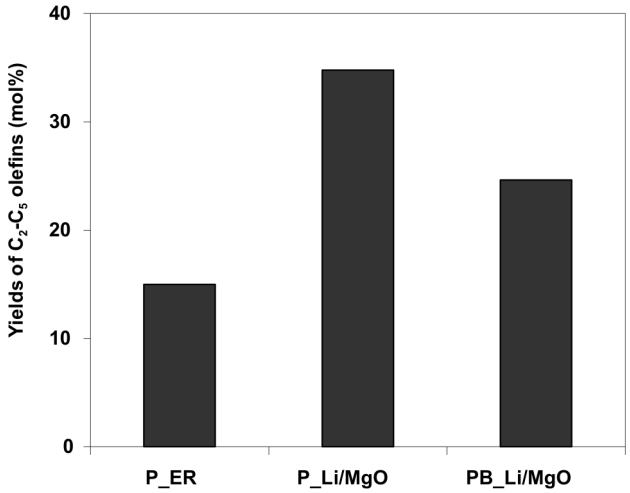

Figure 4.10. Yields of C_2-C_5 olefins with different reactor configurations. Reaction conditions: 100 ml/min, 10% hexane, 8% oxygen and balance helium, T = 600 ^oC.

In order to explore the potential for industrial application of the integrated plasma-Li/MgO system, an estimation of the energy efficiency of the system was attempted. Table 4.4 shows a qualitative estimate of the energy efficiency of the integrated plasma-Li/MgO system. The amount of the energy absorbed by plasma (180 J/min) was compared to the amount of energy needed for dissociation of the C-H bond in the converted hexane (54 J/min). Results indicate that only 30% of energy absorbed by plasma is utilized for hexane conversion. Inefficient utilization of plasma energy, thus, strongly suggests that further improvement in the energy efficiency of the system is required.

Table 4.4. Estimated energy for integrated plasma-Li/MgO.

BDE, 2ndary C-H	Hexane converted	Energy needed	Energy absorbed by plasma	Energy loss
KJ/mol	mol/min	J/min	J/min	%
394	1.38E-04	54	180	70

4.4 Conclusions

Application of both plasma and Li/MgO catalyst in oxidative conversion of hexane results in considerable improvements both in hexane conversions and selectivities to light olefins ($C_2^=$ - $C_5^=$) at a relatively low temperatures of 500 to 600 ^oC. The yields of olefins achieved with the integrated plasma-Li/MgO-catalyst are considerably higher than those achieved with Li/MgO in absence of plasma or in plasma reactor in absence of catalyst.

The combination of plasma and catalyst results in synergy. (i) Presence of plasma creates new [O^-] defect sites in the catalyst. These enhance hexane activation and moreover minimize the unselective interaction of radicals with O^{2-} sites of MgO resulting in alkoxide formation, hence minimize combustion. (ii) Presence of the Li/MgO catalyst in the plasma reactor, results in an increase in both electron-density and -energy, leading to enhanced electron impact dissociations of hexane and oxygen molecules.

In the integrated plasma-Li/MgO system hexane activation takes place *via* three main routes; (i) C-H bond scission *via* the [O^-] defect sites originally present as [Li^+O^-] as well as created *via* photo-excitation of O^{2-} sites of MgO, (ii) C-C, C-H bond scission by electron-impact excitation of hexane molecule with electrons, and (iii) C-H bond scission by O(^{3}P) oxygen atoms formed from collisions of oxygen molecules with electrons.

Temperature influences the performance of the integrated plasma-Li/MgO system, as illustrated by the differences in the product distribution at both temperatures. At 500 ^oC, significant formation of acetylene and ethylene and low formation of the high olefins ($C_3^=$-$C_5^=$) was observed. It is proposed that at this temperature plasma chemistry is more dominant. Acetylene formation is a characteristic of plasma chemistry, and can be formed *via* dimerization of CH species formed in the presence of plasma and through the extensive dehydrogenation of ethane.

At 600 ^oC, the reaction of intermediate radicals with oxygen to from olefins, is more favored, hence more formation of the high olefins was observed, *i.e.;* ($C_3^=$ - $C_5^=$) > C_2H_4. At this temperature the contribution of Li/MgO catalyst in hexane activation and enhancing olefin formation becomes more significant. The absence of acetylene at this temperature together with oxygen depletion, suggest that oxygen depleting conditions are required to minimize acetylene formation.

Despite the significant improvements achieved with the application of plasma in the yields of C_2-C_5 olefins, the integrated plasma-Li/MgO system still can not compete with the conventional cracking processes, due to the low energy efficiency.

References

[1] C.-H. Lin, K.D Campbell, J.-X. Wang, J.H. Lunsford, J. Phys. Chem. 90 (4) (1986) 534-537.

[2] D. J. Driscoll, W. Martir, J. H. Lunsford, J. Phys. Chem. 91 (13) (1987) 3585-3588.

[3] T. Ito, J.-X. Wang, C.-H. Lin, J.H. Lunsford, J. Am. Chem. Soc.107 (1985) 5062-5068.

[4] M. Xu, C. Shi, X. Yang, M.P. Rosynek, J.H. Lunsford, J. Phys. Chem. 96 (15) (1992) 6395-6398.

[5] E. Morales, J.H. Lunsford, J. Catal. 118 (1989) 255-265.

[6] F. Cavani, F. Trifiro, Catal. Today 24 (1995) 307-313.

[7] M.V. Landau, M.L. Kaliya, A. Gutman, L.O. Kogan, M. Herskowitz, P.F. van den Oosterkamp, Stud. Surf. Sci. Catal. 110 (1997) 315-326.

[8] L. Leveles, K. Seshan, J.A Lercher, L. Lefferts, J. Catal. 218 (2003) 307-314.

[9] L. Leveles, K. Seshan, J.A. Lercher, L. Lefferts, J. Catal. 218 (2003) 296-306.

[10] C. Trionfetti, I.V. Babich, K. Seshan, L. Lefferts, Appl. Catal. A 310 (2006) 105-113.

[11] C. Trionfetti, I.V. Babich, K. Seshan, L. Lefferts, Langmuir 24 (2008) 8220-8228.

[12] F. Cavani, N. Ballarini, A. Cericola, Catal. Today 127 (2007) 113-131.

[13] C. Boyadjian, L. Lefferts, K. Seshan, Appl. Catal. A 372 (2010) 167-174.

[14] C. Trionfetti, A. Agiral, ChemPhysChem 9 (4) (2008) 533-537.

[15] C. Trionfetti, A. Agiral, J. Phys. Chem. 112 (11) (2008) 4267-4274.

[16] A. Agiral, Ph.D. Thesis, University of Twente, Enschede,

[17] A. Agiral, C. Boyadjian, K. Seshan, L. Lefferts, J.G.E. Gardeniers, J. Phys. Chem. C, submitted.

[18] S. Ahmed, A. Aitani, F. Rahman, A. Al-Dawood, F. Al-Muhaish, Appl. Cat. A 339 (2009) 1-24.

[19] A.M. Harling, V. Demidyuk, S.J.Fischer, J. C. Whitehead, Appl. Cat. B 82 (2008) 180-189.

[20] X. Zhu, P. Huo, Y.-P. Zhang, D.-g. Cheng, C.-j. Liu, Appl. Cat. B 81 (2008) 132-140.

[21] T. Nozaki, N. Muto, S. Kado, K. Okazaki, Catal. Today 82 (2004) 57-65.

[22] W. Kangjun, L. Xiaosong, W. Hui, S. Chuan, X. Yang, Z. Amin, Plasma Sci. Tech. 10 (2008) (5) 600-604.

[23] S. Kado, K. Urasaki, Y. Sekine, K. Fujimoto, T. Nozaki, K. Okazaki, Fuel 82 (2003) 2291-2297.

[24] K.-I. Aika, J.H. Lunsford, J. Phys. Chem. 81 (14) (1977) 1393-1398.

[25] K.-I. Aika, J.H. Lunsford, J. Phys. Chem. 82 (16) (1978) 1794-1800.

[26] E.V. Kondratenko, M.Yu. Sinev, Appl. Catal. A 325 (2007) 353-361.

[27] T. Berger, M. Sterrer, O. Diwald, E. Knozinger, J. Phys. Chem. B. 108 (2004) 7280-7285.

[28] M. Sterrer, T. Berger, O. Diwald, E. Knozinger, J. Am. Chem. Soc. 125 (2003) 195-199.

[29] O. Diwald, M. Sterrer, E. Knozinger, P.V. Sushko, A. Shluger J. Chem. Phys. 116 (4) (2002) 1707-1712.

[30]http://clippercontrols.com/info/dielectric_constants.html#M

[31]http://farside.ph.utexas.edu/teaching/em/lectures/node100.html

[32] X. Xu, Thin Solid Film 390 (2001) 237-242.

[33] R. Li, Q. Tang, S. Yin, T. Sato, Fuel Process. Technol. 87 (2006) 617-622.

[34] W. S. Kang, J. M. Park, Y. Kim, S. H. Hong, IEEE Trans. Plasma Sci., 31 (2003) 504-510.

Chapter 5

Production of C_3/C_4 Olefins from Naphtha: Catalytic Oxidative Cracking as an Alternative Route to Steam Cracking

A conceptual design of the catalytic oxidative cracking (COC) of hexane as a model compound of naphtha, is reported. The design is based on experimental data which is elaborated through a structural design method to a process flow sheet. The potential of the catalytic oxidative cracking as an alternative process to steam cracking (SC) is discussed through comparing the key differences of both processes. The presence of Li/MgO catalyst in the COC process (i) induces hexane cracking at lower operation temperatures (575 ^oC) than in steam cracking (800 ^oC) and (ii) controls the olefin distribution by increasing the ratio of ($C_4^=$ +$C_3^=$)/$C_2^=$. The product distribution, thus separation train of both processes, is different. Catalytic oxidative cracking is designed to maximize propylene and butylene production, while steam cracking is designed to maximize ethylene production. In comparison to steam cracking, catalytic oxidative cracking process is more energy efficient and consumes 53% less of total duty. However, a preliminary economical evaluation illustrates that the catalytic oxidative cracking process still can not compete with the steam cracking process.

5.1 Introduction

Light olefins (ethylene, propylene, butylenes) are the building blocks for the chemical industry. They are currently the raw materials for the synthesis of: (i) bulk chemicals; *e.g.,* ethylene oxide, acrolein, (ii) polymers; *e.g.,* poly-ethylene, -propylene or –butylenes, or (iii) fuels such as diesel, gasoline; *e.g.,* by butene/butane alkylation. In a rapidly growing world with continuous development in the production of new synthetic materials, the demand of these petrochemicals is increasing tremendously and a growth rate of 4% is predicted for the coming years [1]. The demand for the propylene market is growing faster than that of the ethylene market by ~1% [1]. Thus propylene yields from current production technologies are unlikely to be able to satisfy these demands.

Steam cracking, although being the major route for the production of light olefins, is becoming less attractive both environmentally and economically, as it is the most energy-consuming process in the chemical industry. It is reported [1] that the pyrolysis section of a naphtha steam cracker alone consumes approximately 65% of the total process energy required and approximately 75% of the total exergy loss. Moreover, the process is accompanied with high emissions of CO_2 as result of fuel combustion. The drawbacks of this process have urged substantial interest in the development of alternative routes for light olefin production [1]. Although intensive research is performed in this area, only a few processes have been commercialized. Catalytic dehydrogenation processes (Oleflex, STAR, FDB-4, Catofin) were developed in the early 80's as alternative routes for light olefin production [2-4]. However, these processes have made only limited breakthrough commercially. The major disadvantages of this route is the thermodynamic equilibrium leading to limited yields, and the strong tendency to coking and consequently catalyst deactivation, leading to short life times of the catalyst.

Catalytic Oxidative Cracking (COC) of naphtha to light olefins is conceptually a promising alternative to steam cracking for a variety of reasons; (i) the process runs autothermally; reaction in the presence of oxygen is exothermic and therefore the energy required for cracking can be generated *in-situ*, (ii) presence of oxygen shifts the thermodynamic equilibrium, overcoming the olefin yield limitations encountered during the dehydrogenation reactions and (iii) presence of oxygen limits the extent of coking. Moreover, the presence of a catalyst enhances the C-H, and C-C bond cleavage in the alkane, thus induces activity at lower temperatures than those utilized in steam cracking. We expect that with oxygen co-feeding (autothermal operation) and catalytically induced reaction at relatively low temperatures, the external energy input (fuel combustion) will be minimized, and consequently CO_x and NO_x emissions will be reduced. Moreover, with the presence of catalyst we aim to control olefin distribution increasing the ratio of the high olefins (propylene, butylenes) to ethylene. This is not possible in steam cracking where ethylene is produced as the major product [1].

The development of an efficient oxidation catalyst which minimizes combustion, however, remains a challenge. The right catalyst should be able to selectively activate the alkane in the presence of the very reactive olefins, thus inhibiting the consecutive deep oxidation of the product olefins. Li/MgO catalyst has shown promising performance for the oxidative dehydrogenation/cracking of light alkanes [5-14], and recently for the oxidative cracking of hexane [15]. Li/MgO is basic in nature and possesses no formal red-ox properties. Therefore, unlike the case in oxidic catalysts with red-ox properties *e.g.* V_2O_5/MgO [16], consecutive combustion of olefins over this catalyst is significantly suppressed. Thus the high

selectivities to olefins are maintained even at high alkane conversions [12-15]. In the oxidative cracking of butane and propane over Li/MgO catalyst, despite of the high conversion levels achieved (70 mol% of n-butane and 60 mol% of propane), appreciable selectivity to light olefins of ~60 mol% were obtained [12].

In the present study, the technical feasibility of the catalytic oxidative cracking using hexane as a model compound for naphtha, over the Li/MgO catalyst is reported. Moreover, the technical and economical potential of the process in comparison to steam cracking is discussed. Experimental results from the oxidative cracking of hexane over Li/MgO catalyst previously reported by us [15] are the basis for the mass balance and design calculations. These results are utilized together with a structural design method [17-18] to develop, step-by-step, the process flow sheet for the oxidative cracking process (Figure 5.1).

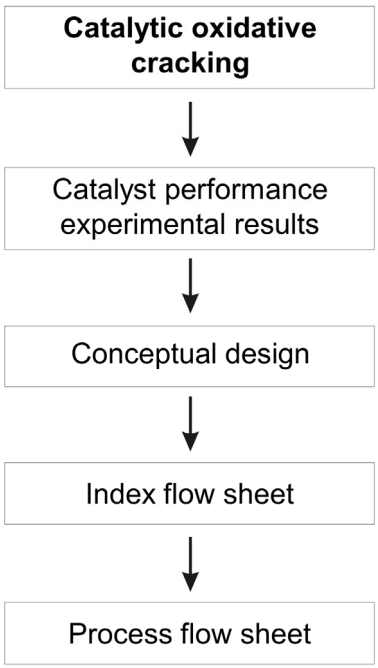

Figure 5.1. Steps to systematically create a process flow sheet.

5.2 Experimental results

Experimental results of catalytic oxidative cracking (COC) of hexane over Li/MgO in the temperature range 425-575 ^{o}C (Figure 5.2), showed a clear influence of temperature on both hexane conversions and selectivity to products [15]. Hexane conversion increased with temperature. Gas phase activation of hexane (not shown here) started to be noticeable, at temperatures above 600 ^{o}C. Therefore, to minimize gas phase non-catalytic conversion of hexane, 575 °C was selected as an optimum temperature. It is generally believed that [$Li^{+}O^{-}$] in Li/MgO is responsible for the catalytic activity. The [O^{-}] site is a strong hydrogen abstractor and induces homolytic scission of the C-H bond in the hexane forming a radical (eq. 1).

$$C_6H_{14} + O^-_s \rightarrow C_6H_{13}\bullet + OH^-_s \quad (1)$$

$$C_6H_{13}\bullet + O_2\,(g) \rightarrow C_1\text{-}C_5\ (\text{paraffins \& olefins}) + CO_x + H_2O + H_2 \quad (2)$$

The formed radical then undergoes complex radical chemistry in the presence of oxygen in the gas phase forming a product mixture of C_2-C_5 olefins, C_1-C_5 alkanes, as well as combustion products (H_2O and CO_x), and by-product H_2 [15]. Thus, oxidative cracking over Li/MgO is a heterogeneously initiated homogeneous reaction. With the increase in temperature a continuous decrease in CO_x formation and a continuous increase in C_2-C_4 olefin formation was observed (Figure 5.2).

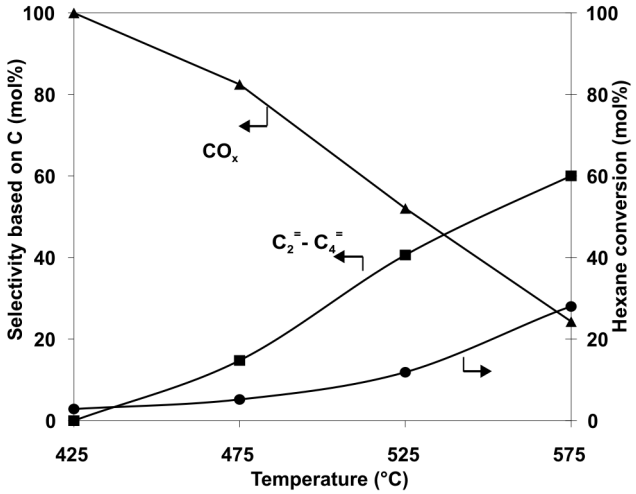

Figure 5.2. Influence of temperature on hexane conversions and selectivities to products during the oxidative cracking of hexane over Li/MgO. Reaction conditions: 100 ml/min, 10% hexane, 8% oxygen and balance He. Catalyst amount = 100 mg [15].

A typical product mixture of COC over Li/MgO at 575 °C is given in Figure 5.3. At this reaction conditions (300 mg catalyst), 45 mol% of hexane conversion and 63 mol% selectivity (based on C) to C_2-C_4 olefins was observed. Carbon and hydrogen balance closed within ±5%.

Further, the influence of the oxygen concentrations in the feed on both hexane conversions and selectivities to olefins has been studied (Figure 5.4). Oxygen in the feed up to 4 mol% has a significant influence on hexane conversions. This is mainly explained by the role of oxygen in regenerating the catalyst by removing hydrogen from the surface [Li^+OH^-] species (eq. 3) formed during the oxidation of hexane. The further slight increase in hexane conversions with the increase in oxygen concentrations above 4 mol%, is explained by the role of oxygen in accelerating the radical chemistry through the formation of $HO_2\bullet$ radicals, which act as chain propagators in gas phase reactions (eq. 4). Oxygen also plays a significant role in inhibiting coke formation. However increase in oxygen concentrations results in increase in CO_x formation. Moreover, increase in explosion risks is expected. Therefore, optimal oxygen concentrations are necessary to maximize hexane conversions and minimize both combustion reactions and explosion risks.

$$2Li^{+}OH^{-} + ½\ O_2 \rightarrow 2Li^{+}O^{-} + H_2O \qquad (3)$$

$$C_nH_{2n+1}\bullet + O_2 \rightarrow C_nH_{2n} + HO_2\bullet \qquad (4)$$

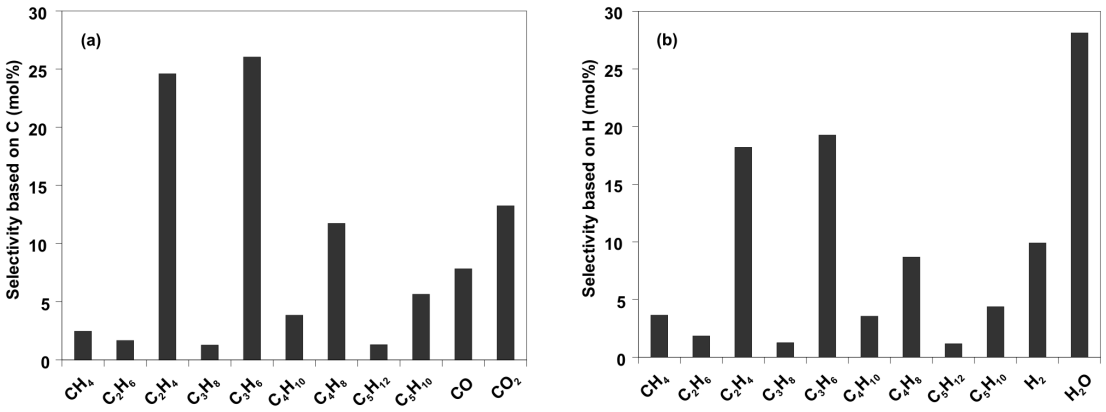

Figure 5.3. Product distribution observed during the oxidative cracking of hexane. Selectivities based on C (a), and based on H (b) are presented. Reaction conditions: 100 ml/min, 10% hexane, 8% oxygen and balance He. T = 575 ^{o}C. Catalyst amount = 300 mg. Hexane conversion = 45 mol% [15].

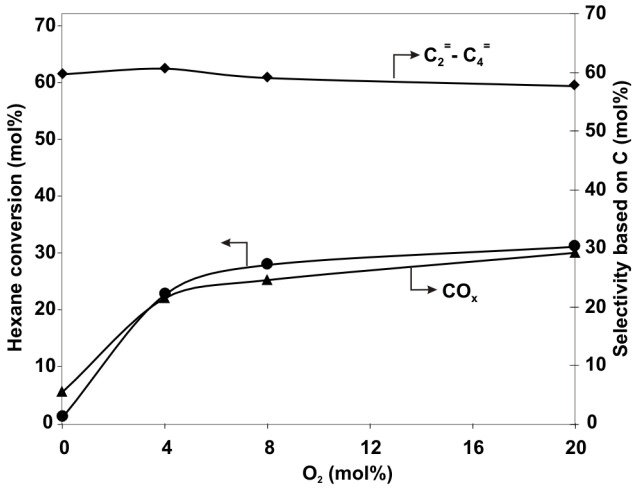

Figure 5.4. Influence of oxygen concentrations on hexane conversions as well selectivity to products. (•) hexane conversion, (▲) selectivity to CO_x, (♦) selectivity to light olefins ($C_2^{=}$-$C_4^{=}$). Oxygen conversions = 69, 65 and 39 mol% at 4, 8 and 20 mol% O_2, respectively. Reaction conditions: 100 ml/min, 10% hexane and balance helium, T=575 ^{o}C. Catalyst amount = 100 mg [15].

The reported experimental data of catalyst activity (45 mol% of hexane conversion) and selectivity to various products presented in Figure 5.3 are further utilized to determine the composition of feed and product streams of the process overall, hence are the basis for the

mass balance and design calculations. However, it is necessary to note that catalytic experiments were performed in conditions far from a real case process. In these experiments hexane was used as a model compound of naphtha. We assume that the product distribution, hence both mass balance and design calculations elaborated in the present work for the catalytic cracking of hexane, is identical when naphtha is used as the feed. This is not unusual, as hexane cracking has been used to model naphtha cracking in FCC processes and the results have been quite relevant [19]. Moreover in the experimental work our objective was to study the performance of the catalyst; hence to minimize gas phase activation of hexane, low concentrations of hexane and oxygen were used by dilution in helium. Hexane–to-oxygen ratio to be used in this process design and choices regarding the dilution is discussed below in the conceptual design section. Figure 5.5 presents a black box sequence of the process, identifying the key process overall parameters.

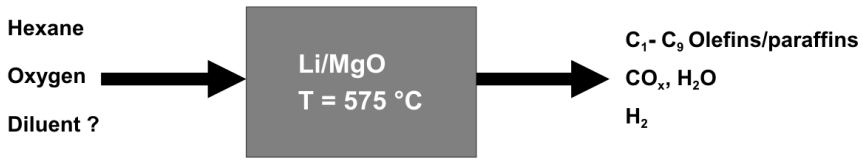

Figure 5.5. Black box of the COC process.

5.3 Conceptual design

Figure 5.6 presents a functional block diagram of the COC process. The process feed consists of hexane and oxygen. The possible use of diluent is discussed later in the alternative and choices section. Due to the low conversion in the reactor (45 mol%), it is decided to recycle the unconverted hexane. Propylene and butylenes are the main desired products and are recovered together and separately from ethylene and the remaining by-products (heavy olefins ($\geq C_5$), C_1-C_5 alkanes, H_2, H_2O, CO_x). Based on various process alternatives and choices, this block diagram is elaborated further to a comprehensive flow sheet.

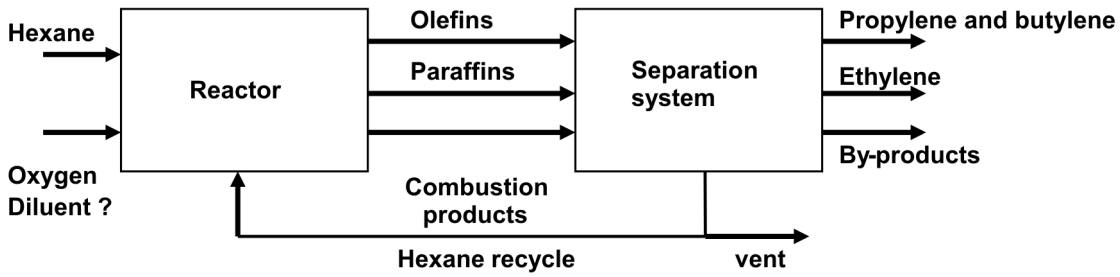

Figure 5.6. Functional block diagram of the COC process.

5.3.1 Alternatives and choices

Overall process alternatives and choices made are given in Figure 5.7. Decisions and choices are further discussed below.

Variable	Alternative 1	Alternative 2	Alternative 3
Feed	Naphtha +air	Naphtha + O_2 + diluent	**Naphtha + O_2**
Reactor	Fixed bed reactor	**Fluidized bed reactor**	Catalytic membrane reactor
Separations			
$C_2^=/C_2$	Absorption	**distillation**	membranes
$C_3^=/C_3$	Pressure swing adsorption (PSA)	**distillation**	membranes
$C_4^=/C_4$	OLEX process	**distillation**	membranes
Separation order	C_2/C_3 first	**C_4/C_3 first**	
Hydrogen	**Sell hydrogen as product**	Use hydrogen	
Heavies removal	With phase separators	**With distillation**	

Figure 5.7. Alternatives and choices.

5.3.1.1 Feed

Hexane and oxygen are the only feeds to the process. Pure oxygen is decided to be utilized instead of air or a mixture of oxygen and diluent, since the separation of the diluent (*e.g.,* air or N_2) is complicated and costly. To avoid explosion, oxygen concentrations in the reactor should be limited. Figure 5.8 presents the ternary diagram of explosion limits for a mixture of octane (as model compound of naphtha), oxygen and hydrogen at reaction conditions. Since the reactor volume consists mainly of a mixture of hydrocarbons, oxygen and hydrogen, the process should be operated at a very high volume percentage of the alkane and a low oxygen volume percentage to avoid explosive mixtures.

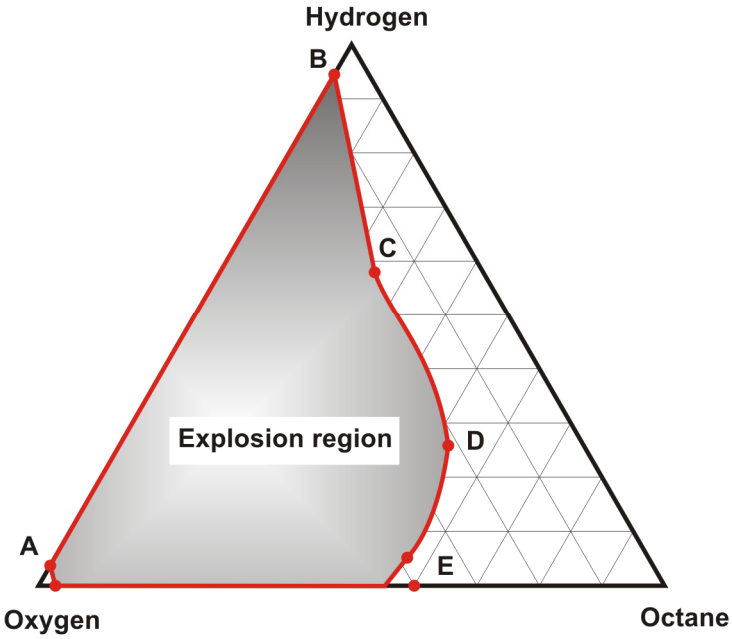

Figure 5.8. Explosion limits of reaction mixture at reaction conditions [20].

Since one of the concepts of COC is the autothermal operation, a certain amount of oxygen is required for the combustion of a part of the alkane feed. The minimum oxygen concentration required for autothermal operation was estimated using the following equations (5-7), and was based on octane as the alkane feed. It is assumed that this estimation is also valid when hexane or naphtha is used as a feed. The values of the required parameters are given in Table 5.1.

$$\underset{[evaporation]}{f_{burned}\Delta H_{combustion}} = (1-f_{burned})(\underbrace{\Delta H_{vap}}_{[evaporation]} + \underbrace{Cp_{liquid}(T_{boil}-T_{feed})}_{[liquid\ heating]} + \underbrace{Cp_{gas}(T_{reaction}-T_{boil})}_{[gas\ heating]} + \underbrace{\zeta\cdot\Delta H_r}_{[heat\ of\ reaction]}) \quad (5)$$

Table 5.1. Physical properties of octane.

properties	value
Cp_{gas} (J/mol/K)	241
Cp_{liquid} (J/mole/K)	255
T_{boil} (K)	399
ΔH_{vap} (KJ/mol/K)	35
HHV (KJ/mol)	5074
HHV (KJ/Kg)	44419
$\Delta H_{reaction}$ (KJ/mol)	416
$T_{reaction}$ (K)	775

It is assumed that the un-combusted octane reacts to four molecules of ethylene and one molecule of hydrogen (eq. 6).

$$C_8H_{18} \rightarrow 4C_2H_4 + H_2 \qquad \Delta H_r = 416 \text{ (KJ/mole)} \qquad (6)$$

Assuming an inlet temperature of 25 °C and a 45% of conversion of octane equation 5 was solved. Results indicate that 6.25mol% of the octane feed needs to be combusted to provide enough heat for autothermal operation of reaction 6. Assuming complete combustion of the octane according to reaction 7, the concentration of oxygen needed (if fed totally at the reactor inlet) for sufficient heat production for autothermal operation was calculated to be 45 mole%.

$$C_8H_{18} + 12.5O_2 \rightarrow 8CO_2 + 9H_2O \quad \Delta H_r = -5074 \text{ KJ/mol} \qquad (7)$$

However, according to the explosion limits, this percentage of oxygen is not within the safe operating zone. Since safe operation necessitates maximum oxygen concentrations of 20-30%, we conclude that in case of co-feeding oxygen in one stage at the reactor inlet, it is impossible to operate autothermally. Autothermal operation, however, would be possible when using a multiple oxygen feed, where local oxygen concentrations are kept low.

5.3.1.2 Reactor

To prevent coupling reactions in the reactor during the COC process, products must be rapidly removed from the reaction zone. Thus high gas hourly space velocities should be utilized (ranging from 100,000 h^{-1} – 1,000,000 h^{-1}) to minimize the residence time inside the reactor. The reactor selection is done according to the method of Krishna and Sie [21].

Fixed bed, fluidized bed and catalytic membrane reactors (Figure 5.7) are conceptually potential reactor choices for oxidation reactions [22]. The significant advantage of the FLBR is the possibility of achievement an isothermal catalytic bed, thus avoiding the hot spots typical of FBRs. For an autothermal operation at low residence time, the utilization of a FLBR leads to better selectivities compared to a FBR. For the oxidative dehydrogenation of propane, butane and iso-butane, the use of these reactors led to remarkable selectivities to olefins [22]. The high selectivities achieved with this reactor were explained by the total oxygen consumption close to the distributor, hence inhibiting the consecutive combustion of the olefins formed at the beginning of the catalytic bed.

In addition, in a FLBR it is possible to utilize a distributed oxygen inlet along the catalytic bed [22]. Oxygen differentiation allows maintaining a constant high hexane-to-oxygen ratio and ensures safe operation simultaneously. Thus, it is decided to use multiple oxygen feeds along the fluidized bed.

The utilization of catalytic membrane reactor although conceptually promising, is not considered for this process due to the cost issues for ceramic membranes.

5.3.1.3 Separation

The separation order is determined using the method of Barnicki [23]. Based on this method alternative separation routes were developed (Figure 5.7) and compared to each other resulting in an optimized method of separation. Similar to steam cracking, the reactor outlet has to be quenched directly after the reactor to prevent coupling reactions. After quenching the process stream consists of six groups of components that need to be separated: heavy oil (≥ C_5), light olefins (C_2-C_4) and alkanes (C_1-C_4), unconverted feed, combustion products (CO, CO_2, H_2O) and by product H_2. The liquid phase products *i.e.,* unconverted feed, quench fluid (quench oil and ≥C_5 products) and water should be separated first to prevent the formation of solids at high pressure and low temperature conditions later in the separation process. For similar reasons, removal of CO_2 at early stages is favorable. Figure 5.9 presents a functional flow sheet of the process, with block A representing the first separation unit and block B the second separation unit. In block A the quench oil, water and the unconverted feed are separated and recycled. Afterwards, CO_2 and remaining water are removed. In the last separation unit (block B) light olefins (C_2-C_4) and alkanes (C_1-C_4) as well as the by-products H_2 and CO are separated**.**

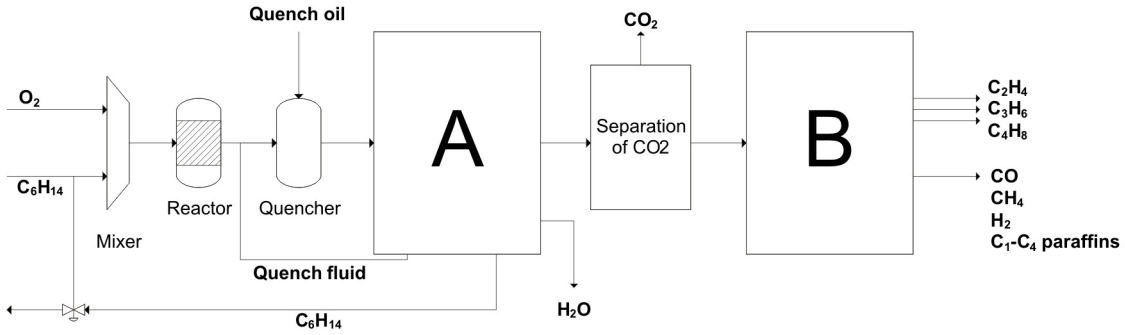

Figure 5.9. Functional flow sheet of the COC process.

Block A

Figure 5.10 represents the separation units of block A. To increase efficiency of separation, the utilization of two distillation columns is favored over the phase separators.

In the first distillation column, 100% of the quench oil and ≥ C_5 products modeled as nonane (C_9), 94% of the water and 78% of the unconverted hexane are recovered in the bottom stream. The remaining products (22% of the unconverted hexane, 6% of the water, C_1-C_4 olefins and alkanes, CO_2, CO and H_2) are fully recovered in the top stream. In the decanter water is separated from the apolar hydrocarbons. The hydrocarbon stream leaving the decanter consists only of 0.7% of water. The hydrocarbons are then separated with the second distillation column. The hexane stream (99.9% recovery) is sent to the reactor, and the nonane stream (99.5% recovery) is sent to the quench.

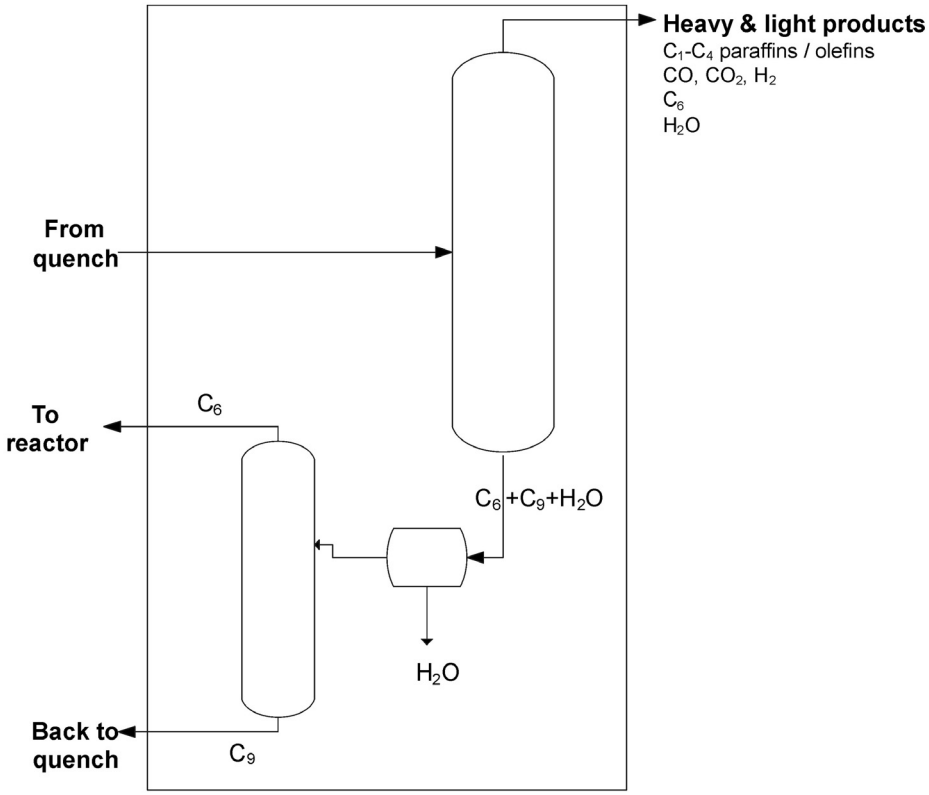

Figure 5.10. Separation units of block A.

Sour gas and water removal

In practice sour gasses (CO_2, H_2S) are removed using absorption towers with amine solutions [24]. This technique is commercially available and is also used in this process design for CO_2 removal. The remaining 6% of water from the top stream of block A, together with water from CO_2 absorption unit (amine-water solution) is separated by a molecular sieve (MS 13X).

Block B

Distillation columns are selected for the separation of all hydrocarbon streams. Compared to alternatives mentioned in Figure 5.7, *e.g.*, absorption and PSA (99.5% recovery), distillation results in more efficient separation (99.99% recovery). The Olex process [25] can provide an efficient separation as in distillation. However this process requires a liquefied feed, hence is not considered as a suitable choice.

Because of the low relative volatility of C_2/C_1, C_2/C_3, $C_2/C_2^=$ and $C_3/C_3^=$, cryogenic distillation is needed for the separation of these products. Regarding the order of separation of the light products *i.e.*, C_1-C_4 olefins/alkanes, CO and H_2, it is decided unlike in steam cracking, to first separate the C_4 products from C_3 and all remaining lighter products (C_2, C_1, CO, H_2). C_4/C_3 separation is easier than C_2/C_3 separation and can be operated at low pressures. Pressurizing the stream after C_4 removal for C_2/C_3 separation will be less energy consuming. Figure 5.11 presents a block scheme for the separation block B. Butane and

butylene are first separated from the process stream. Afterwards, C_2/C_3 hydrocarbons are separated, followed by separation of C_1/C_2, $C_2^=/C_2$ and $C_3^=/C_3$. H_2 is recovered with a palladium-silver membrane, which is a method already used industrially.

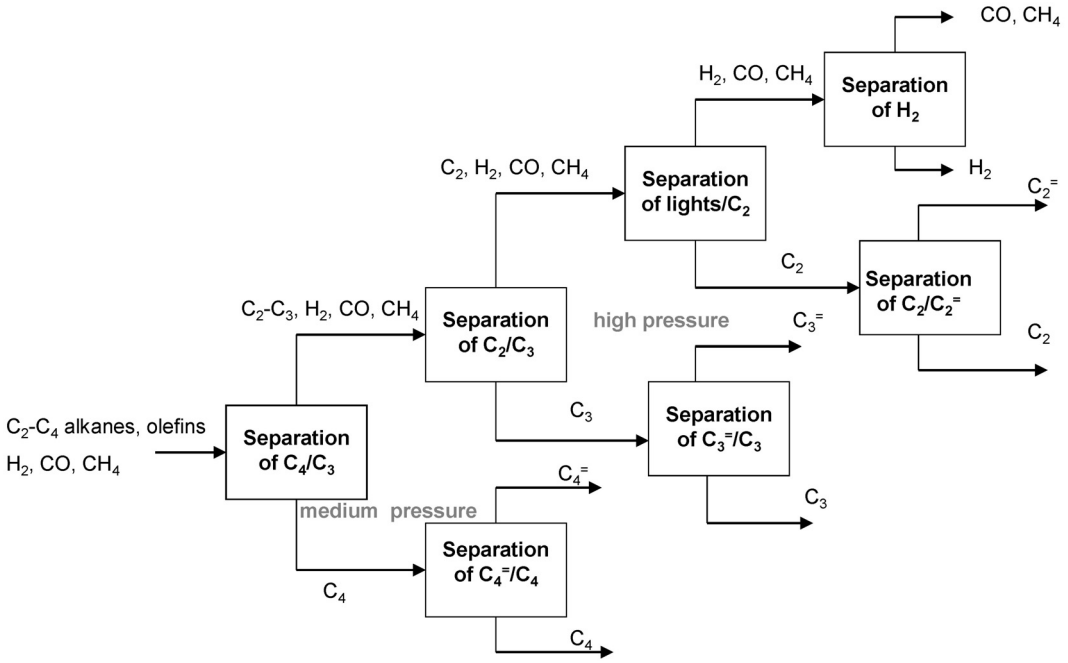

Figure 5.11. Block scheme for separation block B.

5.4 Process flow diagram

For the simulation of the process UNISIM Design Suite R380 is used. The property set chosen for the simulation is the Peng-Robinson equation of state. The process is designed for a total capacity of 300 kton/yr of $C_2^=$-$C_4^=$ products. Due to the lack of sufficient kinetic data, a simplified conversion model was used for the reactor and simulation was performed starting from the reactor outlet. Hexane was used as a model compound of naphtha. For process simulation hexane-to-oxygen molar ratio of 5:3 was used. This amount of oxygen is not sufficient for autothermal operation, but was selected to keep consistency with experimental conditions. Multiple oxygen feeds in the FLBR is expected to provide safe operation. A process overall hexane conversion of 45% was considered and complete oxygen conversion was assumed. The reactor outlet composition was based on experimental results presented in Figure 5.3. Some of the separation units (*e.g.,* sour gas removal) involve absorption and/or desorption processes, hence were not modeled. Figure 5.12 presents a process flow diagram and a comprehensive mass balance of the COC process.

	1	2	3	4	5	6	7	8	9	10	11	12	13	14	15
Temperature (C)	20	20	71	300	348	76	60	0	-144	-14	-7	36	44	69	130
Pressure (kPa)	100	100	100	100	101	100	1000	950	2950	2950	2950	1500	1500	950	950
molar flow (Kmol/hr)	1220	877	659	1540	4243	1553	2536	1912	625	339	83	417	20	161	249
mole balance (Kmol/hr)															
n-hexane	0	873	657	1530	842	657	185	185	0	0	0	0	0	0	185
oxygen	932	0	0	932	0	0	0	0	0	0	0	0	0	0	0
hydrogen	0	0	0	0	206	0	208	208	208	0	0	0	0	0	0
water	0	0	5	5	368	346	22	0	0	0	0	0	0	0	0
CO	0	0	0	0	304	0	304	304	304	0	0	0	0	0	0
CO2	0	0	0	0	596	0	596	0	0	0	0	0	0	0	0
Ethane	0	0	0	0	29	0	29	29	0	0	29	0	0	0	0
propane	0	0	0	0	21	0	21	21	0	0	0	2	19	0	0
n-butane	0	0	0	0	64	0	64	64	0	0	0	0	0	0	64
ethylene	0	0	0	0	393	0	393	393	0	338	54	0	0	0	0
propylene	0	0	0	0	416	0	416	416	0	0	0	415	0	0	0
1-butylene	0	0	0	0	161	0	161	161	0	0	0	0	0	161	0
methane	0	0	0	0	49	0	49	49	49	0	0	0	0	0	0
$=C_5$ (modeled as n-nonane)	0	0	3.5	3.5	110	110	0	0	0	0	0	0	0	0	0
Carbon and hydrogen balance closed within ±5%															

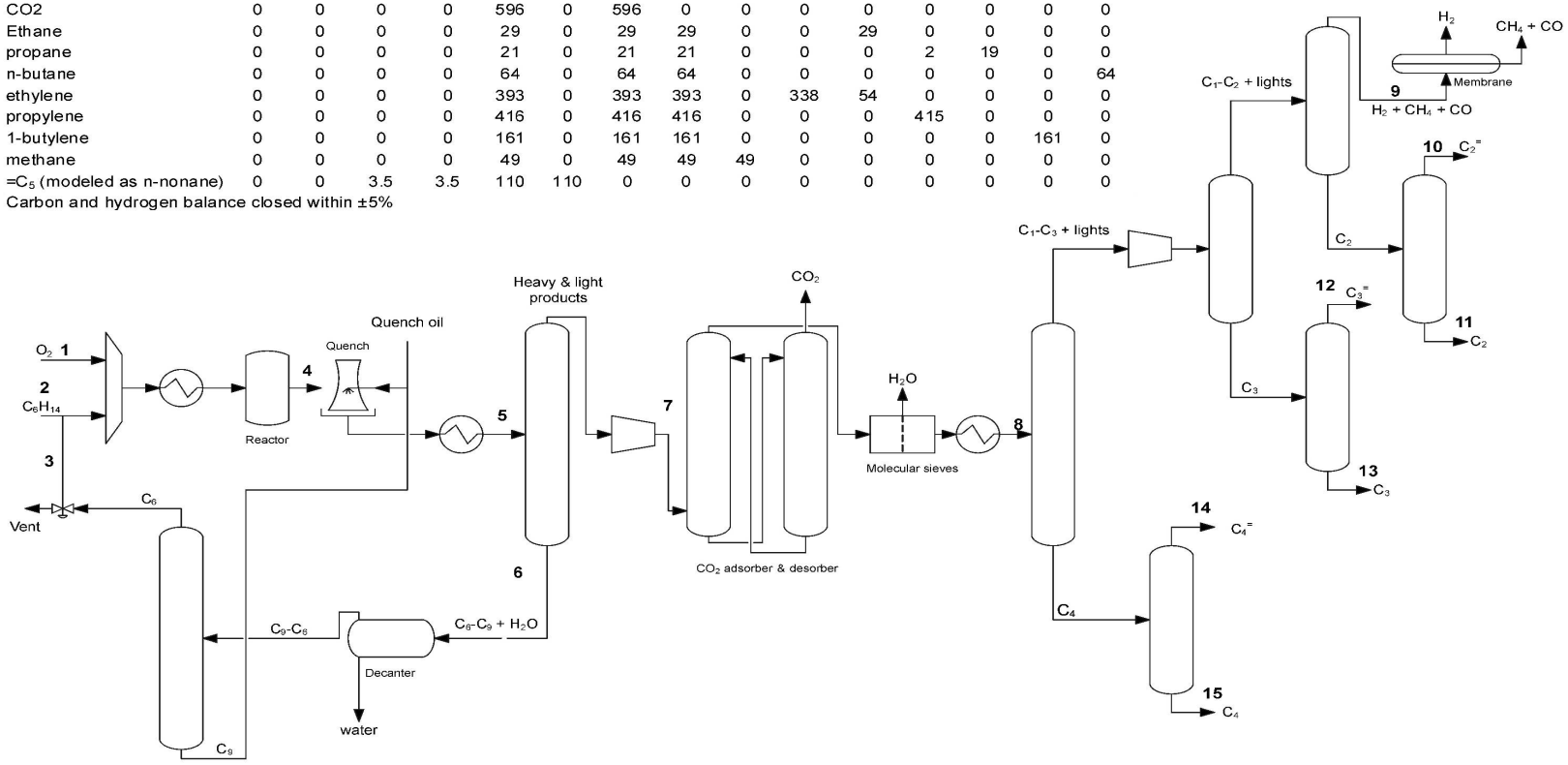

Figure 5.12: Process flow sheet of COC process and comprehensive mass balance

Fire and explosion index (F&EI) as well as HAZOP studies for the COC process indicate that the process has an intermediate degree of danger. Specifically the risk of explosions demands extra safety precautions; therefore extra pressure, temperature and flow controls should be installed near the reactor. Extra safety valves are as well advisable near the reactor. The Chemical Exposure Index (CEI) indicates that in relation to toxicity the process is relatively safe, as there are no highly toxic chemicals in the process. Of course this is no permit to neglect the general safety procedures considering toxic chemicals. With the extra safety measures this plant is safe enough to be built.

5.5 Differential study of catalytic oxidative cracking (COC) *vs.* steam cracking (SC)

The potential industrial application of the COC process depends on the both technical and economical advantages the process is able to achieve, as compared to the conventional steam cracking process. Thus, to evaluate the COC process a comparative study of both COC and SC processes is essential. The key process differences between the two processes are; (i) the presence of the catalyst in the COC, (ii) the feed; COC uses O_2 in the feed with no diluent while steam cracking uses steam as diluent, (iii) temperature of operation; SC operates at 800 ^{o}C while the COC at 575 ^{o}C, (iii) SC uses external source of heating, while in COC part of the heat of reaction is provided autothermally inside the reactor, thus reducing the external fuel combustion and (iv) products formed. These parameters introduce differences in the reactor design, product distribution and separation trains, hence significant differences in the energy consumption of the two processes. The functional block diagram of both processes is shown in Figure 5.13 and presents the key differences between these two processes.

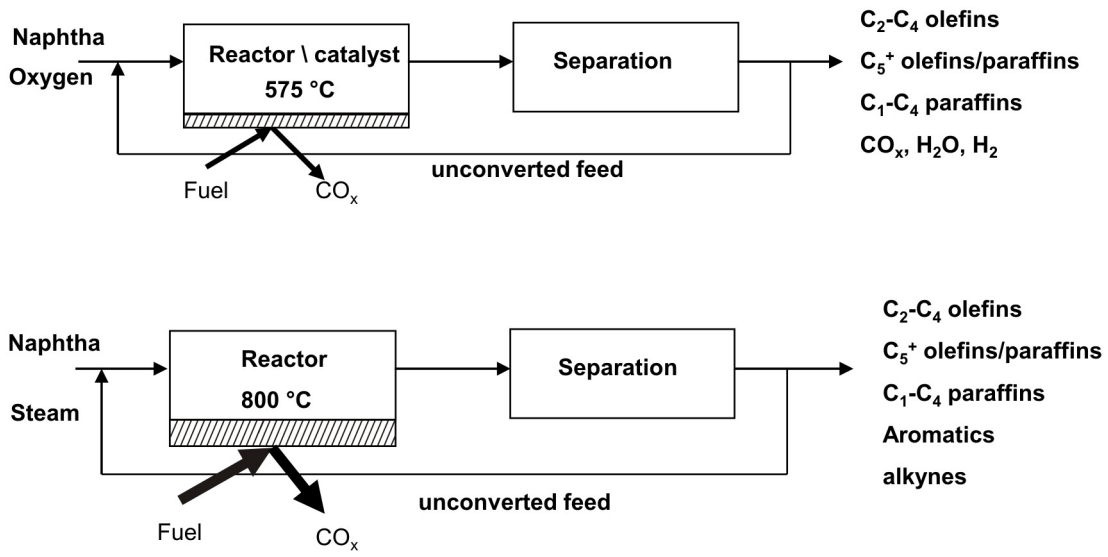

Figure 5.13. Key process differences between the COC and SC processes.

The COC process, due to the presence of the catalyst and oxygen in the feed, operates at much lower reaction temperatures (575 °C) and results in a completely different product distribution than in steam cracking. A simplified comparison of reactor outlet products of the both processes based on 100 moles of hexane/naphtha conversion is shown in Table 5.2. The presence of the catalyst provides control over the olefin distribution increasing the selectivity to total butylenes and propylene.

Table 5.2: Reactor outlet of both COC and SC processes**.**

	COC	SC [27]
	mol/mol hexane converted	mol/mol naphtha converted
H_2	0.3	0.4
CO	0.4	–
CO_2 (from cracking reaction)	0.9	–
H_2O	0.5	2.5
C_1-C_4 paraffins	0.2	0.9
$C_2^=$	0.6	1.0
$C_3^=$	0.6	0.4
$C_4^=$	0.3	0.1
alkynes/diolefins	–	0.1
naphthenes/aromatics	–	0.1
other C_5^+	0.2	0.1
$(C_4^=+C_3^=)/C_2^=$	1.5	0.4
CO_2 emissions from external fuel combustion (mol/mol hexane or naphtha converted)		
	0.3[a]	1.5 [1]

[a] calculated CO_2 emission from methane combustion to provide sufficient heat to operate the reactor

COC results in $(C_4^=+C_3^=)/C_2^=$ molar ratio of 1.5 against $(C_4^=+C_3^=)/C_2^=$ molar ratio of 0.4 in steam cracking. Previously, during the oxidative conversion of propane to propylene, Sinev and co-workers [26] reported that the abstraction of a secondary hydrogen atom from the alkane by surface $[O^-]$ sites ($[Li^+O^-]$ in Li/MgO) is energetically more favorable. Similarly, in the case of hexane, the high $(C_4^=+C_3^=)/C_2^=$ molar ratios are explained by the involvement of the catalyst in the process and the related preference for hydrogen abstraction from a secondary carbon atom forming iso-hexyl radicals. β-scission of iso-hexyl radicals at this relatively mild cracking conditions (575 °C) will result in higher ratio of high olefins to ethylene. However, steam cracking follows a radical chemistry route [27]; the carbon radicals (primary or secondary) formed initially *via* C-H bond cleavage, after subsequent β-cleavage result in primary radicals. Every further β-cleavage of the primary radicals formed results in C2 product.

In the COC process, in addition to hydrocarbons, an amount of 1.3 moles of combustion products ($CO + CO_2$) per mol of hexane converted is formed. Carbon loss is hence considered a drawback of this process. In steam cracking, however, by products like aromatics and acetylene have revenues. Total CO_2 emissions from the COC process (1.2 mol/mol hexane converted) are slightly lower than emissions from the steam cracking process (1.5 mol/mol naphtha converted).

The differences in product distribution in both processes, lead to differences in the separation trains. The separation of heavy products and quench oil in both processes is

similar. In steam cracking however, there are more water and heavy components to be separated. In addition, in steam cracking due to the higher reactor outlet temperature, approximately double the amount of quench oil is needed to cool down the products. The composition of the light product stream, however, is very different in both processes. Therefore the separation order of the light product stream is fundamentally different. The SC process is designed for a maximum ethylene production and recovery; hence light olefins are separated first. The COC process is designed for production and recovery of propylene and butylene; hence these olefins are separated first. In addition, a significant difference in the separation train of both processes is the need for CO_2 separation in the COC process. Figure 5.14 presents a process flow sheet of the steam cracking obtained from literature [27].

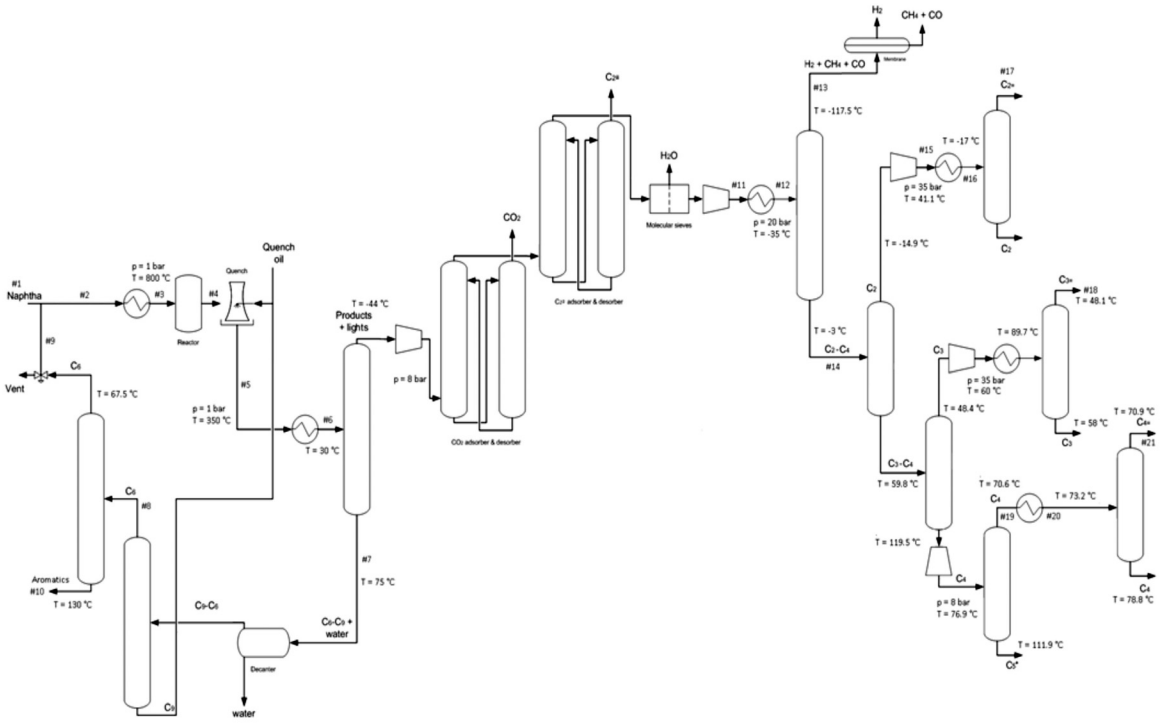

Figure 5.14. Process flow sheet of steam cracking process [27].

The utilities (hot/cold) required for both COC and SC processes were estimated through performing heat integration of both processes. Heat integration was based on the identification of both cold and hot streams and determining the pinch temperature [18]. Heat integration results of both COC and SC processes are presented in Table 5.3.

Results indicate that the COC process consumes 53 % less total duty than the SC process, making the process much more energy efficient. The high energy consumption in steam cracking is mainly due to the large amount of hot utilities required for vaporization of water as diluent in the feed, as well as energy needed to heat the crackers to 800 °C. The COC process however, due to the lower operating temperatures, uses significantly less hot utilities, which makes the heat integration much more efficient than in SC (see Table 5.3). Heat integration of COC reduced the amount of utilities required for the process by 60%, while this was only 38% in SC. The specific amount of energy consumed in SC process was

calculated to 17 GJ/ton of light olefins produced, while this was 8 GJ/ton of light olefins in the COC process. The claim that the COC process is more energy efficient is proven valid.

Table 5.3. Hot and cold duties of the COC and SC processes, before and after heat integration.

		SC process	COC process
before heat integration	Cold utilities (MW)	107	121
	Hot utilities (MW)	189	92
	Total duties (MW)	296	213
after heat integration	Cold utilities (MW)	50	57
	Hot utilities (MW)	133	27
	Total duties (MW)	183	85
	Reduction by heat integration	38%	60%
	Total duties compared to SC	100%	47%

5.6 Economic evaluation

The method of Hill and the method of Lang (± 50% accuracy) were used to estimate the capital costs of the COC process [28]. The capital costs of the plant were estimated, utilizing equipment design and costs data (not shown here), to be $147 million. The operational costs consist of costs of raw materials, utilities, maintenance and operations, depreciation (8% of total depreciable capital) and general expenses (12% of sales). The pie diagram in Figure 5.15 presents the distribution of the operational costs. The total operational costs were estimated at $281 million per year, of which 77% is the cost of naphtha feed. The heat utilities present only 3% of the total operational costs. This implies that although of the more energy efficiency of the COC process, it still can not compete with the steam cracking. Carbon loss as result of combustion of part of the valuable naphtha feed makes the COC process economically less attractive compared to steam cracking, where methane which is a cheaper fuel than naphtha is utilized.

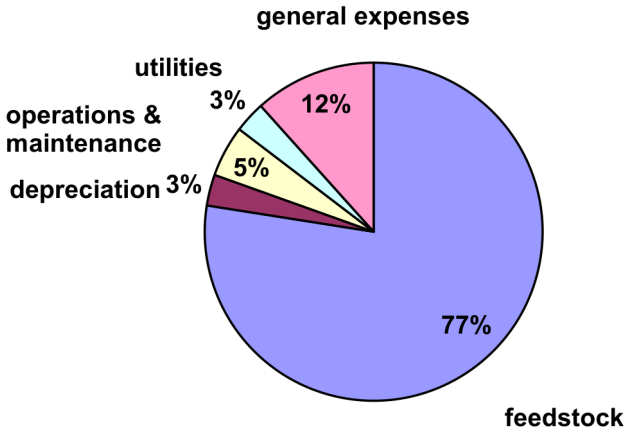

Figure 5.15. Pie diagram of operational costs.

Using the current market prices in the Middle East of naphtha, ethylene, propylene and butylenes [29-30] the revenues of the COC process were estimated at $283 million per year. However, as it is predicted that in the upcoming years the demand for propylene and butylene will increase, it is relevant to assume that the prices of these chemicals will also increase. Similarly, the demand for oil will probably as well increase, leading to an increase in prices of naphtha. Therefore, NPV analysis [18] for different scenarios was performed. The scenarios were defined as follows; *Scenario 1*: current market prices were used; *Scenario 2*: current market price of naphtha was used and 25% increase in price of propylene and butylene was estimated; *Scenario 3*: 25% increase in price of each of propylene, butylene and naphtha was estimated; *Scenario 4:* prices as they were in 2008; *Scenario 5:* average price of naphtha over the years 2008 and 2009 was used and 25% increase in price of propylene and butylene was estimated. Table 5.4 presents the NPV analysis of the five scenarios. It is clear both from scenarios 4 and 5, that the increase in the price of naphtha has a detrimental effect on the NPV. The most promising scenario is *scenario 2* with a $193 million profit at year ten. *Scenario 5* would be, however, the most probable and realistic scenario. Nevertheless, even with this scenario the break even point will not be reached after 10 years and the loss after 10 years was estimated to $510 millions.

Table 5.4: NPV analysis [a]

	Scenario 1	Scenario 2	Scenario 3	Scenario 4	Scenario 5
Naphtha ($/Kg)[b]	0.5	0.5	0.6	1.0	0.8
Ethylene ($/Kg)[b]	1.0	1.0	1.0	1.5	1.0
Propylene ($/Kg)[b]	1.0	1.3	1.3	1.5	1.3
Butylene ($/Kg)[c]	0.8	1.0	1.0	1.0	1.0
BEP (year)	–	4	–	–	–
NPV (mln USD)	-136	193	-158	-679	-510

[a] It is auumed that the plant is built in year 0 and lifetime is 10yrs.Discount rate is assumed 10%.
[b] Prices obtained from YNFX [29]
[c] Prices obtained from ICIS [30]

The performance of the Li/MgO catalyst and the selectivity to C_2-C_4 olefins is also an influential factor in the economical feasibility of the COC process. Thus a feasibility study was preformed to see at which selectivity to olefins the process becomes economically attractive. Revenues were calculated using the current market prices, for 100% conversion and a C_2-C_4 olefin selectivity of 60%, 77.5% and 100%. For the calculation purpose, the following overall reaction equation was used.

$$C_6H_{14} + O_2 \rightarrow C_2H_4 + C_3H_6 + C_4H_8 + C_5H_{10} + H_2O + CO_x \qquad (10)$$

Figure 5.16 shows the revenues per ton of naphtha against the overall selectivity. Results indicate that the selectivity to C_2-C_4 olefins should be above 63 mol% for the COC process to break even. Thus we conclude that based on the C_2-C_4 selectivities (63 mol%) achieved with the Li/MgO catalyst and the current market prices, the COC process will not be profitable.

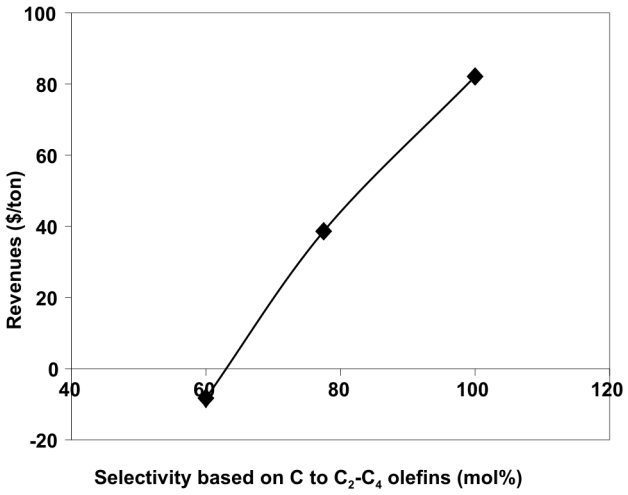

Figure 5.16. Revenues *vs*. selectivity.

The profitability of the COC process is thus highly dependent on (i) the development of the market prices of ethylene, propylene and butylene, and (ii) the design of more selective catalysts with C_2-C_4 selectivities above 65mol%. Catalysts that will enhance C-C bond cleavage in the alkane, and further minimize combustion are essential. Moreover, it is highly recommended to investigate reactor design parameters, specifically the catalyst volume-to-empty reactor volume ratio. Burch and Crabb [31] suggested during the oxidative conversion of propane, that the combination of heterogeneous (catalytic) and homogeneous (gas phase) reactions is necessary to obtain commercially acceptable yields of olefins. Similarly, in the case of oxidative cracking of naphtha, an optimized ratio of heterogeneous surface reactions to homogeneous gas phase reactions is expected to significantly enhance the yields of olefins.

5.7 Conclusions

A conceptual design of the catalytic oxidative cracking process as an alternative to steam cracking for light olefins, proved that the process is technically feasible. However there are some constraints because the design is based on experimental data where reactants (hexane and oxygen) were diluted in helium. The presence of diluent in the process is economically not feasible, thus pure hexane and oxygen have been considered as the feed. Safe operation, out of the explosion window, places severe restrictions on the feed composition. It is concluded that fully auto-thermal operation of the process is only possible with multiple oxygen feeding along the FLBR.

In comparison to steam cracking, the presence of the Li/MgO catalyst in the COC process, (i) allows operation at 575 °C which is much lower than temperatures utilized in steam cracking, and (ii) controls the olefin distribution increasing the ratio of $(C_4^= + C_3^=)/C_2^=$. The

presence of oxygen is crucial to (i) internally provide heat for the endothermic cracking reaction, (ii) regenerate the catalyst, and (iii) inhibit coke formation.

The reactor products and separation train are very different for both processes. The separation of the light hydrocarbon product stream is separated in opposite order for both processes. The SC process is designed for a maximum ethylene production and recovery, while the COC process is designed for production and recovery of propylene and butylene.

Energy evaluation of both processes clearly indicates that compared to SC, the COC process is more energy efficient with 53% less total duty use. However, utilities present only a minor fraction of the operational costs, and the latter is controlled by the costs of the feedstock. Therefore, loss of valuable feedstock as result of combustion of part of the naphtha feed, makes the COC process economically less attractive compared to steam cracking.

Finally, an economic evaluation of the COC process showed that in a realistic scenario, this process is not yet economically attractive. For the process to be profitable the market prices of propylene and butylene should rise about 25%. The design of more active and selective catalysts with selectivity to C_2-C_4 olefins above 65% should also be considered to increase the industrial applicability potential of the process. It is also highly recommended to investigate reactor design parameters, specifically the catalyst volume-to-empty reactor volume ratio.

Symbols

f_{burned}	= fraction of hydrocarbon burned	[mol]
$\Delta H_{combustion}$	= heat of combustion	[J/mol]
ΔH_{vap}	= heat of vaporization	[J/mol]
HHV	= higher heating value	[J/mol]
T_{boil}	= boiling temperature	[K]
$T_{reaction:}$	= reaction temperature	[K]
Cp_{liquid}	= specific heat capacity of the liquid	[J/mol.K]
Cp_{gas}	= specific heat capacity of the gas	[J.mol.K]
ζ	= conversion	[mol]
ΔH_r	= heat of reaction	[J/mol]

References

[1] T. Ren, M. Patel, K. Blok, Energy 31 (2006) 425-451.

[2] P.R. Cortelli, S.T. Bakas, M.F. Bentham, J.H. Gregor, C.R. Hamlin, L.F. Smith, Oleflex process – The proven route to olefins; UOP, Des Plaines, III,1992.

[3] H. Bolt, H. Zimmerman, in: M. Baerns, J. Whitelamp (Eds.), DGMK Proc, Kassel, 1993, 175-185.

[4] P.R. Sarathy, G.S. Suffridge, Hydrocarbon Processing 72 (1993) 89-92.

[5] T. Ito, J.-X. Wang, C.-H. Lin, J.H. Lunsford, J. Am. Chem. Soc. 107 (1985) 5062-5068.

[6] C.-H. Lin, K.D. Campbell, J.-X. Wang, J.H. Lunsford, J. Phys. Chem. 90 (1986) (4) 534-537.

[7] E. Morales, J.H. Lunsford, J. Catal. 118 (1989) 255-265.

[8] F. Cavani, F. Trifiro, Catal. Today 24 (1995) 307-313.

[9] M. Xu, C. Shi, X. Yang, M.P. Rosynek, J.H. Lunsford, J. Phys. Chem. 96 (1992) (15) 6395-6398.

[10] M.V. Landau, M.L. Kaliya, A. Gutman, L.O. Kogan, M. Herskowitz, P.F. van den Oosterkamp, Stud. Surf. Sci. Catal. 110 (1997) 315-326.

[11] L. Leveles, K. Seshan, J.A. Lercher, L. Lefferts, J. Catal. 218 (2003) 307-314.

[12] L. Leveles, K. Seshan, J.A. Lercher, L. Lefferts, J. Catal. 218 (2003) 296-306.

[13] C. Trionfetti, I.V. Babich, K. Seshan, L. Lefferts, Appl. Catal. A 310 (2006) 105-113.

[14] C. Trionfetti, I.V. Babich, K. Seshan, L. Lefferts, Langmuir 24 (2008) 8220-8228.

[15] C. Boyadjian, L. Lefferts, K. Seshan, Appl. Catal. A 372 (2010) 167-174.

[16] F. Cavani, N. Ballarini, A. Cericola, Catal. Today 217 (2007) 113-131.

[17] H. van den Berg, Process Plant Design course, University of Twente, Enschede, the Netherlands, 2009.

[18] W.D. Seider, J.D. Seader, D.R Lewin, Product and Process Design Principles: Synthesis Analysis and Evaluation, 2nd ed, Wiley: New York, 2004, pp. 243-396.

[19] T.F. Narbeshuber, A. Brait, K.Seshan, J.A. Lercher, J. Catal. 172 (1997) 127-136.

[20] J.W. Bolk, K.R. Westerterp, Influence of Hydrodynamics on the Upper Explosion Limit of Ethene-Air-Nitrogen Mixtures.1999, 45, pp. 124-144.

[21] R. Krishna, S.T. Sie, Chem. Eng. Scien. 49 (1994) (24 PART A) 4029-4065.

[22] G. Centi, F. Cavani, F. Trifiro, in: M.V. Twigg, M.S. Spencer (Eds.), Selective Oxidation by Heterogeneous Catalysis, Fund. Appl. Catal.7, Kluwer Acedemic: New York, 2001, pp 37-74.

[23] S.D. Barnicki, J.R. Fair, Ind. Eng. Chem. Res. 31 (1992) 1679-1694.

[24] A.L. Kohl, R.B. Nielsen, Gas Purification, 5th ed, Gulf. Publ: Houston TX, 1997, pp 148-181.

[25] R.A. Meyer, Handbook of Petroleum Refining Processes, 2nd ed, McGraw-Hill:New York, 1997, pp 10.79-10.81.

[26] E.V. Kondratenko, M.Yu. Sinev, Appl. Catal. A 325 (2007) 353-361.

[27] A. Chauvel, G. Lefebvre, N. Marshall, Petrochemical Processes: Synthesis-Gas Derivatives and Major Hydrocarbons; Gulf: Houston, 1989, pp 118-165.

[28] M.S. Peters, K.D. Timmerhaus, R.E. West, Plant Design and Economics for Chemical Engineers, 5th ed, McGraw Hill: Boston, 2003, pp 226-278.

[29]http://www.yarnsandfibers.com/textile-pricewatch

[30] http://www.icis.com/staticpages

[31] R. Burch, E. Crabb, Appl. Catal. A 100 (1993) 111-130.

Conclusions and Recommendations

1 Introduction

Steam cracking, the current major existing route for light olefin production, is the most energy consuming process in the chemical industry. The need for energy efficient processes, urged substantial research work for the development of new catalytic technologies for light olefin production [1].

Steam cracking maximizes ethylene formation, and propylene is produced as a secondary product. The faster increase in demand of propylene than that of ethylene [1-2], makes steam cracking a less attractive route for the production of this olefin. Thus, catalytic pathways that provide for more propylene formation are essential.

The present research work investigated catalytic pathways for n-hexane cracking, as a model compound of naphtha, in the presence of oxygen. The work aimed towards achieving; (i) lower cracking temperatures and (ii) higher selectivities to both propylene and butylenes than in the steam cracking process.

Li/MgO catalyst has shown to be promising for the oxidative dehydrogenation/cracking of light alkanes (*e.g.*, methane [3], ethane [4], propane [5-8] and butane [7]). The catalyst has no formal red-ox character and together with its inherent strong Bronsted basicity, minimizes re-adsorption and sequential combustion of formed olefins. Therefore, in the present work for the oxidative conversion of n-hexane, to maximize olefin yields, Li/MgO catalyst was selected and studied.

2 Oxidative cracking of n-hexane over Li/MgO catalyst

In the oxidative cracking of n-hexane [9], Li/MgO shows a similar behavior as in oxidative dehydrogenation of ethane, propane and butane; *i.e.*, heterogeneously initiated homogeneous reaction. However, as hexane is more active than C_2-C_4 alkanes, it is possible to operate at lower reaction temperatures (575 ^oC), much lower than temperatures used in conventional steam cracking (800 °C). Due to the low oxidation activity of Li/MgO limited hexane conversions (28 mol%), however excellent selectivity to C_2-C_4 olefins (60 mol%) are observed. Selectivities obtained are similar to those achieved during oxidative conversion of C_2-C_4 alkanes [5]. In agreement with the performance of Li/MgO for the oxidative conversion of low alkanes, an olefin selectivity which is invariant with hexane conversion is observed. Oxygen plays a significant role in (i) regenerating the active sites, (ii) accelerating the radical chemistry, and (iii) inhibiting coke formation.

Unlike steam cracking, catalytic oxidative cracking results in a relatively higher ratio of butylenes + propylene to ethylene. Thus presence of the catalyst provides a better control over olefin distribution. Active sites of the catalyst, however, are susceptible for deactivation due to poisoning by product CO_2, which interacts with the $[Li^+O^-]$ catalytic active sites forming stable Li_2CO_3. Both Mo and Bi promoted Li/MgO, however, maintain activity during time on stream due to less formation of Li_2CO_3, and hence show considerably higher yields of C_2-C_4 olefins than Li/MgO. Mo promoted Li/MgO was selected for detailed study in this work.

3 Mo/Li/MgO: Efficient catalyst for the oxidative cracking of n-hexane

Chapters two and three addressed the drawbacks of the Li/MgO catalyst. These consist of (i) deactivation during time on stream as result of the poisoning of the $[Li^+O^-]$ active sites by product CO_2, and (ii) sintering when exposed to high temperature treatments (> 500 ^oC), due to Li_2CO_3 originally present in the catalyst. Promotion of Li/MgO with Mo results in significant improvements in both surface area and stability of the catalyst. It is established both in chapters two and three, that minimum loadings of Mo (~0.3wt%) is sufficient to bring the following advantages; (i) reduce the amount of Li_2CO_3 originally present in Li/MgO, thus promote the catalyst to maintain higher surface area upon high temperature treatment, and (ii) prevent the poisoning of the $[Li^+O^-]$ by product CO_2 during reaction, hence improve stability of the catalyst. Increase in Mo loadings above 0.3wt% affects both catalyst activity and selectivity negatively.

Further, chapter three presented a structure-performance study of the Mo/Li/MgO catalysts. The chemical structures of the different molybdena species were identified and their presence correlated to the high surface area and stability, as well as the activity and selectivity observed for the Mo promoted catalysts. Characterization with Raman spectroscopy showed that the Mo/Li/MgO catalyst contains three types of phases; (i) monomeric $Mg[MoO_4]$, $Li_2[MoO_4]$, where Mo is in tetrahedral coordination, (ii) polymeric species such as $Li_2Mo_4O_{13}$ where Mo is in octahedral coordination, and (iii) an amorphous lithium molybdate phase also where Mo is in octahedral coordination. The amorphous lithium molybdate species are proposed to enhance catalyst stability by hindering Li_2CO_3 formation from catalytically active $[Li^+O^-]$ sites during oxidative conversion reaction. The formation of Lithium molybdates (Li_2MoO_4, $Li_2Mo_4O_{13}$) from reaction of MoO_3 with Li_2CO_3, is proposed to reduce the amount of Li_2CO_3 originally present in the catalyst. At the high Mo loadings, however, the formation of the dispersed phases is enhanced, leading to poor activity and selectivity.

It is concluded that 0.3 wt% Mo promoted Li/MgO catalyst is very efficient for the selective conversion of hexane to olefins. The catalyst is stable and keeps characteristics of Li/MgO; *i.e.*, the high olefin selectivities (~60 mol%) are maintained even at high hexane conversions.

4 Integrated plasma-Li/MgO system for the oxidative cracking of n-hexane

Kinetic results from the oxidative conversion of alkanes over the Li/MgO show that C-H bond splitting is the rate limiting step in these reactions [6]. Even in the presence of strong H• abstractor, high temperatures ≥ 550 ^oC are still required to induce this step. For the oxidative conversion of hexane, in an attempt to enhance hexane conversions, thus yields of olefins, chapter four investigated the role of plasma in introducing new pathways for hexane conversion.

Indeed, similar as in the oxidative conversion of propane in a plasma micro-reactor previously reported by us [10-11], in the oxidative conversion of hexane plasma introduces additional pathways for hexane and oxygen activation *via* electron impact excitations. Thus, in the integrated plasma-Li/MgO system hexane activation takes place *via* three main routes;

(i) C-H bond scission *via* the [O^-] defect sites on the surface of Li/MgO, (ii) C-C, C-H bond scission by electron-impact excitation of hexane molecule with electrons, and (iii) C-H bond scission by oxygen atoms formed from collisions of oxygen molecules with electrons.

Combination of plasma and Li/MgO results in a synergistic effect, hence significantly higher C_2-C_5 olefin yields (35 mol%) than those achieved with plasma in the absence of catalyst (15 mol%) or with catalyst in the absence of plasma (19 mol%).

Temperature has clear influence on the performance of the integrated plasma-Li/MgO system. At 500^{o}C, plasma chemistry is dominant leading to significant formation of acetylene (17 mol%) and ethylene (32 mol%) and low formation of the high olefins ($C_3^=$-$C_5^=$ =11 mol%). At the higher temperature (600 ^{o}C), however, contribution of the catalyst both in hexane activation and olefin formation becomes significant leading to more formation of C_3-C_5 olefins (38 mol%) than ethylene (26 mol%). Interestingly at this temperature no acetylene formation is observed, and is explained by the complete oxygen consumption, which minimizes combustion of the CH radicals, thus enhances their reaction to olefins.

5 Catalytic oxidative cracking (COC) *vs.* Steam cracking (SC)

The technical and economical feasibility of the catalytic oxidative cracking, as an alternative process to steam cracking, was investigated in chapter five.

A conceptual design, elaborated from experimental data of the oxidative conversion of hexane over the Li/MgO, proved that the process is technically feasible. The key process differences between both SC and COC processes were established. The COC process operates at lower temperatures (575 ^{o}C) than steam cracking (800 ^{o}C), thus reduces the external fuel combustion. Moreover, the presence of oxygen in the COC process allows for an auto-thermal operation where part of the heat of reaction is provided *in situ* from combustion of part of the feed.

The reactor products and separation train are very different for both processes. The SC process is designed for a maximum ethylene production and recovery, while the COC process is designed for production and recovery of propylene and butylene. Moreover, in the COC process an additional CO_2 separation unit is necessary.

Energy evaluation of both processes clearly indicates that compared to SC, the COC process is more energy efficient with 53% less total duty use. However, an economic evaluation of the COC process showed that the naphtha feedstock presents 77% and the utilities only 3% of the operational costs. This implies that carbon loss in the COC process, as result of combustion of part of the valuable naphtha feed, makes it economically less attractive compared to steam cracking.

An NPV analysis showed that in a realistic scenario, this process is not yet economically attractive. The profitability of the COC process is highly dependent on the development of the market prices of ethylene, propylene and butylene, and the design of more selective catalysts with C_2-C_4 selectivities above 65 mol%.

6 Recommendations

It is established in the present thesis that Mo promoted Li/MgO is an efficient catalyst for the oxidative conversion of n-hexane. The catalyst maintains activity over time on stream, moreover, exhibits invariant selectivities to C_2-C_4 olefins (60 mol%) with hexane conversions. However, it is demonstrated in chapter five that experiments in this research work were conducted at conditions far from a real case process; *i.e*, hexane was used as a model compound of naphtha and reactants (hexane, oxygen) were diluted in helium. Therefore, in order to gain better insight on the potential industrial application of the process, it is highly recommended to investigate the oxidative conversion of naphtha over the newly developed catalyst (Mo/Li/MgO), using naphtha and oxygen feed streams in the absence of the diluents.

Nevertheless, a preliminary economical evaluation of the catalytic oxidative conversion of hexane, utilizing current research results, strongly suggests further improvements in the selectivities to C_2-C_4 olefins. In order to achieve higher selectivities to olefins and minimize combustion, two approaches are recommended: (i) Improve performance of the catalyst and (ii) investigate reactor design parameters.

Improving the performance of the catalyst necessitates the presence of new selective sites that minimize the secondary combustion reactions of the formed olefins. It is also recommended to investigate promoters other than Mo. Mo has facile red-ox properties and at the high loading, it enhances the secondary combustion of the olefins. The promoter, thus, should be a cation that does not undergo a change in oxidation state easily. Bi promoted Li/MgO, investigated in chapter one, showed promising performance; *i.e.*, stability with time on stream and high yields to olefins. In agreement to literature work by Grasselli and co-workers [12-13], Bi promoted the selective oxidation of hydrogen to water and showed minimal CO_x formation. It is, thus, recommended to carry a detailed study of this catalyst and investigate the influence of varying Bi loading on the performance of Li/MgO for the oxidative conversion of naphtha.

Regarding the second approach, as demonstrated in chapter five, a fluidized bed reactor with distributed oxygen inlet is a suitable reactor choice for this reaction. Distributed oxygen inlet will minimize combustion and provide safe operation outside the flammability window. It is recommended to conduct research work to further investigate reactor design parameters. It is agreed in the oxidative conversion of alkanes that the combination of heterogeneous and homogeneous radical reactions are essential to obtain high yields of olefins [14]. Therefore, an optimal catalyst-volume-to-empty reactor volume ratio is necessary. A disadvantage of the FLBR, however, is that it requires a catalyst with specific mechanical properties, *e.g*., resistance to attrition. These issues need to be as well addressed.

Integrated plasma-Li/MgO is a promising technology for light olefin production. However, inefficient energy utilization is a major drawback of this technology. Hence, it is recommended to research methodologies to improve the efficiency of the system. The use of more efficient power supplies and numbering up of plasma reactors are options for better utilization of plasma energy.

In addition, a better understanding of the influence of plasma on catalyst surface is highly recommended. This necessitates the utilization of *in situ* spectroscopic techniques under plasma conditions. *In situ* EPR is suggested to characterize the generation of new [O^-] sites on surface of Li/MgO, from the photo excitation of O^{2-} sites of MgO by UV light from plasma.

References

[1] T. Ren, M. Patel, K. Blok, Energy 31 (2006) 425-451.

[2] http://www.plastemart.com/upload/Literature/Global-ethylene-propylene-demand-capacity-to-change.asp

[3] T. Ito, J.-X. Wang, C.-H. Lin, J.H. Lunsford, J. Am. Chem. Soc.107 (1985) 5062-5068.

[4] E. Morales, J.H. Lunsford, J. Catal. 118 (1989) 255-265

[5] L. Leveles, K. Seshan, J.A Lercher, L. Lefferts, J. Catal. 218 (2003) 307-314.

[6] L. Leveles, K. Seshan, J.A. Lercher, L. Lefferts, J. Catal. 218 (2003) 296-306.

[7] C. Trionfetti, I.V Babich, K. Seshan, L. Lefferts, Appl. Catal. A 310 (2006) 105-113.

[8] C. Trionfetti, I.V Babich, K. Seshan, L. Lefferts, Langmuir 24 (2008) 8220-8228.

[9] C.Boyadjian, L. Lefferts, K. Seshan, Appl. Catal. 372 (2010) 167-174.

[10] C. Trionfetti, A. Agiral, ChemPhysChem 9 (4) (2008) 533-537.

[11] C. Trionfetti, A. Agiral, J. Phys. Chem. 112 (11) (2008) 4267-4274.

[12] R.K. Grasselli, D.L. Stern, J. G. Tsikoyiannis, Appl. Catal. A 189 (1999) 1-8.

[13] J. G. Tsikoyiannis, D. L. Stern, R.K. Grasselli, J. Catal. 184 (1999) 77-86.

[14] R. Burch, E. Crabb, Appl. Catal. A 100 (1993) 111-130.

List of Publications

1. C. Boyadjian, L. Lefferts and K. Seshan, *Catalytic Oxidative Cracking of n-Hexane as a Route to Olefins*. Appl. Catal. A 372 (2010) 167-174.

2. C. Boyadjian, B. van der Veer, I.V. Babich, L. Lefferts and K. Seshan, *Oxidative Cracking of n-Hexane over MoO_3-Li/MgO.* Catal. Today in press (2010).

3. C. Boyadjian, S. Crapanzano, I.V. Babich, B.L. Mojet, L. Lefferts and K. Seshan, *Structure and Performance of Li/MgO Supported Molybdenum Oxide for the Oxidative Cracking of n-Hexane*. J. Catal. (2010) submitted.

4. C. Boyadjian, L. Lefferts, K. Seshan, A.G.J. van der Ham and H. van den Berg, *Production of C_3/C_4 Olefins from Naphtha: Catalytic Oxidative Cracking as an Alternative Route to Steam Cracking*. Ind. Eng. Chem. Res. (2010) submitted.

5. C. Boyadjian, A. Agiral, J.G.E. Gardeniers, L. Lefferts and K. Seshan, *Oxidative Cracking of n-Hexane - Influence of Plasma and Catalyst on Reaction Pathways*, Plasma Chem. Plasma Process. (2010) submitted.

6. A. Agiral, C. Boyadjian, J.G.E. Gardeniers, L. Lefferts and K. Seshan, *Pathway Study on DBD Plasma Conversion of Hexane.* J. Phys. Chem. C in press (2010).